UNDERSTANDING THE SOURCES, ATMOSPHERIC EVOLUTION AND RADIATIVE EFFECT OF BROWN CARBON AEROSOL PARTICLES

A Dissertation
Presented to
The Academic Faculty

by

Linghan Zeng

In Partial Fulfillment
of the Requirements for the Degree
Doctor of Philosophy in the
School of Earth and Atmospheric Sciences

Georgia Institute of Technology
December of 2021

UNDERSTANDING THE SOURCES, ATMOSPHERIC EVOLUTION AND RADIATIVE EFFECT OF BROWN CARBON AEROSOL PARTICLES

Approved by:

Dr. Rodney J. Weber, Advisor
School of Earth and Atmospheric Sciences
Georgia Institute of Technology

Dr. Nga Lee (Sally) Ng
School of Chemical and Biomolecular Engineering
Georgia Institute of Technology

Dr. Yuhang Wang
School of Earth and Atmospheric Sciences
Georgia Institute of Technology

Dr. Jack E. Dibb
College of Engineering and Physical Sciences
University of New Hampshire

Dr. Lewis G. Huey
School of Earth and Atmospheric Sciences
Georgia Institute of Technology

Date Approved: November 3, 2021

To my parents

ACKNOWLEDGEMENTS

First and foremost, I would like to thank my advisor, Dr. Rodney J. Weber, for his continuous and generous support throughout my Ph.D. study. I am sincerely grateful for his guidance and trust. There are many things Rodney has taught me, but nothing was more precious than his passion for atmospheric science, especially for aerosols. In the past six years, it was truly a great experience that we have done several field campaigns together. Without his motivation and help, this thesis and many studies not covered here would undoubtedly have never achieved fruition. I am also grateful to my Ph.D. thesis committee members: Dr. Yuhang Wang, Dr. Lewis G. Huey, Dr. Nga Lee (Sally) Ng, and Dr. Jack Dibb, for their constructive suggestions in helping me become more productive and professional.

I would also like to thank the current members and alumni of Rodney's group. It is a great pleasure working with Dr. Amy A. Sullivan, Dr. Jiumeng Liu, Dr. Hongyu Guo, Dr. Ting Fang, Dr. Qian Zhang, Dr. Dong Gao, Dr. Jenny P.S. Wong, Dr. Theo Nah, Dr. Yuzhong Zhang, Yuhan Yang, Rime EI Asmar, Dr. Michael Battaglia, Dr. Kayane Dingilian, and Sukanya Kumar. I also thank students of other professors in the EAS department, including Dr. Lu Xu, Dr. Aoxing Zhang, Dr. Yunle Chen, Dr. Qiyang Yan, Taekyu Joo, Young Ro Lee, for their help and support with my research.

I am also very grateful for attending two NASA projects (ATom and FIREX-AQ). I especially thank Dr. Jack Dibb and Eric Scheuer from the University of New Hampshire for their help with sample collection on the airplane. I appreciate all my coauthors for their insightful comments and suggestions.

Finally, I would like to express my endless gratitude to my parents for their unconditional love, companionship, and support throughout my life.

TABLE OF CONTENTS

LIST OF TABLES

LIST OF FIGURES

LIST OF SYMBOLS AND ABBREVIATIONS

SYMBOLS

A_λ	Raw absorbance signal at wavelength λ
Abs_λ	Light absorption coefficient at wavelength λ in liquid
$b_{ap,\lambda}$	Light absorption coefficient at wavelength λ in aerosol phase
b_{BC}	Light absorption coefficient due to BC in aerosol phase
b_{BrC}	Light absorption coefficient due to BrC in aerosol phase
b_{scat}	Light scattering coefficient in aerosol phase
E_λ	Absorption enhancement for BC particle due to coating effect
I	Light intensity
j_{NO2}	The photolysis rate of NO_2
K^+_{BB}	Potassium ion from biomass burning
K_λ	Conversion factor for estimating the particle light absorption coefficient from the solution data
m	Refractive index; m=n+k*i*
λ	Wavelength, nm

ABBREVATIONS

AAE	Absorption Ångström Exponents
AAOD	Absorption Aerosol Optical Depth
Aeronet	Aerosol Robotic Network
AMS	Aerosol Mass Spectrometer
ATom	Atmospheric Tomography Mission

BC	Black Carbon
BrC	Brown Carbon
CCN	Cloud condensation nuclei
CH_3CN	Acetonitrile
CO	Carbon Monoxide
COVID-19	Coronavirus Disease
CSU	Colorado State University
DACOM	Differential Absorption Carbon Monoxide Measurements
DC3	Deep Convective Clouds and Chemistry
DI	Deionized
DRE	Direct Radiative Effect
DTT	Dithiothreitol
EESI-Tof-MS	Extractive Electrospray Ionization Time-of-Flight Mass spectrometer
EC	Elemental Carbon
ER	Emission Ratio
FLAME-4	The fourth Fire Lab at Missoula Experiment
FIREX-AQ	Fire Influence on Regional to Global Environments and Air Quality
FIRMS	Fire Information for Resource Management System
FRP	Fire Radiative Power
GFS	Global Forecast System
HCN	Hydrogen Cyanide
HEPA	High Efficiency Particulate Air
HIMIL	High-Performance Instrumented Airborne Platform for Environmental Research Modular Inlet
HR	High Resolution

HRRR	High-Resolution Rapid Refresh
HULIS	Humic-like Substance
HYSPLIT	Hybrid Single-Particle Lagrangian Integrated Trajectory
IC	Ion Chromatography
LAS	Laser Aerosol Spectrometer
LOD	Limit of Detection
IPCC-AR5	Intergovernmental Panel on Climate Change Fifth Assessment Report
LWC	Liquid Water Content
LWCC	Liquid Waveguide Capillary Cell
MAC	Mass Absorption Cross-section
MASTER	MODIS/ASTER airborne simulator
MC	Mist Chamber
MCE	Modified Combustion Efficiency
MOUDI	Micro-orifice Uniform Deposit Impactor
MS	Methonal-soluble
M-BrC	Moderately Absorbing Brown Carbon
NAM	North American Mesoscale Forecast System
NASA	National Aeronautics and Space Administration
NCAR	National Center for Atmospheric Research
NEMR	Normalized Excess Mixing Ratio
NOAA	National Oceanic and Atmospheric Administration
NOx	Oxides of Nitrogen
NO_3	Nitrate Radical
OA	Organic Aerosol
OC	Organic Carbon

OH	Hydroxyl Radical
O_3	Ozone
ODR	Orthogonal Distance Regression
PAH	Polycyclic Aromatic Hydrocarbon
PALMS	Particle Analysis by Laser Mass Spectrometry
PAS	Photoacoustic Spectrometer
PILS	Particle-into-Liquid Sampler
PM	Particulate Matter
PMF	Positive Matrix Factorization
POA	Primary Organic Aerosol
PTFE	Polytetrafluoroethylene
PTR-MS	Proton-transfer-reaction mass spectrometry
rBC	Refractory Black Carbon
R	Pearson Correlation Coefficient
RH	Relative Humidity
ROS	Reactive Oxygen Species
SAE	Scattering Ångström exponent
SBDART	Santa Barbara DISORT Atmospheric Radiative Transfer
SEAC^{4}RS	Studies of Emissions and Atmospheric Composition, Clouds and Climate Coupling by Regional Surveys
SLPM	Standard Liters per Minute
SMAI	Submicron Aerosol Inlet
SOA	Secondary Organic Aerosol
SP2	Single Particle Soot Photometer
STP	Standard Temperature and Pressure

S-BrC	Strongly Absorbing brown carbon
TFA	Trifluoroacetic Acid
TOA	Top of the Atmosphere
TOC	Total Organic Carbon
ToF	Time-of-flight
UV	Ultraviolet
Vis	Visible
VOC	Volatile Organic Compound
VW-BrC	Very Weakly Absorbing Brown Carbon
WE-CAN	Western wildfire Experiment for Cloud chemistry, Aerosol absorption and Nitrogen
WS	Water-soluble
W-BrC	Weakly Absorbing Brown Carbon
4-NC	4-Nitrocatechol

SUMMARY

Organic aerosols (OA) have long been thought to only scatter incoming solar radiation and have a cooling effect on the Earth's climate. However, a fraction of OA, referred to as brown carbon (BrC) absorbs light at wavelengths in the lower visible to ultraviolet range. BrC can be emitted from incomplete combustions and can also be generated through secondary processes. The radiative impact of BrC on climate is difficult to assess owing to the lack of knowledge about emissions and how BrC aerosol evolves once emitted into the atmosphere. This dissertation aims to gain a better understanding of the sources, atmospheric evolution, and radiative impact of BrC aerosol.

As part of the thesis work, the light absorption of BrC aerosol was measured with filters sampled from research aircraft during the NASA ATom mission. The aircraft flew from near surface to up to ~ 13 km altitude nearly pole to pole along the central Pacific and Atlantic Ocean basins and across the southern and Arctic Oceans. This work provides the first direct measurement of BrC aerosol on a global scale. The results suggest that the concentration of BrC was very low in most of the remote atmosphere, and detectable levels were only found in specific regions, including the mid-Atlantic Ocean and regions of the Arctic. The observed BrC was associated with biomass burning from air mass back trajectory analysis. The radiative impact of BrC was assessed by a radiative transfer model and the average direct radiative effect (DRE) due to BrC absorption accounted for 7-48% of the DRE due to absorption by all carbonaceous aerosols, suggesting that BrC can substantially affect the global climate.

As biomass burning is an important source of BrC, the next part of this thesis work investigates the characteristics and evolution of BrC emitted from wildfires in the western US as part of the FIREX-AQ study. An optical closure analysis was performed to compare the overall light absorption measured by a photoacoustic spectrometer (PAS) and the sum of the light absorption by individual light absorbers, including black carbon (BC) and BrC. The emission ratio of BrC at 405 nm relative to CO from wildfires was estimated to be 0.131 Mm^{-1} $ppbv^{-1}$. The evolution of BrC was examined in the first few hours after emissions, but no consistent fate of BrC was observed. We found that BrC did not behave in the same way as bulk OA or as a single BrC compound (4-Nitrocatechol) in response to temperature increases. In searching for factors driving changes in BrC in fresh smoke as it aged, evidence was found that oxidation by ozone could cause BrC enhancement under high NOx conditions, while BrC could be bleached by ozone when NOx levels were low. Other possible pathways, including aqueous reaction, reaction with ammonium, direct photolysis, were not found to have a discernible effect on BrC evolution.

Besides BrC measurement with filters and the PAS instrument, an online BrC measurement system was developed and deployed in the FIREX-AQ to provide direct water-soluble BrC measurements with a better time resolution possible than using filter sampling. The newly built system was compared to two other systems with similar detection methods but different aerosol collection methods. In general, all three instruments can make effective BrC measurements in airborne campaigns, but baseline drift and signal hysteresis were observed. A possible approach to correct the baseline drift and hysteresis effect was proposed, along with possible methods for future improvements for these systems.

CHAPTER 1. INTRODUCTION

1.1 The importance of the aerosol particles

Atmospheric aerosol particles, also known as particulate matter (PM), are suspended liquid or solid particles in the atmosphere, with typical diameters from a few nanometers to hundreds of micrometers. Despite their small sizes, the impacts of aerosols on air quality, visibility, human health, climate, and atmospheric chemistry are not negligible and are closely related to everyday life. Aerosols affect Earth's climate system in both direct and indirect ways. Aerosols can absorb or scatter solar radiation to affect the climate directly. In the Intergovernmental Panel on Climate Change Fifth Assessment Report (IPCC-AR5), light scattering by most atmospheric aerosols is the largest negative radiative forcer globally, which cools the Earth; however, some fraction of aerosols can absorb incoming solar light resulting in global warming. Black carbon (BC), brown carbon (BrC), and mineral dust have been investigated to be major contributors to the aerosol warming effect. Among these, BC aerosols contribute the third-largest positive radiative forcing at 0.6 W m^{-2}, behind only CO_2 and methane. Meanwhile, aerosols can also serve as cloud condensation nuclei (CCN) to indirectly change the global energy balance. Additionally, deposition of BC onto snow and ice can alter the surface albedo resulting in positive radiative forcing. However, in all models, the radiative effect of aerosols in both direct and indirect pathways is subjected to a large degree of uncertainty. The aerosol extinction, mainly by light scattering, can reduce visibility and cause haze events (Friedlander, 1977; Appel et al., 1985). Air pollution from fine aerosols caused more than 4.2 million premature deaths worldwide in the year 2015 (Cohen et al., 2017). Aerosols

can also provide surfaces for heterogeneous chemical reactions with trace gases, and thereby affect their abundance, distribution, and atmospheric residence time (Dentener et al., 1996; Pöschl et al., 2007).

1.2 Current understanding of brown carbon aerosol

Carbonaceous aerosols are one of the most abundant constituents of ambient aerosols. According to different thermostability, carbonaceous aerosols can be divided into two groups: elemental carbon (EC) and organic carbon (OC), which is also called organic aerosol (OA) (Schauer, 2003). OC will evaporate when aerosols are heated to temperatures in the range of 550 °C to 870 °C depending on the operating procedures, whereas in contrast, EC, which is the residual after heating, is refractory and light absorbing. Carbonaceous aerosols can also be classified as black carbon (BC), brown carbon (BrC), and non-absorbing organic aerosols based on operational defined optical properties. BC is a strong light absorber across the ultraviolet (UV) – visible (Vis) – near-infrared (NIR), and has been extensively studied (Bond and Bergstrom, 2006; Bond et al., 2013). Soot is also a term used to described light absorbing aerosols, which are usually generated in combustion related processes, and it is composed of graphene-like layers of carbon and adsorbed organic materials. In the research literature, EC, BC, and soot are usually used interchangeably or even mistakenly (Buseck et al., 2012). In past studies, OA has been thought to be clear (complex component of refractive index is zero), which means it only scatters light. However, more evidence shows that a fraction of OC does absorb light and has been referred to as brown carbon (BrC) because of its yellow or brown appearance. Unlike BC that absorbs light with little difference over all wavelengths, BrC has been observed to absorb light preferentially towards lower wavelengths (UV), and this strong

wavelength dependence feature can be described by the absorption Ångström exponent (AAE; $Abs_\lambda = C \cdot \lambda^{-AAE}$). In general, nonrefractory OC typically consists of low molecular weight hydrocarbons and is colorless, while refractory EC/BC has a graphene layer structure and is very absorptive. BrC is composed of higher molecular weight compounds, such as polycyclic aromatic hydrocarbons (PAH) and humic-like substances (HULIS), and many properties of BrC lie in between BC and clear OA, for example, absorptivity, volatility, and solubility.

BrC can be produced by incomplete combustion of fossil or biomass fuels, and it can also be formed during secondary processes involving carbonyl groups or nitrogen-containing compounds (Hoffer et al., 2006; Haan et al., 2009; Chen and Bond, 2010; Hecobian et al., 2010; Sareen et al., 2013), or from biomass burning emissions (Zhong and Jang, 2014; Wong et al., 2017; Wong et al., 2019b). A few studies have described changes of BrC aerosol following emission. Field observations of wildfires in California (Forrister et al., 2015), the Amazon (Wang et al., 2016), and Crete (Wong et al., 2019b) have suggested the half-life of BrC is between 9 and 24 hours. During the fourth Fire Lab at Missoula Experiment (FLAME-4), burning of differing fuel types under conditions that simulated fire emissions found a BrC half-life of ~16 hours (Lin et al., 2016). Laboratory studies have also investigated the aging of BrC chromophores in solvents. Secondary BrC formed from dark reactions of glyoxal or methylglyoxal with ammonium sulfate undergoes rapid photo-bleaching with a lifetime on the order of minutes to hours (Sareen et al., 2013; Zhao et al., 2015; Wong et al., 2017; Aiona et al., 2018), although secondary organic aerosol (SOA) from aromatic species is more stable, with a half-life of 12-24 hours (Lee et al., 2014; Liu et al., 2016).

BrC is found to behave on a continuum, where BrC aerosols composed of larger molecule weight compounds tend to be more thermostable and darker with less wavelength dependence, while particles composed of smaller BrC chromophore are lighter in color and less stable (Saleh, 2020). They have grouped BrC into four categories: very weakly absorbing BrC (VW-BrC), weakly absorbing BrC (W-BrC), moderately absorbing BrC, and strongly absorbing BrC (S-BrC), mapping these classifications by how absorptive BrC aerosol is, described by the mass absorption cross-section (MAC) or the imaginary part (k) of the refractive index (m=n+k*i*), and its wavelength dependence (AAE).

The complex nature of BrC hinders the estimation of its impact on the planetarty radiative balance. Previous studies have estimated the top of atmosphere (TOA) BrC direct radiative effect (DRE), which is its instantaneous radiative impact on Earth's energy (Heald et al., 2014), to range from +0.04 to +0.57 W m^{-2} with BrC contributing from 20 to 40% of the carbonaceous absorbing aerosol (Feng et al., 2013; Lin et al., 2014; Saleh et al., 2015; Jo et al., 2016). Most current model simulations depend on highly parameterized BrC predictions, which are based on the BC-to-OA ratio or modified combustion efficiency (MCE), and assume an invariant BrC following emission (Saleh et al., 2014; Jo et al., 2016). However, as noted, both field and laboratory data show that the absorption by BrC has been found to decay during atmospheric processing. Wang et al. (2018) included BrC bleaching utilizing a one-day photochemical lifetime and predicted a much lower global BrC DRE of +0.048 W m^{-2}. Another modeling study that included bleaching, but also the added effect of BrC enhancement above clouds (Zhang et al., 2017), found that this enhancement offset the bleaching of BrC on DRE (Zhang et al., 2020a). In these models, predictions are often assessed by comparison with BrC inferred from Aerosol Robotic

Network (AERONET) data, leading to substantial uncertainty (Schuster et al., 2016). The global-scale radiative impact of BrC is hard to assess due to the lack of BrC observations in the field and highly variable BrC properties that evolve following emissions.

1.3 Outline

The overarching goal of this dissertation is to gain a better understanding of sources, atmospheric evolution, and radiative effects of BrC aerosol. In this thesis, the following topics were investigated (1) the sources and direct radiative effect (DRE) of BrC aerosol on a global scale; (2) the characterization and evolution of relatively fresh BrC in aerosols from wildfires in the western US; (3) the development of an online BrC measurement system utilizing a set of mist chambers as the aerosol collection method and comparing this method with two similar systems based on the particle-into-liquid sampler (PILS).

Specifically, the remainder of this thesis has the following structure:

In Chapter 2, we conducted a global survey of BrC aerosol in an airborne study, Atmospheric Tomography Mission (ATom), which happened during 2016 to 2018. During ATom, the NASA DC-8 research aircraft sampled air across the globe, reaching near pole-to-pole along the central Pacific and Atlantic oceans during different seasons. Samples for BrC collected on this mission provided the first direct BrC measurement on a global scale. A radiative transfer model was run to estimate the radiative impact of this BrC.

Chapter 3 investigates BrC aerosol emitted from wildfires in the western US as a part of FIREX-AQ campaign in 2019. BrC from wildfires was measured with two methods: one based on aerosol liquid extracts with a spectrophotometer and a long path waveguide,

and the other used a photoacoustic spectrometer (PAS). This is the first comparison in a field study for these two methods, both of which have been used widely. The overall behavior of BrC level with transport time was examined, and multiple factors for cause of vairous trends were investigated.

In Chapter 4, we developed an online system for measuring water-soluble BrC with mist chambers to collect aerosols into water. Then, the light absorption by the sample was quantified in a long path liquid waveguide capillary cell (LWCC) when exposed to a broad wavelength (UV-Vis) light source. Together with this newly built system, two similar systems that followed similar detection methods, but with a PILS as the aerosol collection method, were deployed on separate research aircraft targeting wildfires as part of the FIREX-AQ and WE-CAN studies. Detection limits, baseline correction, and signal hysteresis are discussed and compared, and improvements to these water-based systems are provided.

Chapter 5 summarizes the findings in Chapters 2-4 and provides recommendations for future work.

CHAPTER 2. GLOBAL MEASUREMENTS OF BROWN CARBON AND ESTIMATED DIRECT RADIATIVE EFFECTS

2.1 Abstract

Brown carbon (BrC) is an organic aerosol material that preferentially absorbs light of shorter wavelengths. Global-scale radiative impacts of BrC have been difficult to assess due to the lack of BrC observational data. To address this, aerosol filters were continuously collected with near pole-to-pole latitudinal coverage over the Pacific and Atlantic basins in three seasons as part of the Atmospheric Tomography Mission. BrC chromophores in filter extracts were measured. We find that globally, BrC was highly spatially heterogeneous, mostly detected in air masses that had been transported from regions of extensive biomass burning. We calculate the average direct radiative effect due to BrC absorption accounted for approximately 7 to 48% of the top of the atmosphere clear sky instantaneous forcing by all absorbing carbonaceous aerosols in the remote atmosphere, indicating that BrC from biomass burning is an important component of the global radiative balance.

2.2 Introduction

Atmospheric aerosols affect the global radiative balance by scattering and absorbing radiation (Chýlek and Coakley, 1974). The main light absorbing component of aerosols is black carbon (BC) (Horvath, 1993; Bond and Bergstrom, 2006), however, some components of mineral dust (Sokolik and Toon, 1999) and organic aerosols (OA) also absorb visible light. Organic chromophores in aerosol particles are the least well

understood and are overall referred to as brown carbon (BrC) because they absorb most strongly in the UV and near-visible wavelengths, resulting in a brownish or yellow appearance.

One known major source for BrC are products of incomplete combustion of fossil and biomass fuels (Hoffer et al., 2006; Chen and Bond, 2010; Hecobian et al., 2010; Desyaterik et al., 2013; Zhang et al., 2013). The complex molecular structures of organic chromophores are challenging to exactly determine, although nitro-aromatic compounds have been identified in urban and biomass burning aerosols (Claeys et al., 2012; Lin et al., 2016). Other compounds, such as polycyclic aromatic hydrocarbon derivatives and polyphenols may contribute to aerosol light absorption properties as well (Lin et al., 2016). Field observations of wildfires in California (Forrister et al., 2015), the Amazon (Wang et al., 2016), and Crete (Wong et al., 2019b) have indicated that a large fraction of emitted BrC can be depleted over time by bleaching, with a half-life varying between 9 and 24 hours. However, studies show a small fraction of emitted chromophores of high molecular weight resist bleaching. Low molecular weight chromophores that rapidly bleach would then mainly contribute to BrC absorption near sources, while high molecular weight chromophores with longer lifetimes could continue to contribute to light absorption in aged biomass burning plumes over large spatial scales (Di Lorenzo and Young, 2016; Wong et al., 2017).

Estimation of the global aerosol direct radiative effects in past studies treated OA as wholly non-absorbing (Haywood and Boucher, 2000; Bellouin et al., 2005), whereas a variety of recent studies have attempted to estimate the global radiative impact of BrC. These studies are limited by incomplete knowledge of BrC sources, sinks, evolution, and

chemical composition-driven optical properties, and there is little data to assess model predictions. They estimate that the global average top of atmosphere (TOA) BrC direct radiative effect (DRE), which is its instantaneous radiative impact on the Earth's energy balance (Heald et al., 2014), ranges from +0.04 to +0.57 W m^{-2}, with BrC contributing from 20 to 40% of DRE from total carbonaceous absorbing aerosol (i.e., BC+BrC) (Feng et al., 2013; Lin et al., 2014; Saleh et al., 2015; Jo et al., 2016). These model simulations depend on parameterized BrC emissions, often based on the BC-to-OA ratio, or modified combustion efficiency (MCE) (Saleh et al., 2014; Jo et al., 2016). They also assumed an invariant (non-bleaching) BrC following emission. In contrast, Wang et al. (2018) included BrC bleaching utilizing a one-day photochemical lifetime and predicted a global BrC DRE of +0.048 W m^{-2} and a similar BrC contribution to DRE by all carbonaceous aerosol absorption (23%). Other modeling studies that included both bleaching and the added effect of BrC enhancement relative to BC with increasing altitude (Zhang et al., 2017), found that DRE due to upper troposphere BrC can largely offset BrC bleaching (Zhang et al., 2020a). Model skill has often been assessed by comparison with BrC inferred from AERONET data, but these data have substantial uncertainty themselves (Schuster et al., 2016). Global-scale data sets of measured BrC are needed for evaluation of model predictions and an assessment of its importance in the radiative balance. Here, the first estimates of BrC DRE and importance relative to BC, based on direct observational data over large spatial scales, is reported.

2.3 Method

2.3.1 The ATom Mission (Atmospheric Tomography Mission)

The NASA DC-8 aircraft conducted research flights nearly pole to pole along the central Pacific (north to south) and Atlantic (south to north) Oceans at altitudes systematically alternating from near surface (180 m) to ~13 km above sea level over four deployments, one in each season (see Table 2-1), (Prather et al., 2017). A map is shown in Figure 2-1. (BrC measurements were made in ATom-2, 3, and 4 deployments).

2.3.2 Filter Sampling, Extraction and Analysis

The particle filter sampling system and offline analysis was identical to that used in two previous studies on the DC-8, Studies of Emissions and Atmospheric Composition, Clouds and Climate Coupling by Regional Surveys (SEAC^{4}RS) and Deep Convective Clouds and Chemistry (DC3) and the method described in those publications (Liu et al., 2014; Forrister et al., 2015; Liu et al., 2015a; Zhang et al., 2017). Particles with aerodynamic diameter less than nominally 4.1 μm (McNaughton et al., 2007) were collected onto Teflon filters over all altitudes at intervals typically <5 minutes at altitudes below 3 km and a maximum of 15 minutes for higher altitudes. For all three missions, 1074 filters were collected and analyzed, including two or three blank filters per flight. Filters were extracted in water first and then methanol sequentially, and extracts were filtered by an in-line syringe filter to filter out insoluble compounds like BC. Light absorption spectra of the extract were measured with a spectrophotometer utilizing a 2.5 m long liquid waveguide. A schematic of the method is shown in Figure A-1, along with a more detailed description of the method. Light absorption coefficient of chromophores in solution was calculated following Hecobian et al. (2010). In the following, the absorption coefficient averaged between 360 and 370 nm (avg. 365 nm) was used as a measure of particle BrC levels; water-soluble BrC (WS BrC) was determined from Abs_{365nm} for water extracts,

while total BrC was the sum of Abs_{365nm} for water and methanol extraction. BrC Absorption Ångström Exponents (AAE; $Abs_\lambda = C \cdot \lambda^{-AAE}$) were also determined from the measured spectra (see Figure A-2 for example spectra). Note that all data presented here are at standard temperature and pressure (273K & 1013 mb), however, these are converted to ambient conditions for the radiative calculations discussed below.

Limit of detection (LOD) was determined by three times the standard deviation of field blank filters, combining all blanks from a given deployment (Table 2-1). (See also Figure A-3 for frequency distribution of all water-soluble BrC data relative to calculated LODs for each mission). In the following analysis we focus on only WS BrC due to high blanks associated with methanol extractions. BrC measurement uncertainty was calculated by propagating the uncertainties from sample collection to data analysis and is estimated at 20%, where the uncertainty associated with subtracting the blank contributed 40 to 60% of this overall estimate.

The light absorption measured in this study are largely by individual chromophores (molecules) dissolved in solution, not the absorption of suspended particulate. This technique was used since it exclusively measures BrC optical properties (BC is not included), resulting in a highly sensitive approach required for this remote atmosphere study, however when used for analysis of filters, the main limitation is blank variability, as noted above. Past studies, based on measured BrC aerosol size distributions and Mie theory, indicate that a multiplication factor of 1.8 to 2.1 (roughly 2±0.2, or ±10%) can be used to estimate the light absorption by aerosol particles based on measurements of chromophores in the bulk liquid extracts (Liu et al., 2013; Washenfelder et al., 2015; Zhang

et al., 2017; Shetty et al., 2019). We include this in the subsequent overall uncertainty analysis, which is discussed more below.

2.3.3 Other Measurements on the DC-8, Back Trajectories and Fire Events

Refractory black carbon (rBC, or just BC here) content of individual particles was measured with a single particle soot photometer (SP2). Integrated BC concentrations have been adjusted to account for accumulation-mode BC outside of the SP2's detection size range (Schwarz et al., 2008), and in-cloud measurements were removed based on cloud-probe data. In the following analysis, solvent-extracted BrC and SP2 BC are assumed to encompass all absorbing carbonaceous aerosols. Methanol has been shown to extract greater than 92% of BrC from laboratory-generated smoke (Chen and Bond, 2010), but other forms of light absorbing aerosols from wild fires may not be included in BrC by solvent extraction (Shetty et al., 2019), nor SP2 BC measurements, which would lead to our under-measuring carbonaceous aerosol absorption in this study (Adler et al., 2019). Aerosol scattering was derived from particle number size distributions for dry sizes between 2.7 nm to 4.8 μm in diameter which were measured at 1 Hz using a suite of particle counters (Brock et al., 2019). The NOAA Particle Analysis by Laser Mass Spectrometry (PALMS) instrument was used to assess both the relative contributions and mass concentrations of biomass burning sources to the ambient aerosol that encompasses particles of sizes between 0.1 and 4.8 μm (Froyd et al., 2019; Schill et al., 2020).

Airmass 72 hours back trajectories were computed using the Hybrid Single-Particle Lagrangian Integrated Trajectory (HYSPLIT) analysis method (Stein et al., 2015; Rolph et al., 2017). Locations and fire radiative power (FRP) of large biomass burning regions for

each ATom deployment were obtained from the Fire Information for Resource Management System (FIRMS, https://firms.modaps.eosdis.nasa.gov/map/). Only fires with FRP greater than 100 MW are included in the analysis. Air mass transport time from fire emissions to the point of aircraft sampling was estimated based on HYSPLIT back trajectories from the sampling location to the nearest FIRMS-identified wildfire intersected by the trajectory. Type of fuel, or other variables that may affect emissions, were not considered. More details are provided in APPENDIX A.2.

2.3.4 Radiative Impact of BrC

Radiative transfer calculations were performed with the Santa Barbara DISORT Atmospheric Radiative Transfer (SBDART) model (Ricchiazzi et al., 1998) to compute the direct short-wave (0.25-4 μm) radiative effect at the top of the atmosphere (TOA). Accuracy of the model is discussed by Obregón et al. (2015) and more details are described in Zhang et al. (2017). Estimates of aerosol scattering from dry aerosol size distributions, and measurements of BC and BrC collected during aircraft vertical profiling were used in the calculations. In-cloud data were excluded. Either for a complete ATom mission, or for a given geographical region, all vertical profile data were averaged (mean) and then used in the radiative calculation. The ambient aerosol scattering coefficient (b_{scat}) at multiple wavelengths was calculated with dry aerosol size distribution and measured temperature, pressure and relative humidity (RH) using κ-Köhler approximation for hygroscopic growth (Brock et al., 2016; Brock et al., 2019). Data were fitted with a power law ($b_{scat} = A \cdot \lambda^{-SAE}$, A is a constant and SAE is the scattering Ångström exponent), which was then used with light scattering data to determine the aerosol scattering over all wavelengths in the radiative forcing calculation. The light absorption coefficient for BC (b_{BC}) was calculated

from the measured BC mass concentration using a mass absorption cross-section (MAC) of 10.0 m^2 g^{-1} at 660 nm and AAE of 1 to compute absorption at other wavelengths. This is equivalent to a factor of 1.6 lensing effect due to BC coatings (i.e., for uncoated BC a MAC of 6.25 m^2 g^{-1} at 660 nm is typically used) (Zhang et al., 2017). If BC absorption is actually larger than this due to greater lensing effects, or AAEs > 1, we will overestimate the BrC contribution to radiative forcing. For BrC, measured absorption at 365 nm (Abs_{365nm}) and an AAE value of 5 (the average of the measured WS BrC AAE, discussed below), was used to compute absorption at all wavelengths (b_{BrC}).

The water-soluble light absorption data were converted to an overall aerosol BrC absorption coefficient by the combination of two factors. First, the factor to convert water-soluble BrC to total BrC in solution. Based on our data (Table 2-1), the ratio of WS BrC to total BrC for all ATom data is 53%±17%. Other studies have reported the WS BrC to total BrC ratio for aged aerosols to be in the range of 25% to 80% (Chen and Bond, 2010; Zhang et al., 2013; Liu et al., 2015a; Phillips and Smith, 2017; Wong et al., 2017; Satish and Rastogi, 2019; Shetty et al., 2019). Here we assume the ratio is 0.5 with ±40% uncertainty, meaning the WS BrC is multiplied by 2 (±40% uncertainty) to estimate the contribution of all chromophores to BrC. We then convert the chromophores absorption to an aerosol light absorption coefficient. This factor depends on the particle size distribution of BrC, which is, as discussed in Section 2.3.2, estimated to be a factor of 2 ± 0.2 (10%), meaning the overall conversion factor is 4. More recent simultaneous measurements in smoke plumes of aerosol absorption with a photoacoustic instrument and the same BrC filter sampling system utilized here show an overall conversion ratio of 3.21 (R^2=0.84) for WS BrC to aerosol absorption at a wavelength of 405 nm, consistent with the factor of 4 here,

considering uncertainly (see Figure A-4). Including the uncertainty in BrC measurement of 20% (discussed above), we estimate the overall BrC aerosol light absorption coefficient determined by this method has an uncertainty of ±46%.

To parse out the various aerosol contributions to TOA radiative effects, we performed 3 SBDART runs to determine: (1) DRE due to only scattering; (2) DRE due to scattering and BC absorption; (3) DRE due to scattering, BC absorption and BrC absorption. We estimated the DRE of BC by subtracting (1) from (2), and the DRE of BrC by subtracting (2) from (3). More model details are provided in the APPENDIX A.3.

2.4 Results and Discussion

2.4.1 Global Distribution of Fires and BrC

BrC measured in ATom-2, 3 and 4 is shown in Figure 2-1, along with air mass back trajectories for those regions where WS BrC was above the LOD. Locations of burning are shown with indicated fire radiative power (FRP), for fires with FRP >100 MW. We find that WS BrC was very low over vast areas (also see Table 2-1), however, there were regions of significant WS BrC; these include the mid-Atlantic Ocean, northern Pacific Ocean, and southern Pacific Ocean near islands in Oceania (Australia, New Zealand, etc.).

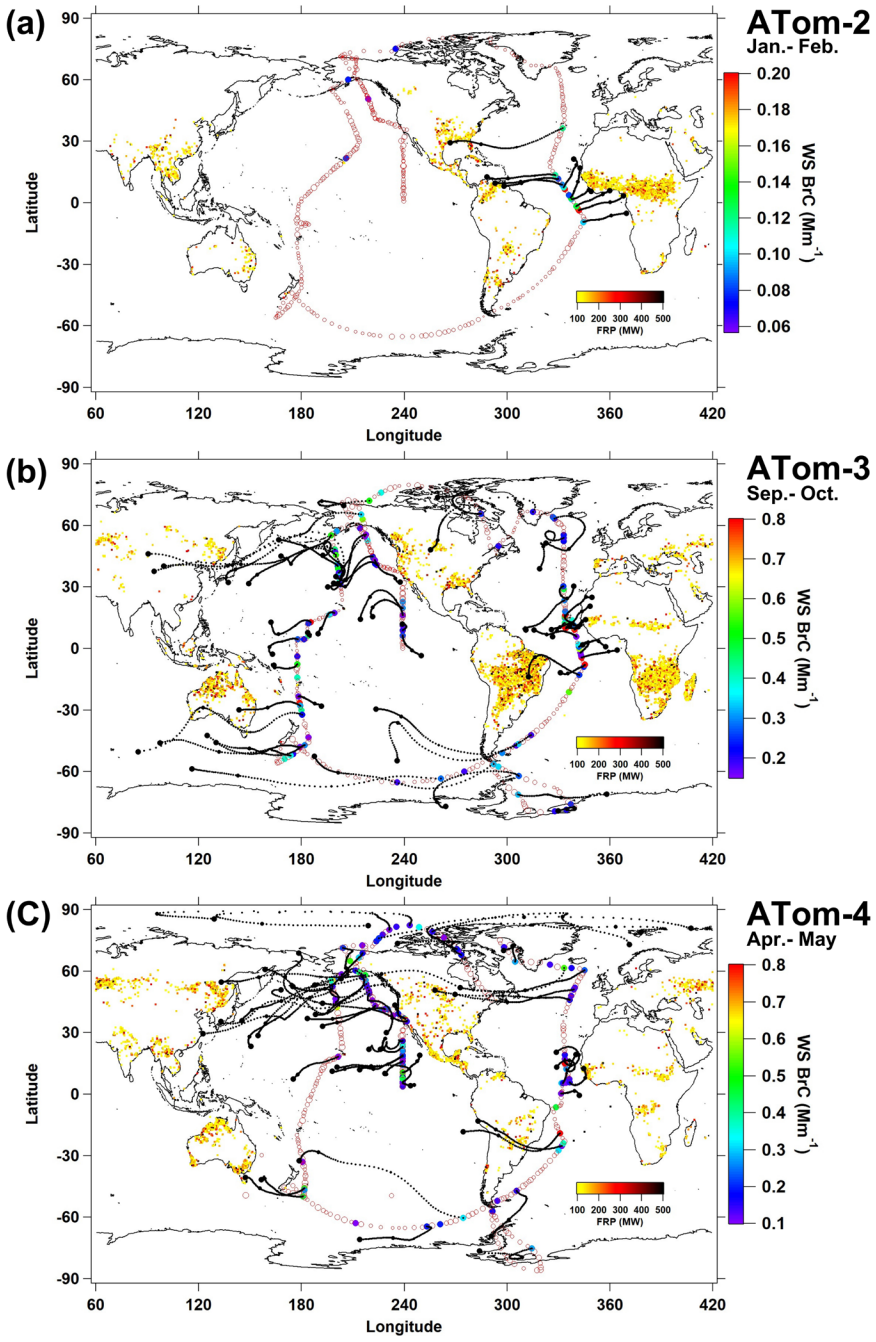

Figure 2-1 Water-soluble (WS) BrC (Absorption coefficient at 365 nm) global distribution measured in ATom-2 (a), ATom-3 (b), and ATom-4 (c). Filled circles are colored by the magnitude of WS BrC for data above the LOD and open circles represent data below the LOD, sized by relative magnitude. Fire dots with greater than 100 MW fire radiative power (FRP) are colored by FRP magnitude in all plots. HYSPLIT air mass back trajectories are shown for up to 72 hours, where black dots indicate locations every 24 hours.

Table 2-1 ATom data summary. BrC absorption data are for only water-soluble species.

	ATom-2	ATom-3	ATom-4
Deployment dates	26 Jan. to 21 Feb. 2017	8 Sept. to 27 Oct. 2017	24 Apr. to 21 May 2018
BrC LOD, Mm^{-1}	0.05	0.15	0.10
% of filters above LOD	5.1	28.4	27.3
BrC Mean: Data below LOD set to ½ LOD, Mm^{-1}	0.003	0.172	0.099
BrC Median: No adjustment for below LOD (Median for only data above LOD), Mm^{-1}	-0.001 (0.098)	0.066 (0.276)	0.042 (0.172)
Water−soluble BrC to Total BrC Ratio	N.A.	57%±17%	50%±16%
AAE mean: wavelength ranges from 300 to 500 nm	4.1	4.3	6.5
Number of FIRMS identified fire counts with FRP greater than 100 MW globally	13,905	33,070	18,408
BrC mean DRE, (BrC set to zero for data below LOD), W m^{-2}	+0.033 (+0.01)	+0.29 (+0.25)	+0.15 (+0.11)
BC mean DRE, W m^{-2}	+0.11	+0.31	+0.17
Scattering Mean DRE, W m^{-2}	-8.07	-17.02	-8.99

To estimate corresponding aerosol absorption coefficients, liquid absorption coefficients should be multiplied by a factor of 1.8 to 2 (see text). The Direct Radiative Effect (DRE) was based on total-soluble BrC, which is a factor of ~2 greater than WS BrC (see WS BrC/Total BrC row above).

In the tropical mid-Atlantic region, enhanced levels of WS BrC were recorded in all three missions. FIRMS-identified wildfires and back trajectories suggest that the BrC source for this region was either fires in South America or Africa. In ATom-2 (Jan.-Feb.), most fires were in equatorial regions in northern South America and Africa, coinciding

with the dry period for these regions (Jan.-Apr.). These measurements accounted for a majority of the observed BrC above LOD for the complete ATom-2 mission. During ATom-3 (Sept.-Oct.), the fires in South America were found further south, following the movement of dryer regions southward, dictated by the annual movement of the Inter-Tropical Convergence Zone. Compared to ATom-2, the wildfires were also more extensive in ATom-3 in terms of both fire density and radiative power (FRP). In the last mission, ATom-4 (Apr.-May), the extent of fires in these regions decreased to the lowest levels relative to the ATom-2 and 3 missions. Levels of BrC recorded in the mid-Atlantic tracked these seasonal trends.

For the North Pacific Basin in Figure 2-1, WS BrC was observed in ATom-3 and 4 and back trajectories indicated that the BrC was from northeastern China, but occasionally from fires in western North America. Nearly no WS BrC was above the LOD in ATom-2 in this region, which could be due to differences in emissions and transport with season. BrC from biofuels or other forms of incomplete combustion may also contribute, but would not be evident from the FRP data. For the tropical mid-Pacific Ocean (Figure 2-1), BrC above LOD was only observed in ATom-3 and 4, possibly from scattered islands in the region, such as Hawaii. In the south Pacific, BrC was observed downwind of Indonesia, Australia and New Zealand (Oceania), mainly during ATom-3, suggesting it was also highly seasonal. For example, the Oceania region fire counts with FRP greater than 100 MW during ATom-2 was 419, while there were 6721 and 3749 counts during ATom-3 and 4, respectively. BrC was occasionally above LOD when sampling near or within polar regions (Antarctic and Arctic) during ATom-3 and 4, where back trajectories show the air masses were mainly from high latitude regions, although it was difficult to locate specific

sources for this region. BrC in polar regions may persist longer due to low sunlight limiting BrC photochemical bleaching.

As can be seen in Figure 2-1, the number of fire events identified from FIRMS varied significantly with region and season (i.e., ATom deployment). In general, trends of fire counts and levels of WS BrC were similar; highest fire counts were mainly seen in ATom-3 and highest BrC levels were generally recorded in that mission (Table 2-1). However, significant scatter in this relationship can be expected since the aircraft did not necessarily sample plumes from all fires identified by FIRMS and there are uncertainties in both WS BrC and fire events identified by MODIS (Schroeder et al., 2008). Overall, we conclude that biomass burning appears to be the predominant source for BrC in the remote atmosphere since most regions of recorded BrC could be traced to a burning region, and we also found regions where measured BrC<LOD did not intercept burning regions, see Figure A-5. Given that the smoke plumes were transported over great distances (>10,000 km), some portion of the fire-emitted BrC persisted for at least 3 days, the limit of our back trajectory analysis, consistent with laboratory studies that high molecular weight BrC species resist photobleaching (Di Lorenzo and Young, 2016; Wong et al., 2017).

2.4.2 BrC Correlation with BC

Correlations provide further evidence that the BrC was mainly associated with biomass burning. Biomass burning emits BC and BrC, although there are differences in emissions rates depending on fuel and burning temperature, and how these species may be altered with atmospheric age. More BrC is emitted per unit mass of fuel burned in smoldering compared to flaming fires (Chakrabarty et al., 2016), whereas more BC is

emitted in flaming than smoldering (Echalar et al., 1995). Some fraction of BrC will bleach over time, whereas BC is chemically stable, and only undergoes removal from the air with an estimated lifetime of about <5 to 10 days globally (Cooke and Wilson, 1996; Koch et al., 2009; Lund et al., 2018). Also, there is evidence that BrC is lofted to higher altitudes by convection more efficiently than BC (Zhang et al., 2017), (which was also observed in ATom as an increasing ratio of BrC to BC with increasing altitude, Figure A-9), thus some scatter between BrC and BC is expected even if both are emitted from wild fires in a given region. The Pearson correlation (R) between BrC and BC was 0.86, 0.75 and 0.53 for Atom-2, 3 and 4, respectively (for scatter plots, see Figure A-6, also see Table A-1). Despite high correlations, there is significant variability at lower levels, suggesting that BC cannot solely be used to infer BrC optical effects. Data with moderate to low WS BrC, but very low BC, were mostly observed at higher altitudes (>9 km), possibly due to differences in advection of these species through clouds (Zhang et al., 2017), whereas periods (filter samples), that contained moderate to low BC, but very low WS BrC were mainly found in the mid-Atlantic Ocean region. Causes may be different burning conditions (smoldering/flaming) and processing during transport.

Comparing amongst separate ATom missions, the highest correlation between BrC and BC was found in ATom-2 (0.86); the correlation was weaker in ATom-3 (0.75) and lowest in ATom-4 (0.53). A similar, although somewhat stronger correlation trend was found for BrC vs. estimated biomass burning potassium (K^+_{BB}), and between K^+_{BB} vs. BC (see Table A-1 and supplemental material discussion for calculation of K^+_{BB}). The trend was also seen in BrC and the PALMS estimate of biomass burning particle mass (See Figure A-6). A possible explanation is BrC observed in ATom-2 was mainly from two

concentrated regions of burning (see Figure 2-1a), whereas in ATom-3 and 4, data were from fires located in different geographic regions. Thus, although the total impact of fires may be higher for ATom-3 and 4, the characteristics of the emissions and effects during transport might be broader and more complex, which weakened the correlations.

2.4.3 Direct Radiative Effect of BrC Aerosol

Light absorption over the full spectral wavelength range is necessary to simulate the radiative impact of BrC aerosol. As noted in the Methods, we use a constant BrC AAE of 5, the mean for all missions. For the three ATom missions, AAE values ranged from 2.5 to 8.6 (10^{th} and 90^{th} percentile) and the mean AAE was similar for ATom-2 and 3, but higher for ATom-4 (Table 2-1). No geographical dependence for AAE was observed, but higher AAE values were always found at high altitude or near the surface. The cause for variability in AAEs is not clear but adds uncertainty to model predictions of radiative effect, which we include in the overall estimated uncertainty.

A summary of the radiative calculations is shown in Figure 2-2, where we compare averages for each ATom mission for different groups of data. (DREs of each aerosol component for various latitudes ranges can be found in Table A-2). Figure 2-2a shows the DRE for scattering, and BC and BrC absorption, for data in which the measured WS BrC was above the LOD. For just these data, BrC accounted for 19 to 59% of the carbonaceous aerosol absorption instantaneous forcing, and carbonaceous aerosol absorption DRE offset total light scattering DRE by ~5%. These are periods (BrC>LOD) of sampling in plumes of fairly strong biomass burning influence, as confirmed by the PALMS tracer analysis; for the three ATom missions when BrC>LOD, median contribution of biomass burning to

aerosol mass was 30% and median aerosol mass from biomass burning was 0.24 µg m^{-3}. This contrasts with periods when BrC<LOD shown in Figure 2-2b, where the magnitudes of the TOA DRE was much smaller for scattering and absorption (contrast scales in Figure 2-2a and 2b). Based on the PALMS data, for these periods only 8% of the aerosol mass was from biomass burning and the concentration median was 0.03 µg m^{-3} (see bar and whisker plot in Figure A-7). BC concentration followed a similar trend, BC was substantially higher when BrC>LOD (i.e, periods of smoke sampling), especially in ATom-2 (Figure A-8).

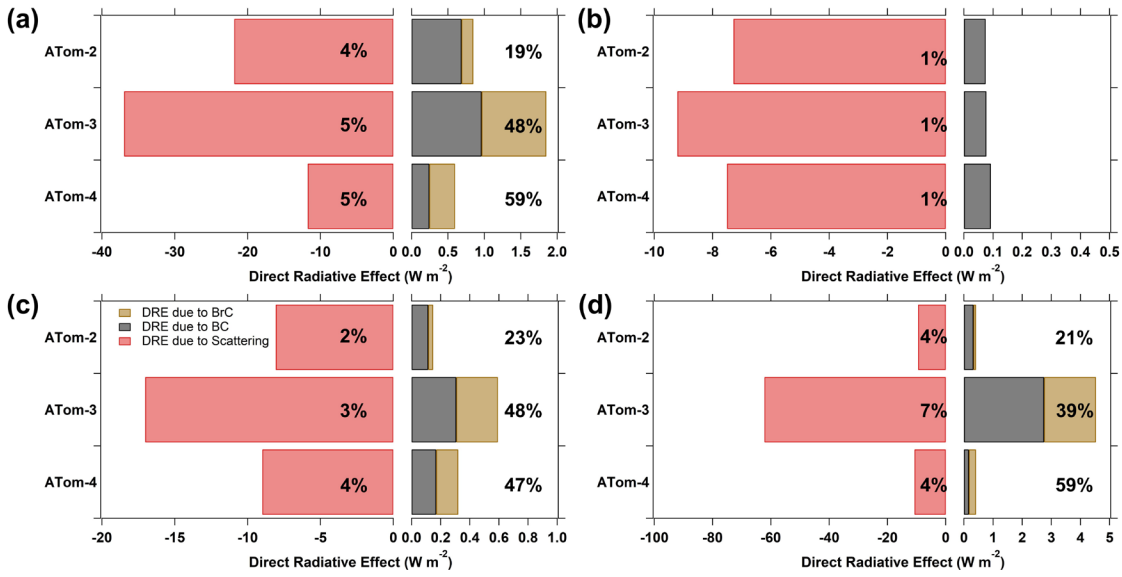

Figure 2-2 Instantaneous clear-sky DRE at the top of atmosphere (TOA) computed with ATom data (a) for the average of each ATom mission when BrC data are above LOD, (b) average of each ATom mission when BrC data are below LOD, (c) global average of each ATom mission for all data with BrC < LOD set to ½ LOD, and (d) just for data in the mid-Atlantic (see Figure 2-1). The percentages shown in the scattering bar are the fraction of DRE due to carbonaceous aerosol absorption relative to scattering, Abs(BC+BrC)/Scat., and the percentages shown to the right of the bar are the fraction of DRE due to BrC of all carbonaceous absorbing species, Abs(BrC)/Abs(BC+BrC). Note the scale changes at the point zero since aerosol scattering dominates TOA DRE in remote regions.

The average DRE for each mission was also calculated. Figure 2-2c shows the mean instantaneous DRE at TOA that includes all data, and where BrC < LOD was set to ½ LOD. The ratio of averaged DRE due to BrC was 44% of the averaged total light absorption by carbonaceous aerosols among three ATom missions. The mission average was 38% when BrC set equal to 0 for BrC<LOD, (not plotted). The mean results are similar to those periods of BrC>LOD (Figure 2-2a) since the mean is dominated by the higher magnitude values. Figure 2-2d gives the DRE results for smoke detected in just the mid-tropical Atlantic, and Table A-2 summarizes results from other latitude ranges. These data show that the BrC contribution can be substantial, but with significant variation, ranging from 21% to 59% of the total carbonaceous absorption DRE for the three ATom missions.

The fraction of carbonaceous aerosol DRE due to BrC for these data are similar to or surpasses the high end of the range reported by other studies (Feng et al., 2013; Saleh et al., 2014; Lin et al., 2015b; Jo et al., 2016; Wang et al., 2016; Zhang et al., 2020a). A possible reason is the models are truly global averages, whereas this is data only from where the aircraft sampled. Another possible reason is the sensitivity of DRE to the vertical distribution of BrC and BC, which most modeling studies may not correctly simulate. Throughout this study, BC was mainly found from near the surface to mid altitudes, whereas BrC was observed to decrease less slowly with altitude compared to BC, resulting in increasing BrC/BC with altitude (Figure A-9), as has been seen in continental aerosols (Liu et al., 2014).

The approach used to investigate BrC based on dissolving aerosol in a solvent and measuring the molecular chromophores exclusive of BC generally has higher sensitivity than instrumentation that measures aerosol light absorption without altering the particle,

such as the multiwavelength photoacoustic measurement. Even so, the majority of samples in the remote atmosphere were below detection limit using the solvent method. However, measuring dissolved chromophores and then estimating aerosol optical effects introduces uncertainty, as discussed in the Methods section. Sensitivity tests indicate there is nearly a 1:1 correspondence between the change in BrC absorption coefficient and its DRE, implying the uncertainty in BrC TOA DRE is roughly ± 45%, similar to the overall BrC absorption coefficient uncertainty at 365nm. The use of a constant BrC AAE of 5, based on the average of all ATom data, also adds uncertainty to the DRE; the mean DRE due to BrC increases by about 10% for a BrC AAE of 3 instead of 5 and decreases by about 30% for an AAE of 7. Combining these uncertainties, we estimate the overall uncertainty in BrC DRE is roughly 50%. Assuming the uncertainty of DRE due to BC is significantly smaller, the fraction of BrC DRE to total carbonaceous DRE is estimated to be 7 to 23% for ATom-2, 45 to 48% for ATom-3, and 39 to 47% for ATom-4 (range for setting BrC below LOD to zero or ½ LOD) with ±24% uncertainty.

In summary, the smoldering combustion of wildfires is known to be a significant source of BrC. We find on a global scale, based on the regions measured during ATom-2, 3 and 4 deployments (Jan./Feb., Sept./Oct., Apr./May), that measurable amounts of BrC were associated with tracers of smoke such as BC, potassium, and PALMS single particle composition. Such smoke contained variable amounts of BrC, which was often detected great distances from the burning regions (greater than 10,000 km), persisting for more than 3 days following emissions. This BrC made a significant contribution to the overall absorption by carbonaceous aerosols and the top of atmospheric direct radiative effect, however the spatial distribution of the BrC forcing was highly heterogeneous.

CHAPTER 3. CHARACTERISTICS AND EVOLUTION OF BROWN CARBON IN WESTERN UNITED STATES WILDFIRES

3.1 Abstract

Brown carbon (BrC) aerosol material in western United States wildfires was measured between Jul. and Aug. 2019 from the NASA DC-8 research aircraft during the Fire Influence on Regional to Global Environments and Air Quality (FIREX-AQ) study. Two BrC measurement methods are investigated: highly spectrally-resolved light absorption in solvent extracts of particles collected on filters (water and methanol), and in situ bulk aerosol light absorption measured at three wavelengths (405, 532, 664nm) with a photo acoustic spectrometer (PAS). A light absorption closure analysis for wavelengths between 300 and 700 nm was performed. The combined light absorption of aerosol pure black carbon material including enhancements due to internally mixed materials, plus soluble BrC and a Mie-predicted factor for conversion of soluble BrC to aerosol particle BrC, was compared to absorption spectra from a power law fit to the three PAS wavelengths. At a wavelength of roughly 400 nm they agreed, at lower wavelengths the individual component-predicted particle light absorption significantly exceeded the PAS and at higher wavelengths the PAS absorption was consistently higher, but more variable. Limitations with extrapolation of PAS data to wavelengths below 405 nm and missing BrC species of low solubility that more strongly absorb at higher wavelengths may account for the differences. Based on measurements closest to fires, the emission ratio of PAS measured BrC at 405 nm relative to CO was on average 0.131 Mm^{-1} $ppbv^{-1}$, emission ratios for soluble BrC are also provided. As the smoke moved away from the burning regions the

evolution over time of BrC was observed to be highly complex; BrC enhancement, depletion, or constant levels with age were all observed in the first 8 hours after emission in different plumes. Within 8 hours following emissions, 4-nitrocatechol, a well characterized BrC chromophore commonly found in smoke, was largely depleted relative to the bulk BrC. In a descending plume where temperature increased by 15 K, 4-nitrochatehol and bulk organic aerosol dropped, but bulk BrC remained largely unchanged. Evidence was found for reactions with ozone as a pathway for secondary formation of BrC under both low and high oxides of nitrogen (NOx) conditions, while BrC was also observed to be bleached in regions of higher ozone and low NOx, consistent with complex behaviors of BrC observed in laboratory studies. Although the evolution of smoke in the first hours following emission is highly variable, a limited number of measurements of more aged smoke (15 to 30 hours) indicate a net loss of BrC. Whether insight into processes that affect BrC in smoke relatively near fires provides information on the characteristics of smoke over longer time and spatial scales, where its environmental impacts are likely to be greater, is yet to be determined.

3.2 Introduction

Open biomass burning, which includes wildfires and prescribed burning, emits massive quantities of trace gases and aerosol particles into the atmosphere (Andreae, 2019). In the US, wildfires account for a large burned areas (Kolden, 2019) and are increasing in frequency, especially in western regions (Burke et al., 2021). While wildfires can be beneficial to certain ecosystems (Thompson et al., 2011), aerosol particles produced from wildfires pose a substantial health threat (Akimoto, 2003; Regalado et al., 2006; Laumbach and Kipen, 2012; Fang et al., 2016; Chen et al., 2017); wildfire smoke may be more toxic

than other sources of aerosol particles, in terms of adverse respiratory impacts (Aguilera et al., 2021) and exposure can increase susceptibility to other respiratory hazards (Zhou et al., 2021). Smoke aerosol particles also produce observable optical effects and influence the planetary radiation balance (Zhang et al., 2020a). However, wildfire smoke impacts are highly complex. Following emissions, both the toxicity and optical properties substantially change as the particles undergo atmospheric processing (Forrister et al., 2015; Wong et al., 2019a; Kleinman et al., 2020). Because the atmospheric lifetime of fine aerosol particles can range from about 5 to 30 days (Williams et al., 2002; Kristiansen et al., 2016), wildfire particles can have substantial environmental impacts over local, regional, and global-scales (O'Dell et al., 2021).

By mass, particles emitted from wildfires are mainly carbonaceous, such as black carbon (BC) and organic aerosol (OA) species. Unlike most of OA that predominately scatters light (i.e., imaginary part of the complex refractive index is near zero), a small mass fraction of the OA absorbs light. For these species, the spectral light absorption is characterized by increasing absorption with decreasing wavelength, resulting in a yellow or brown appearance, and is hence referred to as brown carbon (BrC). Globally, biomass burning is likely the predominant source of BrC (Zeng et al., 2020), with lesser contributions from incomplete combustion of bio- (Saleh et al., 2015; Lei et al., 2018) and fossil-fuels (Healy et al., 2015; Olson et al., 2015). BrC is chemically complex and, unlike BC, unstable. Saleh (2020) has proposed a framework to help reduce this complexity by grouping BrC into four broad categories that lie on a continuum from very weakly absorbing (VW-BrC), through weakly absorbing (W-BrC) and moderately absorbing (M-BrC), then up to strongly absorbing (S-BrC) where the BrC has optical and physical

properties approaching those of BC (Adler et al., 2019; Cheng et al., 2021) (see Figure 3-3). These classifications separate BrC by sources and characteristics such as molecular weight, volatility and solubility. By this method, all the characteristics are delineated by the BrC light absorption wavelength dependence (Absorption Angstrom Exponent; AAE) and mass absorption cross-section (MAC) or imaginary part of the complex component (k) of the refractive index at a specific wavelength (e.g., 405 nm or 550 nm).

Characterizing BrC can provide greater insight on the environmental effects of wildfire emissions. Estimates from early model simulations suggest that BrC is a non-negligible warming agent (Feng et al., 2013; Saleh et al., 2015; Wang et al., 2018). Pole-to-pole BrC measurements through the Atlantic and Pacific Basins showed that for the regions where measurements were made, BrC contributed in the range of 7 to 48% to the top of atmosphere direct radiative effect (DRE) relative to all light absorbing carbonaceous particles (BC+BrC), and that most of the BrC was from biomass burning emissions transported over long distances (> 1,000's of km) (Zeng et al., 2020). Measurements have also shown that the prevalence of BrC relative to BC increases in the atmospheric column with increasing altitude, especially in the range of about 5 to 13 km (Liu et al., 2014), possibly due to differences in cloud processing of BrC versus BC (Zhang et al., 2017). Including differences in atmospheric column BrC and BC distributions in a global simulation predicted that BrC, largely from biomass burning, globally accounted for more than 25% of the DRE compared to BC, and atmospheric heating in the tropical mid- and upper-troposphere due to BrC was larger than BC (Zhang et al., 2020a). BrC may also reduce the ultraviolet actinic flux sufficiently to affect atmospheric photochemical reactions (Jo et al., 2016; Mok et al., 2016; Dasari et al., 2019). In terms of toxicity, BrC

has been found to often correlate with aerosol oxidative potential (Verma et al., 2015), which has been linked to adverse cardiorespiratory effects (Bates et al., 2019). By slowing the photochemical aging processes of pollutants, such as heavy metals or other organic compounds, BrC could increase the dispersion of co-emitted carcinogenic compounds (Shrivastava et al., 2017).

Molecular level characterization of BrC particles provides insights on optical properties, formation and scavenging mechanisms, and toxicity. In early studies, nitroaromatic compounds were identified as BrC chromophores in particles from incomplete combustion, including biomass burning emissions (Claeys et al., 2012; Lin et al., 2016). Not only do they absorb light, nitroaromatic species are known to be highly toxic (Bandowe and Meusel, 2017; Tian et al., 2020). Zhang et al. (2013) reported eight nitro-aromatic chromophores in urban ambient aerosols accounting for only ~4% of the light absorption at 365 nm wavelength, whereas Desyaterik et al. (2013) found that these same compounds comprised approximately 50% of BrC in cloud water samples influenced by agricultural burning events. 4-nitrophenol, 4-nitrocatechol, and their derivatives, are now commonly identified BrC species (Bluvshtein et al., 2017; Hems and Abbatt, 2018); other identified chromophores, include a range of PAH derivatives and polyphenols that span wide molecular weights and structures (Lin et al., 2016). Species with carbonyl functional groups are a common feature of BrC chromophores (Laskin et al., 2015; Lin et al., 2015a; De Haan et al., 2017). Evidence suggests that strongly absorbing chromophores comprise a small mass fraction of OA in biomass burning smoke, but dominate the overall BrC absorption (Nguyen et al., 2012; Laskin et al., 2014).

BrC is similar to the overall OA in that it can be directly emitted (primary BrC). A fraction of BrC is semi-volatile (Jai Devi et al., 2016) and may be a component of the secondary organic aerosol (SOA). This secondary BrC can be formed from a range of species and processes, such as reactions between ozone (O_3) or the hydroxyl (OH) or nitrate (NO_3) radicals with aromatic VOCs (Lee et al., 2014; Jiang et al., 2019; Fan et al., 2020), aqueous reactions involving carbonyl function groups with ammonium sulfate or polycyclic aromatic hydrocarbons (PAHs) with illumination (Nguyen et al., 2012; Haynes et al., 2019), and heterogeneous reactions of isoprene on acidic particles (Limbeck et al., 2003).

Laboratory studies demonstrate that the behavior of freshly-formed BrC is highly complex, where soon after emission both photo-enhancement and photobleaching can occur. Table 3-1 provides a brief summary of processes that can affect BrC once emitted by a fire, here we highlight only a few studies amongst many; a number of detailed review articles provide more details (Laskin et al., 2015; Moise et al., 2015; Yan et al., 2018). Zhong and Jang (2014) tracked the light absorption coefficient of ambient aerosols from biomass burning smoke captured in an outdoor smog chamber (with exposure to ambient light), finding the BrC mass absorption coefficient increased in the morning and gradually decreased thereafter. Similar behaviors were observed for aqueous phase BrC from laboratory-generated biomass burning aerosols exposed to UV light and reactions with the OH radical (Zhao et al., 2015; Wong et al., 2017; Wong et al., 2019b). Functionalization of nitrophenol molecules through oxidation by aqueous OH radicals and fragmentation of aromatic structures to smaller oxygenated molecules by direct photolysis was observed to first produce a photo enhancement, followed by photobleaching (Hems and Abbatt, 2018).

Oxidation by O_3 has also been observed to bleach BrC (Sareen et al., 2013; Fan et al., 2020), but BrC absorption can also increase at the beginning of the O_3 oxidation process (Kuang and Shang, 2020). Chemical processing of individual chromophores has also been studied. Light absorption of 4-Nitrocatechol exhibited a wavelength dependent change; a decrease in absorption between wavelengths of 300 and 380 nm and an increase in absorption below 300 nm or above 380 nm with increasing illumination time (Zhao et al., 2015). Reactions with the NO_3 radical produced nitrated organics, such as nitroaromatics, that contributed to aerosol particle BrC (Bluvshtein et al., 2017; Lin et al., 2017; Jiang et al., 2019; Li et al., 2020; Mayorga et al., 2021).

The atmospheric fate of BrC is not well understood, yet this greatly affects its environmental impacts. In laboratory studies, time scales for significant bleaching of secondary BrC are on the order of minutes to several hours to days (Bluvshtein et al., 2017; Lin et al., 2017; Jiang et al., 2019; Li et al., 2020; Mayorga et al., 2021), but atmospheric observations from wildfires show more complex behaviors. For relatively fresh smoke, Palm et al. (2020) conclude that a balance between dilution-driven evaporation of primary wildfire smoke chromophores and formation of secondary BrC led to the observation in nine fire plumes of a near-constant level of light absorption by BrC for smoke up to at least 6 hours old. Wu et al. (2021) found that smoke from West-African prescribed fires that started with minor levels of BrC, but were rich in BC, had continual increases in BrC with plume age for up to 12 hours. Studies tracking smoke over longer time scales have shown an overall loss of BrC, with a BrC characteristic lifetime (e.g., e-folding lifetime) ranging from ~10 hours to days (Forrister et al., 2015; Wang et al., 2016). Some fraction of BrC is very resistant to losses, allowing it to persist and become widely dispersed (Kieber et al.,

2006; Hecobian et al., 2010; Liu et al., 2015a; Washenfelder et al., 2015; Selimovic et al., 2020; Zeng et al., 2020). The longer-term stability of BrC may depend largely on the molecular weight of the chromophores. Laboratory studies show that low molecular weight chromophores tend to by rapidly bleached, whereas high molecular weight BrC species were more recalcitrant and their relative contribution to overall BrC increased as the particles aged (Di Lorenzo et al., 2017; Wong et al., 2017; Wong et al., 2019b). Overall, both field and laboratory studies show that the evolution of BrC from wildfire smoke is highly complex with many competing processes that may produce widely different smoke evolution behaviors in the regions relatively near the fires.

Table 3-1 Summary of processes that produce (enhancement) or remove (bleaching) BrC following emission, which includes competing processes that result in BrC formation (photo-enhancement) and loss (photo-bleaching, dilution-driven evaporation of chromophores).

Mechanism	Fate	Reference
Reaction with OH, O_3 or direct photolysis	Bleaching/enhancement typically first enhancement and then bleaching	Zhong and Jang (2014); Zhao et al. (2015); Wong et al. (2017); Browne et al. (2019); Fan et al. (2020); Fleming et al. (2020); Harrison et al. (2020); Schnitzler et al. (2020)
Aqueous reaction involving or forming carbonyl compounds	Enhancement	Nguyen et al. (2013); Powelson et al. (2014); Kasthuriarachchi et al. (2020)
High NOx, NO_3, associating with night chemistry	Enhancement	Lin et al. (2017); Jiang et al. (2019); Cheng et al. (2020); Li et al. (2020); He et al. (2021); Mayorga et al. (2021)
Dilution-driven evaporation	Bleaching	Palm et al. (2020)

To gain a better understanding of the emissions from wildfires and their evolution within the first hours, airborne measurements were conducted as a part of NASA/NOAA Fire Influence on Regional to Global Environments and Air Quality (FIREX-AQ). The study focused on open biomass burning in the western US in the summer of 2019 (22 Jul. 2019 – 17 Aug. 2019). Here, we report mainly on the characteristics and evolution of BrC chromophores based on a sequential solvent (water, then methanol) extraction method with liquid spectrophotometric measurements and aerosol particle BrC inferred from a photoacoustic spectrometer (PAS).

3.3 Method

3.3.1 Campaign

The FIREX-AQ study of 2019 included measurements from the NASA DC-8 aircraft, two NOAA Twin Otter (FIREX-CHEM and FIREX-MET) aircraft, and additionally, two ground-based Mobile Laboratories. Broad details of the campaign implementation and payload, including the large suite of gas and particle instruments, are provided in the FIREX-AQ white paper (https://www.esrl.noaa.gov/csl/projects/firex-aq/whitepaper.pdf). In the following, we focus on data collected from the NASA DC-8 research aircraft in wildfire smoke.

3.3.2 Instrumentation

3.3.2.1 Light absorption measurements

Two methods were used to determine BrC in this study, an off-line filter-based approach and in situ measurements from a photoacoustic spectrometer (PAS). Following a

number of past studies (Liu et al., 2014; Liu et al., 2015a; Zeng et al., 2020), the light absorption of soluble BrC species (an operationally defined parameter) was measured by a liquid-based spectrophotometric method on solvent extracts of filters. A similar approach was used on a newly developed online mist chamber particle collection system deployed for the first time in this study (Zeng et al., 2021). The spectrometer (USB-4000, Ocean Optics, Dunedin, FL) was coupled with a Long-path Waveguide Capillary Cell (2.5 m optical path; LWCC-3250; World Precision Instruments, Sarasota, FL) and a broadband UV-VIS-NR light source (DH-mini; Ocean Optics, Dunedin, FL). Detailed operating procedures and data processing are described elsewhere (Zeng et al., 2021). Here we only focus on the filter data. Briefly, aerosol particles with aerodynamic diameter less than 4.1 μm were collected onto Teflon filters, which, at a later date, were extracted sequentially, first with water, then after air drying, with methanol. In each case, the resulting liquid extract was filtered (0.22 μm pore size syringe filter) and then injected into the LWCC via a syringe pump. The absorption spectra over wavelengths from 300 to 700 nm at ~1 nm resolution was recorded relative to that of the pure solvent, producing the light absorption spectra of water-soluble (WS) and methanol-soluble (MS) chromophores of species in the ambient aerosol particles. Light absorption measured in the waveguide (A_λ) is converted to an ambient aerosol light absorption coefficient (Abs_λ^{LWCC}) by:

$$Abs_\lambda^{LWCC} = A_\lambda \frac{V_l}{V_a \cdot l} \ln(10) \quad (1)$$

where V_a is the volume of air that passed through the filter, V_l is the volume of solvent used in the extraction, and l is the optical path length (nominally 2.5 m). The total-soluble (TS) light absorption measurement is defined here as the sum of the light absorption coefficients at each wavelength measured from the WS and MS extracts ($Abs_{TS,\lambda}^{LWCC} = Abs_{WS,\lambda}^{LWCC} + Abs_{MS,\lambda}^{LWCC}$), as sequential extraction has been shown to be comparable to methanol extraction alone (Liu et al., 2015a). (Note that water then methanol measurements of BrC were done to provide both WS and total BrC data, since some instruments are only capable of WS BrC measurements, e.g., online systems (Zeng at al., 2021)). As will be discussed, this extraction does not necessarily account for all of the BrC, since some chromophores may not be soluble in these solvents. As in past studies, BrC determined with this technique is primarily characterized by light absorption at one wavelength (365 nm) for both WS BrC and TS BrC ($Abs_{WS,365nm}^{LWCC}$ and $Abs_{TS,365nm}^{LWCC}$). Light absorption data over the whole spectrum are available on NASA data archive (FIREX-AQ 2019; https://doi.org/10.5067/suborbital/firexaq2019/data001). For this method, the limits of detection (LOD) were determined by three standard deviations of the blank measurements and are 0.10 Mm^{-1} and 0.26 Mm^{-1} for WS and MS BrC, respectively at 365 nm. At other wavelengths from 300 nm to 700 nm, the LODs ranges between 0.08-0.52 Mm^{-1} for both $Abs_{WS,\lambda}^{LWCC}$ and $Abs_{MS,\lambda}^{LWCC}$. The uncertainties associated with the absorption measurements were calculated by propagating the uncertainties from sampling (air flow rates and sampling time), filter extraction, and the absorption measurement, and are estimated to be 16% for WS BrC, 19% for MS BrC and 25% for TS BrC at 365 nm. The uncertainties are larger towards higher wavelength because the measured absorption is closer to the blank measurement; the uncertainties are ~60% for $Abs_{WS,700nm}^{LWCC}$ and $Abs_{MS,700nm}^{LWCC}$, and therefore

the uncertainty for $Abs_{TS,700nm}^{LWCC}$ can exceed 85%. There are several advantages of the BrC measurement based on aerosol extracts: (1) the majority of insoluble absorbers, for example BC or mineral dust particles, were filtered out (Zeng et al., 2021) making it a direct measurement of BrC; (2) the absorption was measured over a broad wavelength spanning from UV to visible range at high spectra resolution (300 nm – 700 nm, at ~1 nm resolution). However, aerosol particle size and morphology information are lost, so light absorption (Abs_{λ}^{LWCC}) measured in the LWCC is not directly comparable to results from aerosol optical instruments since it does not consider particle-size and other related effects. In the following, we denote the absorption coefficients for just chromophores in liquids by, Abs_{λ}^{LWCC} and the estimated coefficients for the chromophores in aerosol particles by $b_{ap,BrC,\lambda}$. A further limitation is that a fraction of non-polar chromophores may not be extracted efficiently in water or organic solvents (Corbin et al., 2019; Shetty et al., 2019).

A photoacoustic spectrometer (PAS) was deployed on the DC-8 providing real time measurements of dry aerosol absorption of fine particles (diameters < 2.5 μm) at three wavelengths: 405 nm, 532 nm, and 664 nm (Lack et al., 2012b; Langridge et al., 2013). In this instrument, light at a specific wavelength absorbed by an aerosol particle is converted to an acoustic pressure wave that is detected with a microphone. Uncertainties for these data are estimated to be 20%, mainly from calibration, pressure variation and optical alignment issues (Langridge et al., 2011). Note that the PAS does not directly measure BrC absorption, it must be calculated by the difference between total aerosol light absorption and light absorption by BC (here BC is referred to as the overall light absorption properties of BC, which includes the absorption by BC and any absorption enhancement due to coatings). Since BC, in most cases, dominates the light absorption at all wavelengths, BrC

absorption inferred by optical instruments like the PAS can have a large uncertainty due to BrC being calculated by subtraction of two similar magnitude numbers. In smoldering smoke plumes this is less an issue due to the high levels of BrC relative to BC. As the PAS only provided data at a limited number of wavelengths, mostly in the visible wavelength range, extrapolation from visible to UV wavelengths is required, which also leads to further uncertainties when using these data to infer optical properties over a broad spectral range (Liu et al., 2015c).

3.3.2.2 Other measurements

Refractory black carbon (rBC) mass concentration was measured by a single particle soot photometer (SP2), which quantifies rBC mass in individual particles in the 0.090 to 0.550 μm size range (volume-equivalent diameter assuming 1.8 g cm^{-3} void-free density) based on the incandescence signal they generated when passing through a laser beam (Stephens et al., 2003; Schwarz et al., 2006). The amplitude of the BC incandescence signal is related to the amount of refractory material contained in the illuminated particle. Integrated BC concentrations have been adjusted to account for accumulation-mode BC outside of the SP2's detection size range (Schwarz et al., 2008) on a per-flight basis. Use of a dilution system to reduce particle loads to single-particle instruments on the DC-8, increased total SP2 uncertainty to larger values than typical. Total uncertainty was estimated to be 40% in integrated rBC MMR in its size-range with the dilution system.

OA was measured for particles nominally up to 1 μm diameter by a high-resolution time-of-flight Aerodyne aerosol mass spectrometer (HR-ToF-AMS) (DeCarlo et al., 2006; DeCarlo et al., 2008). The uncertainty of the OA mass concentration was estimated to be

38%, dominated by uncertainty in particle collection efficiency due to particle bounce, and absolute and relative ionization efficiency (Bahreini et al., 2009). A collocated extractive electrospray ionization time-of-flight mass spectrometer (EESI-ToF-MS) (Lopez-Hilfiker et al., 2019; Pagonis et al., 2021), measured the mass concentration of 4-Nitrocatechol (4-NC). The instrument was limited to pressure altitudes of below 7 km above sea level, and the measurement uncertainty was estimated to be 47%. HR-ToF-AMS and EESI-ToF-MS shared the National Center for Atmospheric Research (NCAR) High-Performance Instrumented Airborne Platform for Environmental Research Modular Inlet (HIMIL) (Stith et al., 2009), together with high efficiency particulate air (HEPA) filter for background measurements and a calibration system (Pagonis et al., 2021).

Aerosol number size distribution was measured by a laser aerosol spectrometer (LAS, model 3340, TSI Incorporated, Shoreview, MN), operated behind a monotube Nafion dryer (Moore et al., 2021). The reported size range is from ~100 nm to 4.8 μm. LAS was size-calibrated with ammonium sulfate particles with uncertainty of 20%.

Carbon monoxide (CO) mixing ratios were measured by a diode laser spectrometer system, referred to by its historical name Differential Absorption Carbon Monoxide Measurements (DACOM) with measurement uncertainty of 2 ppbv (Warner et al., 2010). O3 and NOx were measured with the NOAA Nitrogen Oxides and Ozone (NOyO3) 4-channel chemiluminescence instrument with measurement uncertainty of 5-10 pptv (Pollack et al., 2010).

Note that all data presented here are at standard temperature condition and pressure (273K and 1013 mbar). High-resolution 1 Hz data (e.g., measurements by PAS, BC, CO,

OA, and 4-NC) were merged to low time resolution data (i.e., 10s data or filter sampling interval) depending on the analysis performed.

3.3.3 Calculation of various species' light absorption coefficients

Various aerosol particle light absorption coefficients as a function of wavelength are determined from these measurements and compared. From the PAS and SP2 measurements, light absorption due to just BrC ($b_{ap,PASBrC,\lambda}$) is obtained from the difference of the measured (total) absorption ($b_{ap,PAS,\lambda}$) and the absorption by rBC ($b_{ap,rBC,\lambda}$) as a function of wavelength by:

$$b_{ap,PASBrC,\lambda} = b_{ap,PAS,\lambda} - b_{ap,BC,\lambda} = b_{ap,PAS,\lambda} - E_\lambda \cdot b_{ap,rBC,\lambda} \quad (2)$$

where $b_{ap,BC,\lambda}$ is the overall light absorption coefficient of BC, including a lensing effect (enhancement, E_λ) due to coatings on rBC. We estimate the light absorption coefficient of rBC from the published properties of pure BC by:

$$b_{ap,rBC,\lambda} = c_{rBC} \cdot MAC_{rBC,550nm} \cdot \left(\frac{\lambda}{550nm}\right)^{-AAE_{rBC}} \quad (3)$$

where in Eqn (3) the absorption coefficient of rBC ($b_{ap,rBC,\lambda}$) is estimated from the SP2-measured refractory BC mass concentration (c_{rBC}), with an assumed rBC AAE of 1 and mass absorption cross-section ($MAC_{rBC,550nm}$) of pure BC of 7.5 ± 1.2 $m^2\ g^{-1}$ at 550 nm (Bond and Bergstrom, 2006). The AAE of rBC can range from 0.8 to 1.4, and a clear coating does not alter the AAE of rBC significantly (Lack and Langridge, 2013). However, rBC heavily coated with chromophores can result in an AAE of 3 (Zhang et al., 2020b).

The enhancement factor (E_λ) in the rBC absorption due to coatings is not well known as it depends on particle characteristics that are most often not fully measured, such as the coating or BC geometry (Lack and Cappa, 2010; Luo et al., 2018) and the coating optical properties (e.g., clear or absorbing) (Liu et al., 2017; Wu et al., 2018; Zhang et al., 2018). The absorption enhancement has been observed to be less than 5% or as high as 250%, corresponding to E_λ of 1-3.5, and the enhancement effect is larger towards lower wavelengths (Zhang et al., 2017; Zeng et al., 2020). We assume the AAE of rBC (AAE_{rBC}) is 1, as in other studies (Zhang et al., 2017; Zeng et al., 2020). We also use a constant E_λ of 1.6 at all wavelengths which is a typical level reported (Wu et al., 2018; Fierce et al., 2020), and consistent with the E_λ parameterization of Chakrabarty and Heinson (2018) based on our coating levels observed in one smoke plume (average ratio of rBC plus coating mass to rBC mass of approximately 4.5).

We compare the overall PAS-measured light absorption coefficient to a bottom-up estimate of the overall light absorption coefficient resulting from the contributions of individual carbonaceous light absorbing components. This predicted light absorption coefficient as a function of wavelength ($b_{ap,predicted,\lambda}$) is determined by:

$$b_{ap,predicted,\lambda} = E_\lambda\, b_{ap,rBC,\lambda} + b_{ap,TSBrC,\lambda} = E_\lambda \cdot b_{ap,rBC,\lambda} + K_\lambda \cdot Abs_{TS,\lambda}^{LWCC} \qquad (4)$$

which is the sum of the light absorption by pure rBC with an added lensing effect, plus BrC measured in solution (TS BrC, i.e., the sum of all chromophores in the extract solvent, $Abs_{TS,\lambda}^{LWCC}$) and converted to BrC light absorption ($b_{ap,TSBrC,\lambda}$) by aerosol particles by multiplying by a factor, K_λ. Several studies have used Mie theory to calculate the

conversion factor (K_λ) at a specific wavelength, typically 365 nm (Liu et al., 2013; Washenfelder et al., 2015; Shetty et al., 2019). Reported K_{365nm} values are in the range of 1.8 to 2.3 a wavelength of 365 nm. Here we perform a more detailed Mie theory calculation and determine K_λ over the liquid spectrophotometer-measured wavelength range of 300 to 700 nm.

3.3.4 Mie Theory Calculation

Mie theory has been applied to convert the absorption coefficient from soluble BrC (Abs_λ^{LWCC}) in liquid extracts to an ambient aerosol absorption coefficient ($b_{ap,BrC,\lambda}$) from the soluble chromophores. We do this with a conversion factor of K_λ, which is determined based on a number of assumptions, including: (1) The BrC-containing aerosol particles are spherical; (2) BrC chromophores are uniformly distributed through the particle; (3) the size distribution of BrC is the same as that of the OA aerosols (since in intense smoke plumes most of the aerosol is composed of organic species, this is a good assumption); and (4) the BrC aerosol is externally mixed with other light absorbers (BC), since BrC is only a small fraction of OA, most BC coating is likely to be non-absorbing OA species and the majority of BrC part of the OA not containing BC. Aerosol size distribution measured by the LAS (particle diameters between ~ 100 nm and 4.8 μm) were fitted by a log-normal distribution to account for data out of the size range (i.e., particles smaller than 100 nm). The LAS number distribution was scaled by the AMS OA mass concentration to estimate the number distribution of just OA. This was done by calculating the mass distribution from the LAS number distribution, by assuming spherical particles of density 1.4 g cm^{-3}, times the scaling factor, and integrating over the size range of zero to 1 μm. The scaling factor was adjusted

so that the integrated LAS mass distribution equaled the AMS OA. MAC values were calculated based on the AMS OA mass ($Abs_{TS,\lambda}^{LWCC}/OA$). Detailed procedures for Mie theory calculations can be found elsewhere (Liu et al., 2013).

3.3.5 Age of smoke plumes

The age of species in a smoke plume advected from a fire can be estimated in a number of ways, but are only rough estimates due to the large spatial scales of the fires investigated, and other factors. Chemical age can be estimated based on known differential reaction rates of species, or the physical age can be estimated. Here we estimate the physical age based on air mass trajectories comprising two components: advection age and plume rise age (Holmes et al., in preparation). The advection time was estimated by the HYbrid Single-Particle Lagrangian Integrated Trajectory (HYSPLIT; (Stein et al., 2015; Rolph et al., 2017)) from the DC-8 aircraft location relative to the smoke source using the MODIS/ASTER airborne simulator (MASTER; (Hook et al., 2001)) with multiple high-resolution meteorological dataset, including High-Resolution Rapid Refresh (HRRR), North American Mesoscale Forecast System (NAM CONUS nest), and Global Forecast System (GFS). The plume rise time to the trajectory height was obtained from MASTER fire altitude by assuming a vertical velocity of the air mass (12 m s^{-1} in pyroCb and 7 m s^{-1} otherwise). The typical uncertainty of estimated plume age was approximately 27%.

3.3.6 Normalized Excess Mixing Ratio (NEMR)

A number of parameters are used to assess the evolution of species of interest in fire plumes after emission from the burning regions. The normalized excess mixing ratio (NEMR) is the ratio of the enhancement (in-plume minus out of plume, the latter being the

background) in the species of interest to the enhancement of a long-lived co-emitted species, such as CO, or CO_2 (Hobbs et al., 2003; Garofalo et al., 2019). In the following analysis, we use CO as the conservative tracer as its lifetime is ~ 1 month and it is much more enhanced in the plume relative to the background than CO_2. The change of NEMR with plume age indicates the total gain or loss of the species of interest during the plume advection from the burning region by excluding the change in concentration just due to physical dilution. Due to large enhancements in BrC in the smoke plumes relative to the regional background, we assume the BrC (both soluble BrC and PAS BrC) outside the plume was zero, so the $NEMR_{BrC}$ can be estimated to be BrC/ΔCO. The NEMR of rBC ($NEMR_{rBC}$) is also examined to assess if there was any significant change in the burning conditions that affected aerosol particle concentrations when sampling at different down-wind locations in the plume.

3.3.7 Challenges in studying processes in wildfire plumes

After emission, atmospheric evolution involving both physical and chemical processes simultaneously alter the BrC light absorption properties. A goal of FIREX-AQ was to characterize these changes in the first few (~7) hours following emission. Both field and laboratory studies have illustrated that the absorption of BrC can be enhanced or depleted following emission (Table 3-1), with most dramatic changes expected in the first few hours. This includes loss due to evaporation of semi-volatile BrC as the plume disperses and dilutes, formation of secondary BrC due to photochemical reactions or reactions with radicals, and bleaching due to OH, O_3 or photolysis reactions. Except for dilution, many processes are affected by the optical thickness (intensity) of the smoke plume. A recent study shows that photochemical-driven processes often occur at the top

and edges of large smoke plumes, while dark chemistry, including NO_3 radical oxidation, is more likely within or in the lower part of the plume (Wang et al., 2021). Determining what causes the evolution of BrC in a specific wildfire plume is hindered by both the variability within the plume itself, which can be driven by a number of factors, and limitations with the sampling methods. Variability in the plume may be caused by variability in emissions from different regions of the burning area that contribute to the overall plume, meaning different parts of the plume could have a different mix of emissions and observed differences would not be due to some chemical or physical processes. The fire emissions may change in time so that observations of how parameters in the plume change at different downwind distances may be driven by not only chemical and physical evolution, but also changes in emissions between the different times the smoke was emitted (assuming a somewhat steady advection rate). Measurement limitations include the fact that the lawn-mowing patterns do not represent true Lagrangian sampling. High aircraft speed means samples are being integrated over regions of the plume; this is especially a limitation of the filter-based method which integrates over large regions of a plume (i.e., typically average from one transect). Add to this that there may be competing chemical and physical processes occurring simultaneously as the smoke evolves, it is highly challenging to identify key processes that play roles in the chemical and physical evolution of the smoke soon after emission. Some possible way to minimize these limitations is to compare bulk BrC variability to the behavior of a specific BrC chromophore. Another approach is to look at variability across one transect of a plume instead of tracking changes downwind of the fire. We use both methods in the following analysis.

3.4 Results and Discussion

3.4.1 Fire plume sampling

The DC-8 aircraft conducted 23 individual flights during FIREX-AQ, including 13 flights characterizing wildfires in the western United States, 8 flights targeting prescribed burning plumes, and 2 transit flights. Here we focus on the wildfire smoke sampled. Among the 13 flights investigating wildfires, 404 filters were collected in the western US, of these, 268 filters (~66%) were fully or partially within fire plumes. The details of the various plumes are given in Table 3-2.

Table 3-2 Details of the wildfire plumes encountered in the western United States during FIREX-AQ 2019 by the NASA DC-8 aircraft. The Date (month/day) and Time are times the aircraft starting sampling in the plumes, (note that UTC may exceed 24:00 to ensure continuity). Expect for plumes in CA and WA which are in PST the time zone, local time for plumes encountered in other states is in MT.

Date (2019)	Plume Name	Time (UTC)	Local Time	State	Fire Location	Fuels (inciweb)
7/25	Shady	22:45-23:26	16:45-17:26	ID	43.56, -112.89	Timber and Tall grass
		23:47-25:08	17:47-19:08			
		25:46-26:45	19:46-20:45			
7/29	North Hill	23:22-24:51	17:22-18:51	MT	46.75, -111.96	Tall grass, and medium logging slash
	Tucker	26:38-28:13	19:38-21:13	CA	41.73, -121.24	Timber, brush, and tall grass
7/30	Tucker (Aged)	21:30-22:37	14:30-15:37	CA	41.73, -121.24	Timber, brush, and tall grass
7/30	Lefthand	25:34-27:37	18:34-20:37	WA	46.93, -120.99	Logging slash and timber
8/2	Lick Creek	25:06-26:10	18:06-19:10	ID	47.16, -115.91	Logging slash and timber
8/3	Williams Flats	22:20-24:03	15:20-17:03	WA	47.94, -118.62	Dead trees, grass, sage, and bitter brush
		24:38-26:14	17:38-19:14			
8/6	Williams Flats	20:58-21:50	13:58-14:50	WA	47.94, -118.62	Timber, brush and short grass.
	Horsefly	22:37-24:32	16:37-18:32	MT	46.96, -112.44	Timber (litter and understory) and medium logging slash
8/7	Williams Flats (Aged)	22:05-23:02	15:05-16:02	WA	47.94, -118.62	Timber, brush and short grass.
8/7	Williams Flats	23:34-24:46	16:34-17:46	WA	47.94, -118.62	Timber, brush and short grass.
		25:15-26:12	18:15-19:12			
8/8	Williams Flats (Aged)	21:51-26:14	14:51-19:14	WA	47.94, -118.62	Timber, brush and short grass.
8/12	Castle	24:15-26:29	18:15-20:29	AZ	36.53, -112.23	Timber (litter and understory)
		27:08-27:53	21:08-21:53			
8/13	Castle	23:13-24:56	17:13-18:56	AZ	36.53, -112.23	Timber (litter and understory)
		25:22-27:10	19:22-21:10			
8/15	Sheridan	25:06-28:42	19:06-22:42	AZ	34.68, -112.89	Grass and Brush
8/16	Sheridan	24:48-28:28	18:48-22:28	AZ	34.68, -112.89	Grass and Brush

As an example of how smoke from a specific fire was investigated (Williams Flats fire, 7 Aug. 2019, UTC 23:34 to 24:46, Table 3-2), the flight path and time series of the

CO mixing ratio and aircraft altitude are shown in Figure 3-1. For this flight, the DC-8 departed from the Boise Airport (BOI, ID) on 7 Aug. 2019 UTC and flew toward the northeast to trace the aged plumes coming from the Williams Flats fires, which had been forecasted by models and observed in satellite images. This smoke was detected as a subtle enhancement in CO between 22:00 – 23:00 UTC (Figure 3-1b). Then, the DC-8 aircraft maneuvered to approach the fresh Williams Flats smoke from the downwind side at altitudes between ~3800-5200 m. Two lawn-mowing patterns were made in the late afternoon local time with 19 individual plume transects; 10 in the first pattern during local time 16:34-17:46 and 9 transects in the second pattern during local time 18:15-19:12. For the filter sampling, although the sampling goal was to only collect particles when the DC-8 was in the smoke plume, an inevitable small amount of background air was also collected on the filter samples due to the fast-moving aircraft (typical speed 200 m s^{-1}) and because the exact edges of the plumes were ambiguous. In-plume sampling was identified by enhancements in concentrations of CO, CO_2, and rBC; for example, in most cases in-plume was characterized by a CO enhancement of at least 200 ppbv over the background CO concentration. Figure 3-1b shows that the plume could be readily identified by large increases in CO. Following this, the aircraft made an excursion to the southeast and then returned to the Boise Airport.

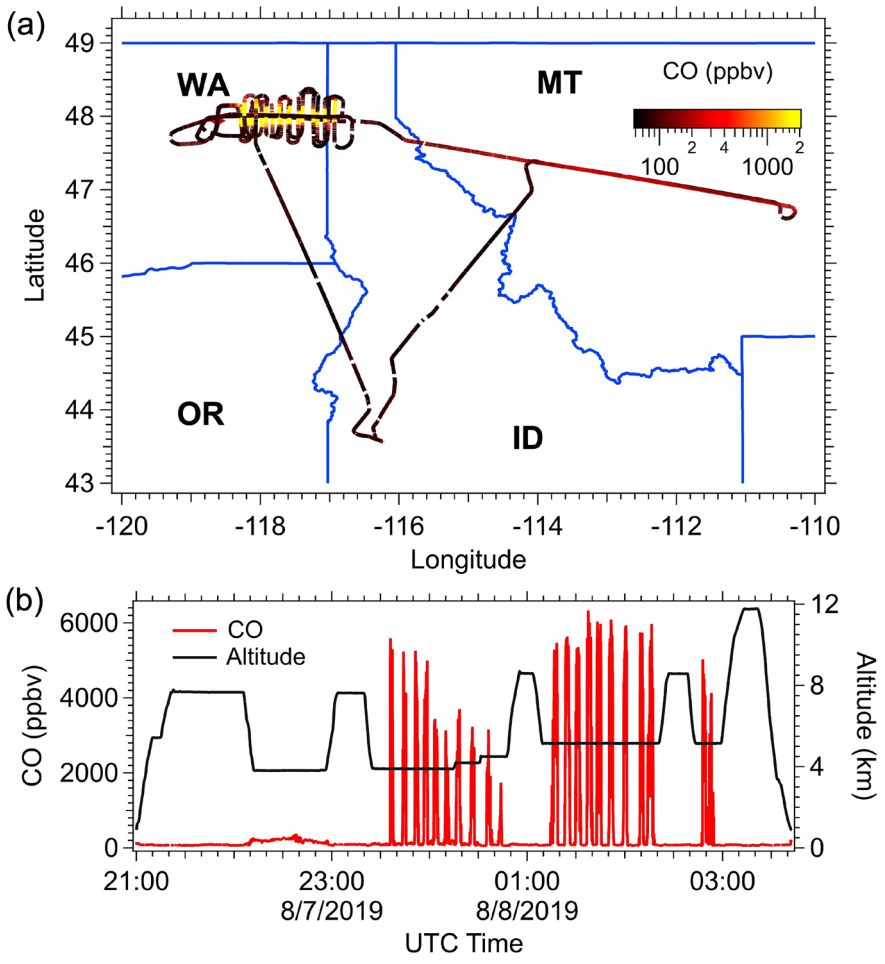

Figure 3-1 (a) Example flight track on 7 Aug. 2019, targeting smoke plumes emitted from the Williams Flats fire, where the flight track color gives the CO mixing ratio. (b) Time series of CO (red) and aircraft altitude (black).

3.4.2 Overall characteristics of BrC in smoke

For data when sampling in the various wildfire smoke plumes, soluble BrC absorption, including WS BrC and TS BrC, and BrC inferred from the PAS were highly correlated with various other gas and aerosol species expected to be emitted by the fires, such as CO, BC, OA, hydrogen cyanide (HCN) and acetonitrile (CH_3CN), the latter two

measured by a Proton-transfer-reaction mass spectrometry (PTR-MS) (see Table 3-3). The various measurements of BrC (WS, TS and PAS) were highly correlated amongst themselves, with the highest correlation between TS BrC and PAS BrC. Compared to WS and TS BrC, PAS BrC also had higher correlations with rBC and gas phase smoke species, possibly due to limitations with the offline filter method, or that PAS BrC is a more comprehensive measurement of BrC (includes possibly insoluble BrC species missed in the filter-solvent extraction method).

Table 3-3 Pearson correlation coefficient (R) for data during the fire events during FIREX-AQ. For filter data (WS BrC and TS BrC at 365 nm), higher time resolution data are averaged to filter times, and for all others the comparisons are for 10 sec merged data. PAS BrC is the absorption coefficient of BrC inferred from PAS and rBC mass from SP2 at 405 nm.

	WS BrC	TS BrC	PAS BrC	CO	rBC	OA	HCN	CH3CN
WS BrC								
TS BrC	0.91							
PAS BrC	0.91	0.96						
CO	0.91	0.95	0.98					
rBC	0.82	0.83	0.92	0.94				
OA	0.89	0.94	0.96	0.97	0.92			
HCN	0.82	0.82	0.91	0.94	0.94	0.87		
CH3CN	0.84	0.81	0.91	0.94	0.95	0.87	0.98	

3.4.2.1 Soluble BrC

For all smoke samples collected during FIREX-AQ, WS BrC ($Abs_{WS,365nm}^{LWCC}$) accounted for 45% ± 16% (mean ± standard deviation) of TS BrC at 365 nm ($Abs_{TS,365nm}^{LWCC}$)

(Figure B-1, TS vs WS BrC at 365 slope=2.23, intercept=0, r^2=0.91), which are similar to levels (~45%) observed in fresh biomass burning plumes during the DC3 campaign that also investigated summertime western US wildfires (Liu et al., 2015a). This fraction is slightly lower than the observation in highly aged biomass burning in the ATom study (smoke transported from the continents to remote marine regions), which was 53% ± 17%, and could be explained by the ATom BrC being more oxidized (more aged) with a higher hygroscopicity (Duplissy et al., 2011).

The spectral characteristics of BrC are often characterized by the Absorption Angstrom Exponent (AAE). To cover as much of the short wavelengths as possible, we calculated the AAE from the light absorption measured between 300 nm to 500 nm. (Note, that calculating the AAE by fitting data with a power law is dependent on the wavelength range utilized (Moosmüller et al., 2011)). Including all measurements in the identified smoke plumes of this study, the AAE for TS BrC (sum of the water and methanol extracts) was on average 4.2 ± 1.6 (± is standard deviation). This is lower than the AAE for just WS BrC (AAE=5.1 ± 1.3), and likely a result from less-polar chromophores that are extracted in methanol and not water absorbing more light in the higher wavelength range compared to water-soluble chromophores (Zhang et al., 2013; Liu et al., 2015a). The AAE of the overall absorbing aerosol determined from fitting the absorption of the 3 PAS wavelength data with a power law for these same smoke plumes was 1.49 ± 0.52 (mean ± stdev). In contrast, the BrC determined from the PAS had an AAE of 2.07±1.01 (mean ± stdev).

3.4.2.2 BrC emissions and classification

The emission ratio of BrC (ER_{BrC}) can be estimated from the various fires as the ratio of ΔBrC to ΔCO (i.e., $NEMR_{BrC}$), assuming there was little atmospheric processing between the emission and time of measurement. To estimate emissions, we only use BrC data from wildfires with transport time less than two hours. The results are shown in Figure 3-2. For PAS-predicted BrC at a wavelength of 405 nm (the lowest PAS measurement wavelength) the ER_{BrC} (slope) was 0.131 ± 0.00028 Mm^{-1} $ppbv^{-1}$ (the ± is the uncertainty in the slope a 1-sigma confidence interval). For just water-soluble BrC the ER_{BrC} was 0.071 ± 0.003Mm^{-1} $ppbv^{-1}$, and for TS BrC 0.163 ± 0.006 Mm^{-1} $ppbv^{-1}$. We calculated the soluble BrC ERs at 365 nm since this is the wavelength most often used to characterize BrC using a single wavelength. Note, that these data are BrC in the solution and not corrected for conversion to ambient particle (factor K_λ, discussed below, is not applied here). (Note that the TS BrC is higher than PAS BrC because it given at a lower wavelength, see Figure B-2).

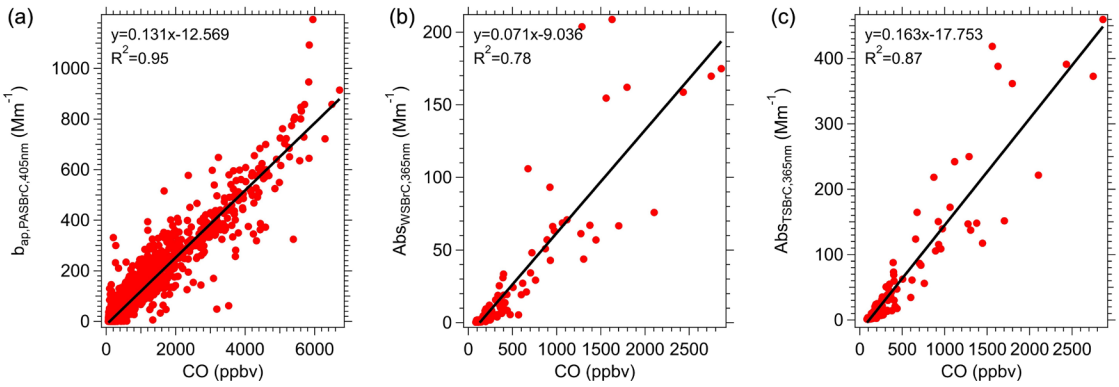

Figure 3-2 BrC emission ratios (ER) determined from the slope of BrC absorption to CO for the studied fires when the smoke transport time was less than 2 hours. Slopes are from orthogonal distance regression (ODR). Plot (a) is for PAS data at 405 nm, (b) WS BrC ($Abs_{WS,365nm}^{LWCC}$) and (c) TS BrC ($Abs_{TS,365nm}^{LWCC}$) both at 365 nm. WS BrC and TS BrC ERs are for chromophores in the solvent and have not been converted to aerosol absorption coefficients (see Figure 3-4 for conversion factor).

The wildfire BrC optical properties can be mapped onto the classification proposed by Saleh (2020) to provide a rough characterization and test the approach as a parameterization. For the PAS and filter data we determined the BrC AAE and the mass absorption cross-section (MAC). For the PAS, the $MAC_{PASBrC,405nm}$ was determined from the ratio of $b_{ap,PASBrC,405nm}$ to OA mass measured by the AMS, and AAE_{PASBrC} was calculated from the power law fit to $b_{ap,PASBrC,405nm}$, $b_{ap,PASBrC,532nm}$, and $b_{ap,PASBrC,664nm}$. PAS data are shown with the Saleh BrC characteristics identified by regions in the boxes. In Figure 3-3a, these wildfires data are best characterized as M-BrC and had little relation to the modified combustion efficiency (MCE). The MCE for samples from wildfires encountered in FIREX-AQ was around 0.9, which is at the boundary of smoldering and flaming burning conditions. However, the MCE did not span a wide range for the fires investigated and so there was little dynamic range to produce a clear separation for different burning conditions. Our smoke data also shows little correlation between BrC AAE_{PASBrC} and $\log_{10}(MAC_{PASBrC,405nm})$. Figure 3-3b shows a similar plot for the TS BrC (without applying the conversion factor K_λ to convert to aerosol absorption). Most of these data are outside of the Saleh's categorization, but they are shifted to the upper left relative to the PAS data, consistent with the idea the soluble BrC contains relatively more weakly absorbing species (or less of BrC chromophores that absorb at higher wavelengths, but are not insoluble in methanol). Like the PAS BrC, TS BrC also does not show a clear trend with MCE, nor a correlation between AAE and $\log_{10}$(MAC).

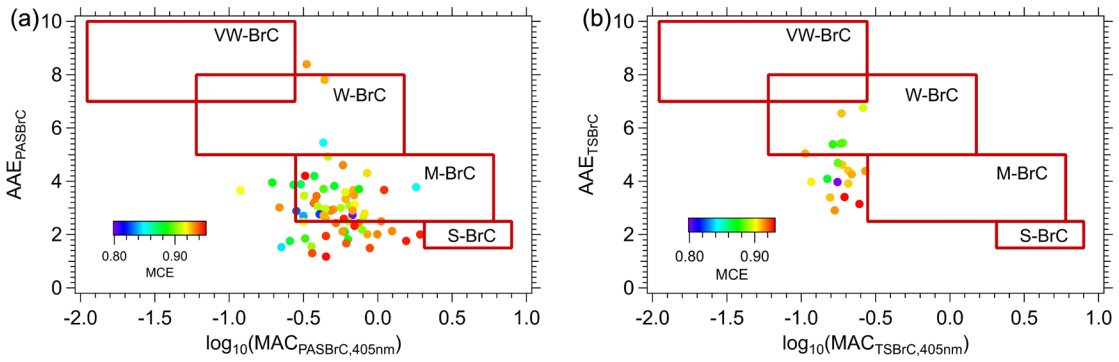

Figure 3-3 The classification framework proposed Saleh (2020) with wildfire BrC data inferred or measured in FIREX-AQ by (a) PAS and (b) soluble TS BrC, where VW-, W-, M- and S-BrC, are very-weakly-, weak-, moderately-, and strongly absorbing BrC. Each datum is one plume transect average.

3.4.3 Comparing methods for determining BrC

A closure analysis is performed to compare the PAS and solution methods for measuring BrC and to assess the magnitude of the various parameters needed for the comparison. Here we focus on the Williams Flats fire measurements on 7 Aug. 2019 as a typical example of the data collected near fires. Detailed calculations are shown for a single plume transect made between 23:34 – 23:39 UTC, which corresponds to the first sampling transect nearest the fire (see Figure 3-1).

To make the comparison, Mie theory and the size distribution data measured in this plume transect were used to determine, K_λ, the conversion factor for estimating the particle light absorption coefficient from the solution data, as described in the Methods section. The results, plotted in Figure 3-4, shows K_λ as a function of wavelength. A sensitivity analysis showing the range in K_λ predicted due to variability in the various Mie theory inputs is shown in the Figure B-3.

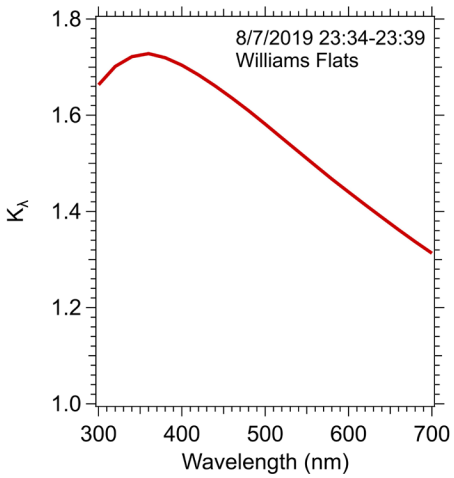

Figure 3-4 Solution-to-particle light absorption conversion factor K_λ versus wavelength calculated for data collected in the first transect of the Williams Flats fire during (23:34-23:39 7 Aug. 2019 UTC).

The contribution of each component to the predicted overall light absorption as a function of wavelength ($b_{ap,predicted,\lambda}$, Eqn (4)) is shown in Figure 3-5a and the total compared to the PAS data. Similar comparison plots to Figure 3-5a for each plume transect of the 7 Aug. 2019 Williams Flats fire are given in the Supplemental Material Figure B-4. In Figure 3-5a, the dotted black line is the "bare" (pure) rBC absorption determined from the rBC mass concentration measured by the SP2 (rBC concentration was 4.8 μg m^{-3}) determined by Eqn (3). The effect of the BC coating enhancement (E_λ=1.6) is also shown, and the resulting overall BC light absorption is the solid black line. Comparing to the PAS data, this coated rBC absorption contributed 61% to the total light absorption at 664 nm, but only about 36% at 405 nm due to BrC contributions. The brown line in Figure 3-5a is $b_{ap,predicted,,\lambda}$, or the ambient light absorption coefficient of TS BrC measured by the LWCC after applying K_λ (conversion of solution to particle BrC, $b_{ap,TSBrC,\lambda} = K_\lambda \cdot Abs_{TS,\lambda}^{LWCC}$) added to the BC absorption (first term in Eqn (4)). The brown shading is then

the aerosol particle TS BrC ($b_{ap,TSBrC,\lambda}$). The red diamond markers in Figure 3-5a are absorption measurements made by the PAS at three wavelengths, representing the overall aerosol absorption. The red curve is from fitting the three PAS measurement points with a power law ($b_{ap,PASBrC} \sim \lambda^{-3.02}$). Note that the area between the red curve and the solid black curve is the estimated PAS BrC absorption from Eqn (2).

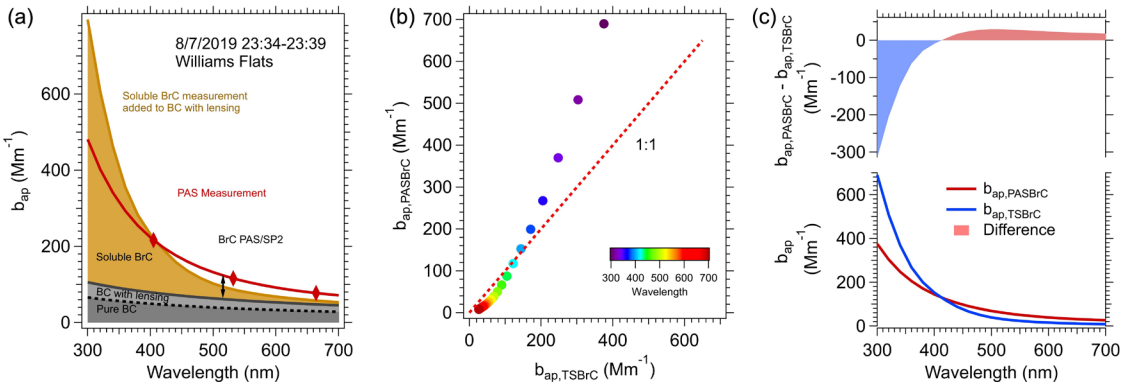

Figure 3-5 Various light absorption coefficients for the average of the first transect made closest to the Williams Flats fire (23:34-23:39 7 Aug. 2019 UTC). (a) Spectral light absorption closure analysis. The dashed black line is the light absorption of bare rBC and the solid line is BC considering the coating effect (E_λ). The brown shading is soluble BrC, $b_{ap,TSBrC,\lambda}$, where Abs_λ^{LWCC} was multiplied by the conversion factor K_λ to convert from solution to aerosol particle absorption. The upper part of the brown curve is $b_{ap,predicted,\lambda}$, given by Eqn 4. (b) Comparison between $b_{ap,TSBrC,\lambda}$ (brown shading in plot (a)) and $b_{ap,PASBrC,\lambda}$ (difference between red and the black solid line in plot (a)), color coded by wavelength. (c) Similar to plot (b), but versus wavelength (i.e., the difference between BrC determined from the soluble measurements with the conversion factor K_λ included, and BrC calculated from the PAS data).

In Figure 3-5b and 5c, a direct comparison is made between PAS BrC ($b_{ap,PASBrC,\lambda}$) and TS BrC ($b_{ap,TSBrC,\lambda}$) as a function of wavelength. At a wavelength near 400 nm the two methods give nearly the same absorption coefficient, but at lower wavelengths the BrC

predicted from the solvent extract is increasingly higher than the PAS-predicted BrC. At wavelengths higher than 400 nm, the PAS BrC tends to be higher by a relatively consistent value. If no conversion from solution to particle absorption factor is applied, (i.e., K_λ=1), the PAS BrC is consistently higher for all wavelengths greater than about 325 nm, see Figure B-5.

Although Figure 3-5 shows data from just one transect through the plume from a single fire (see Figure B-4 for all transects in the first lawn mowing pattern flown in Figure 3-1), these differences between TS BrC and PAS-predicted BrC are consistent between many of the fire plumes investigated in this study. Figure 3-6 show scatter plots comparing the soluble BrC ($b_{ap,TSBrC,\lambda}$) and the PAS BrC ($b_{ap,PASBrC,\lambda}$) at the PAS measurement wavelengths (405 nm, 532 nm, 664 nm) for all smoke plumes. From the linear regression, there is a good correlation between the two methods for determining BrC absorption coefficients, with the highest correlation for the lower wavelength (405 nm), where BrC absorption is a larger fraction of the overall light absorption and BrC absorption coefficients are highest (Figure 3-6a). The data are more scattered and the slope larger (i.e., greater discrepancy) as the wavelength increases from 405 nm to 664 nm.

The wavelength-dependent differences in the soluble BrC and that estimated from the PAS data, shown in Figure 3-5b and 5c, may be due to a number of factors:

1. Measurement artifacts and uncertainties or differences in the particles size ranges measured by the various instruments. We view this as a source of variability in the comparisons, but not a cause for the systematic trends.
2. Uncertainty from the conversion factor K_λ, which is sensitive to the real part of the refractive index and BC-containing-particles size distribution (see Figure

B-3 for sensitivity analysis). Note that changes in the real part of the refractive index do not significantly affect the shape of K_λ with wavelength, so the relative differences when comparing between wavelengths (Figure 3-6) will remain.

3. Uncertainty in the absorption enhancement E_λ, which is associated with aerosol morphology including aerosol geometry, shell thickness, and shell optical properties. E_λ may vary with wavelength, which we did not consider.

4. Contributions of non-soluble species, such as those expected to be characterized as S-BrC. Larger molecular weight chromophores often absorb more into higher wavelengths and are likely less soluble. Thus, missing non-soluble species, but which are included in the PAS BrC, would lead to increasing under-measurement of TS BrC at the higher wavelengths and likely add variability, as observed (Figure 3-6c). However, there is no correlation between the difference in soluble vs. PAS BrC at the higher wavelength (664 nm) as a function of MCE. Note that in Figure 3-6c, the ratio between the two BrC measurements can be very high (all data are far above 1:1 line), which is hard to explain by measurement uncertainties or variations of K_λ and E_λ.

5. Poor spectral resolution of the PAS. The PAS data at three wavelengths may not be sufficient to accurately extrapolate absorption beyond the measurement range, especially to lower wavelengths where BrC aerosol predominantly absorbs light. The PAS data may also not be well characterized by a simple power law fit ($b_{ap,PAS,\lambda} \sim \lambda^{-AAE}$). Jordan et al. (2021) suggest a fitting with a second-order polynomial function for $\log(b_{ap,PAS,\lambda})$ vs $\log(\lambda)$, but this does not change the discrepancy at low wavelengths, (blue curve in Figure 3-7). Adding a data point at a lower wavelength, the predicted BrC at 300 nm ($b_{ap,predicted,300nm}$), to the PAS data and then fitting with a power law tends to produce better agreement with the overall predicted light absorption, although there are still some discrepancies, especially at mid-visible (500 nm) wavelengths. These results suggest that particle absorption instruments that do not measure below wavelengths of ~ 400 nm may significantly under-predict particle absorption contributions when the data is extrapolated to lower wavelengths, if significant levels of BrC are present.

In the following we use soluble BrC at 365 nm (Abs_{365nm}^{LWCC}) (although the conversion factor K is not applied) and PAS at 405 nm to assess causes for BrC variability in plumes, justified by good agreement between the two methods at ~400 nm (Figure 3-6a). Both these measurements of light absorption are normalized by ΔCO to determine the corresponding NEMR.

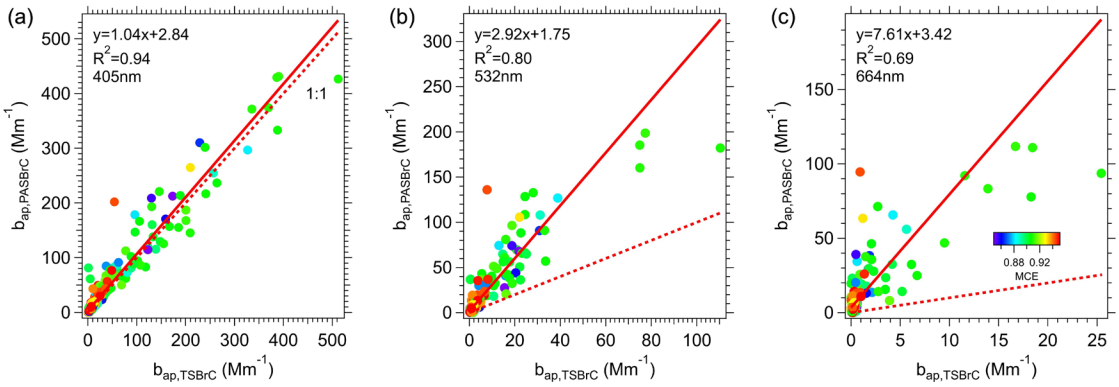

Figure 3-6 Comparisons between BrC inferred from the PAS ($b_{ap,PASBrC,\lambda}$) and total soluble BrC converted to aerosol absorption ($b_{ap,TSBrC,\lambda}$) at (a) 405 nm, (b) 532 nm, and (c) 664 nm, color coded by MCE. The red line is fitted with orthogonal distance regression (ODR). In all plots, the dotted line is the slope=1 line.

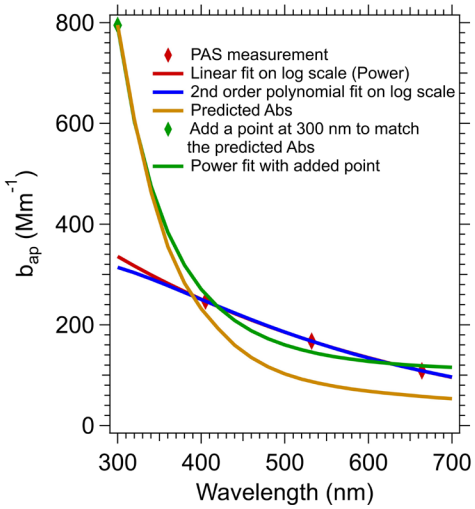

Figure 3-7 Comparison between the predicted absorption from the sum of BC and TS BrC ($b_{ap,predicted,\lambda}$) brown curve (and in Figure 3-5a) and various fits to the PAS data (red diamonds). The red line is PAS data fitted with a line on a log-log scale, which is the typical power law fit, the blue curve is a second order polynomial fit on log-log scale, and the green line is a power law with an added data point from $b_{ap,predicted,300nm}$ at 300 nm.

3.4.4 BrC Evolution

3.4.4.1 Overall trends in BrC

Starting from a wide perspective we compare the down-wind evolution of TS BrC ($Abs^{LWCC}_{TSBrC,365nm}$) of the FIREX-AQ data to the larger scale evolution of smoke (RIM Fire) reported by Forrister et al. (2015) from a previous study. The same filter-based measurement and analytical methods were used in both cases to determine TS BrC. Analysis of the uniquely large RIM fire that was studied on two separate days as it advected from California into Manitoba, Canada, showed a consistent decrease in the $NEMR_{TSBrC}$

(Figure 3-8), and an observed half lifetime of TS BrC of 9 to 15 hours was estimated. We have added to the RIM fire data the various measurements from this study.

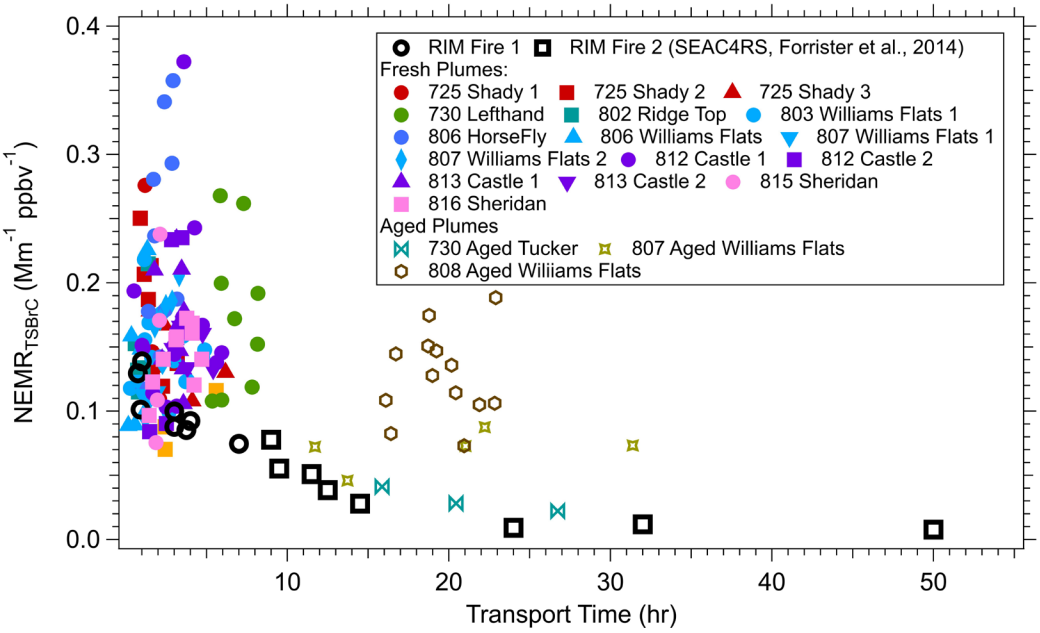

Figure 3-8 NEMR$_{TSBrC}$ at 365 nm measured in liquid extracts (conversion factor K is not applied) versus smoke transport time. Different colors represent different plumes (also see Table 3-2). Open markers (circles and squares) are data obtained from RIM fire in SEAC^{4}RS campaign reported by Forrister et al. (2015).

First noting the more aged (10 to 30 hours) FIREX smoke data in Figure 3-8, which were identified as smoke from the Tucker and two Williams Flats fires. Some of this data (Tucker and some of 8/07 Williams Flats) tend to follow the stead decay of the RIM fire, but other measurements (all of 8/08 and some of 8/07 Williams Flats) have significantly higher NEMR$_{TSBrC}$ at ages between 15 and 30 hours. For these data, a trend is less clear. Since these fires were not tracked continuously, there is a significant measurement gap of

over 10 hours in the plume evolution, the aging process for these smoke plumes is uncertain so causes for the $NEMR_{TSBrC}$ variability cannot be assessed. However, in general, $NEMR_{TSBrC}$ for aged plumes was lower than fresh plumes, suggesting an overall decay of BrC on time scales greater than about 8 hours.

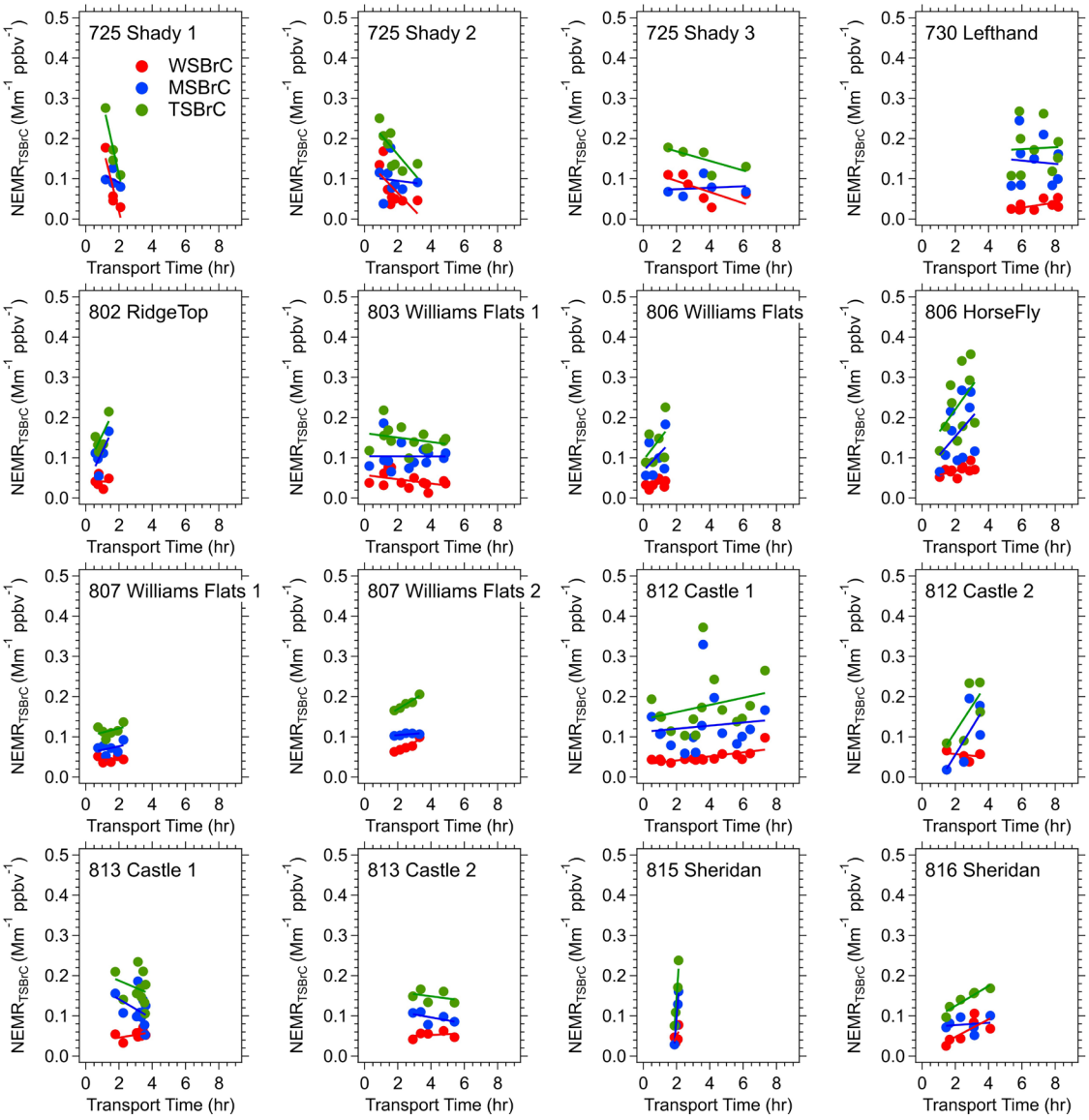

Figure 3-9 Evolution of water, methanol and total soluble forms of BrC relative to CO ($NEMR_{BrC}$ = ΔBrC/ΔCO) within each of the various smoke plumes investigated in detail during FIREX-AQ. All data on one plot are shown in Figure 3-8. Each data point is one plume transect (filter sample). The red data points are WS BrC, the blue MS BrC, and green TS BrC, which is the sum of the red and the blue. Linear fits are included with the data.

Focusing on the higher density of measurements made closer to the fires where the transport ages were less than approximately 8-hour, Figure 3-8 shows that the RIM BrC

data are within the range of the FIREX data, but the FIREX $NEMR_{TSBrC}$ data are highly variable with no clear trend with increasing plume age. Looking at each of the fresh plumes investigated in this study, Figure 3-9 shows that a range of behaviors are seen. No consistent pattern of production nor depletion of BrC is observed in the FIREX-AQ data. In some plumes the data are highly scattered, in others there appears to be a consistent downward or upward trend, or no change in the $NEMR_{TSBrC}$ with increasing time. These trends are similar when using PAS BrC data averaged to the filter sampling times. A similar lack of consistent trends in WS BrC was observed from the Twin Otter measurements as part of FIREX-AQ (Rebecca Washenfelder personal communication) and the WE-CAN study (Amy Sullivan personal communication). The results suggest highly complex and variable evolution. To investigate the changes in $NEMR_{TSBrC}$ we look at the evolution of a specific BrC chromophore and study the variability of species along cross-plume transects.

3.4.4.2 Evolution of bulk BrC compared to 4-Nitrocatechol

One approach to evaluate the evolution of bulk BrC is to compare $NEMR_{BrC}$ as a function of plume age to a specific BrC species with known properties. 4-Nitrocatechol (4-NC) has been observed to be abundant in a variety of BrC sources, including primary emission from biomass burning (Lin et al., 2016) and in secondary aerosol generated from aromatic precursors (Lin et al., 2015b; Vidović et al., 2020), and its evolution has been studied in detail (Zhao et al., 2015). For FIREX, 4-NC mass concentration was measured on 17 of the 23 flights. As it is one of the components of WS BrC chromophores, we compare 4-NC to WS BrC measured in the filter extract. We also compare it to PAS BrC in the aerosol particle phase; both are shown in Figure 3-10. For all available data within smoke plumes, the ratio of the 4-NC absorption coefficient to the WS BrC absorption, both

at wavelength of 365 nm, was 18% ± 16% (Mean ± Stdev), with lower, middle, and lower quartile range of: 10%, 19%, 33%. Figure 3-10a shows the statistics of this ratio for data grouped by estimated plume age. In the first 3 hours following emission 4-NC contributed about 23% (median) to the WS BrC light absorption at 365 nm, although there was significant variability. For smoke plumes in the 3 to 6-hour age range the fraction of 4-NC to WS BrC decreased, with a median of about 18%, and for plumes with transport ages greater than 18 hours, 4-NC was essentially all lost, it contributed only about 0.2% to the light absorption of WS BrC. The absorption ratio of 4-NC and all BrC (PAS BrC) at 405 nm wavelength shows a similar decay in the contribution of 4-NC with smoke age. This indicates that the bulk BrC in these smoke plumes had a lifetime that was significantly longer than the 4-NC. As one of the smaller (in terms of molecular weight) BrC chromophores, 4-NC has been found to have a relatively short lifetime of ~40 min from OH oxidation after the photo-enhancement stage (Zhao et al., 2015).

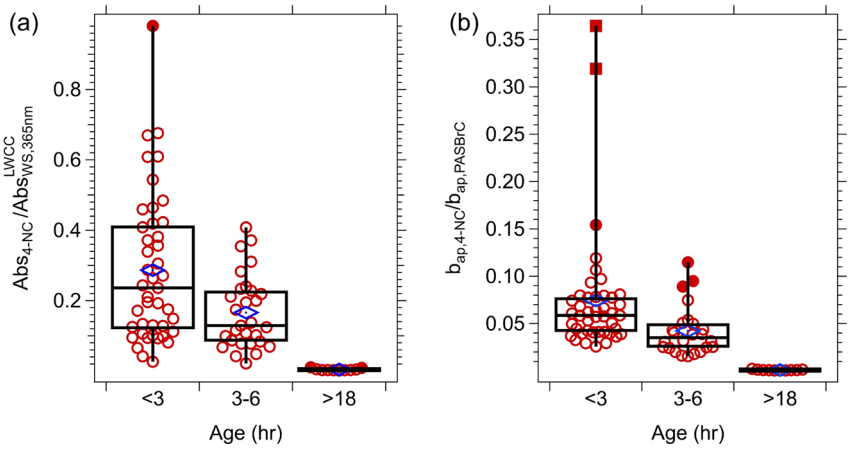

Figure 3-10 (a) Statistics of the ratio of the absorption coefficient in smoke plumes of 4-NC (Abs_{4-NC}) at 356 nm to WS BrC ($Abs^{LWCC}_{WS,365nm}$) for different ranges of transport time. (b) Comparison of the absorption coefficient of 4-NC ($b_{ap,4-NC}$) to BrC ($b_{ap,PASBrC,\lambda}$) inferred from PAS at 405 nm. The MAC of 4-NC used to calculate Abs_{4-NC} and $b_{ap,4-NC}$ is from Zhang et al. (2013), and the conversion factor (K_λ) from liquid to aerosol (K_λ) of 1.6 was applied to convert from Abs_{4-NC} to $b_{ap,4-NC}$. Blue markers are means of each bin and in plot (a) are 28.7%, 16.6%, and 0.5% and for plot (b) 7.4%, 4.2%, and 1.1%, respectively.

3.4.4.3 BrC Volatility: A descending plume with increasing temperature

Unlike BC, which is refractory, OA has a wide range of volatility (Huffman et al., 2009a). Some chromophores that contribute to the overall BrC may also be semi-volatile and evaporate when the temperature increases, or when the plume dilutes, however, this behavior cannot be inferred from the OA evolution since BrC is only a small mass fraction OA. For the Sheridan fire on 15 Aug. 2019, a sampling transect was made along the direction in which the plume was advecting away from the fire. In this particular case, the plume descended as it moved away, resulting in a ~15 K temperature increase from the higher to lower altitude, providing an opportunity to investigate the evolution of BrC in terms of temperature-driven evaporation.

Variation in temperature and the NEMRs (to account for dilution) of various species along the plume as it descended are shown in Figure 3-11. The $NEMR_{rBC}$ (black line) was fairly constant along the plume transect, implying that the combustion conditions (flaming vs smoldering) were relatively stable over time (i.e., since different down-wind distances are related to different times of fire emissions). Thus, we assume that any observed changes with age were mainly from temperature-driven processes. $NEMR_{OA}$ had an average decline of 0.9% K^{-1}, likely driven by evaporation of semi-volatile OA species (Huffman et al., 2009b). Using the higher frequency PAS BrC data, $NEMR_{PASBrC}$ (405 nm) essentially did not change along the plume; the coefficient of variation of $NEMR_{PASBrC}$ was less than 1%. As noted above, 4-NC is less stable than bulk WS BrC, and in this plume it also displayed evidence of volatility-driven loss as advected down-wind, here, at an average rate of 4% K^{-1}. For just this data, the 4-NC contributes ~10 % of the total particle BrC absorption closest to the fire and the fraction decreases to ~3% when temperature increases to 303K. To maintain a constant $NEMR_{BrC}$ despite the substantial decrease of 4-NC, there must be BrC production compensating the evaporation loss. Perhaps gas phase 4-NC and other relatively volatile chromophores were oxidized to some less volatile species that partitioned back to the aerosol phase (Roman et al., 2021), resulting in an unchanged BrC absorption.

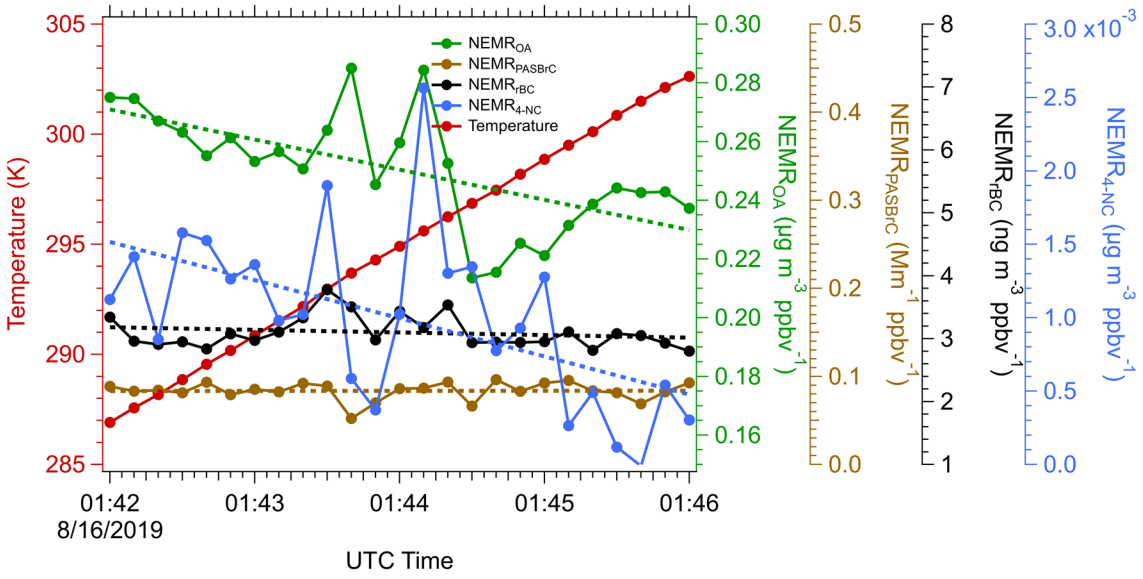

Figure 3-11 Assessment of volatility of various light species by comparing the time series of NEMR$_{rBC}$ (black), NEMR$_{OA}$ (green), NEMR$_{PASBrC}$ (brown), NEMR$_{4-NC}$ (blue), for a measurement period when the temperature (red) increased while sampling within a descending smoke plume from the Sheridan fire on 15 Aug. 2019. Dotted lines are trend lines with time fitted by ODR. Data are 10s averages.

3.4.4.4 Possible role of O_3

In most cases, the DC-8 flew into plumes approximately perpendicular to the direction of smoke transport, generating transverse plume transects, as shown in Figure 3-1. We use these transects with the PAS BrC data to investigate variables that contribute to BrC variability. The filter BrC data could not be used in this analysis since one filter was collected for each transverse transect. Multiple processes, including physical evaporation and chemical reactions, that can be occurring simultaneously may be easier to resolve in a transverse transect analysis. In an idealized transect of a smoke plume, the aircraft would enter the plume from background air, then experience a positive concentration gradient from edge to plume center, then negative gradient from center to the other edge, and finally

exit the plume into background air. Burning is typically not an ideal point source that produces a plume which fans out as advected away, but often occurs in a region or along a line. Smoke generated at different rates along the whole burning area would then contribute to the concentrations of smoke species measured along the transect. If burning conditions or material burned varied in the region this would complicate the analysis. To minimize this effect on aerosol properties, we focus on the analysis of three contrasting plume transects where in all cases the $NEMR_{rBC}$ was relatively constant (coefficient of variation of $NEMR_{rBC} < 10\%$), suggesting minimal variation in overall particle emissions along the transect. The three plumes investigated are shown in Figure 3-12.

Figure 3-12a shows one transect of the Williams Flats plume on 7 Aug. 2019. The CO data suggest smoke from 3 major burning regions had merged into a single plume; three peaks in CO were observed and these plumes had merged since background CO concentrations were not reached in the regions between the plumes. Figure 3-12d is one transect of the Castle plume on 12 Aug. 2019, and Figure 3-12g is one transect of the Williams Flats plume on 3 Aug. 2019. In both of these cases, smoke from two intense burning regions had merged to some extent, based on the CO data. Note the differences in CO concentrations indicting the contrasting levels of emissions from these fires. In most of these cases, the BrC (PAS BrC absorption at 405 nm) profile along the transect had the same shape as CO, suggesting that BrC and CO had the same source, and experienced a similar dilution process, but there were differences. Figure 3-12b, 12e, and 12h show $NEMR_{rBC}$ and $NEMR_{PASBrC}$, which removes the effect of plume dilution. $NEMR_{rBC}$ is relatively constant, suggesting that rBC emissions for these fires did not significantly change, (e.g., flaming vs smoldering). For BrC, if the $NEMR_{PASBrC}$ behaved as $NEMR_{rBC}$,

it would suggest little net effect of any atmospheric processes, other than a simple dilution effect on BrC concentration, or that during the dilution process production balanced loss, but the $NEMR_{PASBrC}$ did vary to different extents in these three cases, and the variation was correlated with O_3.

In the 7 Aug. Williams Flats (Figure 3-12a) and Castle Fire transects (Figure 3-12d), $NEMR_{PASBrC}$ and O_3 concentration had a good positive correlation (Figure 3-12c and 12f), suggesting O_3 oxidation could possibly be linked to the observed BrC enhancement, indicated by the increasing $NEMR_{PASBrC}$. In the Williams Flat 7 Aug. transect, the O_3 concentration was lowest in the center of the plumes (45, 12, and 29 ppbv, respectively for the three CO peaks) and higher in the regions where the plumes mixed and CO was lower (O_3 > 60 ppbv). Lower O_3 in the plume centers was likely due to O_3 titration by NOx with NO_2 photolysis too low to regenerate O_3, consistent with the anticorrelation between O_3 and NOx clearly seen in this transect (Figure 3-12a). Higher O_3 production in the diluted edges of the plume is discussed in detail by Wang et al. (2021). $NEMR_{PASBrC}$ also tended to be higher in the edge regions between the plumes where O_3 was higher leading to a positive correlation between $NEMR_{PASBrC}$ and O_3 (Figure 3-12c). Concentrations of various species were much higher in the 7 Aug. 2019 Williams Flats fire (Figure 3-12a, 12b, 12c); which was a much more intense wildfire than the other two fires shown in Figure 3-12. For the Castle fire transect (Figure 3-12d, 12e, 12f), smoke levels were much lower (much lower CO), O_3 may not have been significantly titrated by NOx (note low NOx levels). O_3 was about ~60 ppbv across the plume, but in this case, there was a slight enhancement in the center of the plume (Figure 3-12d), along with $NEMR_{PASBrC}$ (Figure 3-12e), again leading to a positive correlation with O_3 (see Figure 3-12f). For the

Williams Flats fire on 3 Aug. 2019 (Figure 3-12g, 12h, 12i), which was more intense than the Castle fire but less than 08/07 Williams Flats (compare CO), O_3 was higher in the center of the plumes along with NOx, but $NEMR_{PASBrC}$ was lower, being higher at the edges, leading to a negative relationship with $NEMR_{PASBrC}$. A positive relationship between O_3 and $NEMR_{PASBrC}$ may be linked to BrC photo-enhancement ($O_3 \uparrow \rightarrow NEMR_{BrC} \uparrow$, or $O_3 \downarrow \rightarrow NEMR_{BrC} \downarrow$) while an inverse relationship is indicative of photo-bleaching of BrC ($O_3 \uparrow \rightarrow NEMR_{BrC} \downarrow$, or $O_3 \downarrow \rightarrow NEMR_{BrC} \uparrow$). These types of two divergent behaviors when BrC is oxidized by O_3 have been observed in other studies. Sareen et al. (2013) observed this behavior for secondary BrC (formed with methylglyoxal and ammonium) and Fan et al. (2020) for aerosols from biomass burning.

To look for evidence of these trends in all the data, for each plume transect the relationship between O_3 and $NEMR_{PASBrC}$ was determined, and then grouped as either a positive or negative relationship between $NEMR_{PASBrC}$ and O_3. The transect-average NOx concentration was then compared for these two groups; results are shown in the boxplot in Figure 3-13. When $NEMR_{PASBrC}$ had a positive relationship with O_3, consistent with O_3 enhancing BrC absorption by generating additional BrC chromophores or transforming BrC to more strongly absorbing compounds, high NOx was more likely to be present. When $NEMR_{PASBrC}$ had a negative relationship with O_3, suggesting O_3 contributed to bleaching of BrC, NOx concentrations were generally lower. These observations are consistent with previous studies. Liu et al. (2015b) found that the presence of NOx was associated with the production of organonitrogen compounds via O_3 oxidation, such as nitro-aromatics and organo-nitrates, which enhanced light absorption. However, other studies show fragmentation of chromophores on exposure to O_3 in a NOx-free environment

led to a decrease in BrC absorption (Pillar-Little and Guzman, 2017; Sun et al., 2019). Additionally, the reaction of NO_2 with O_3 produces the NO_3 radical, which has been identified to be an important factor in BrC formation at night (Cheng et al., 2020; Selimovic et al., 2020; Mayorga et al., 2021). In dark optically thick smoke plumes where the nitrate radical loss by photolysis may be suppressed, high O_3 and NOx could also be linked to increases in BrC (Cheng et al., 2020; Selimovic et al., 2020; Mayorga et al., 2021). The correlation is not perfect, since as seen in Figure 3-13, (left box-whisker plot), there were many periods when BrC increased with increasing O_3, and yet NOx levels were very low. This may be a limitation with our analyses, but there is some evidence that BrC can be formed through heterogeneous reactions of ozone with combustion particles (i.e., soot) (Kuang and Shang, 2020). Overall, the range of possible results demonstrate the complexity of processes that may affect BrC in fairly fresh wildfire smoke.

Dilution-driven evaporation resulting in BrC loss has been reported to be an important process in the WE-CAN airborne study, which investigated similar western US wildfires in the summer before FIREX-AQ (Palm et al., 2020). Our analysis comparing the evolution of WS BrC to 4-NC and the change in BrC with changing plume temperature, however, suggested that the dominant fraction of BrC was not volatile. Also, if dilution had a large affect in the 3 plumes above, it is likely that it would have been difficult to discern any trends between $NEMR_{PASBrC}$, O_3, and NOx, which implies that dilution played a minor role compared to the effects of O_3 on BrC. For example, along these transverse transects, air masses experienced different degrees of dilution; air masses at the edge of the plume, or where two plumes had merged, are more diluted with background air than those at the center of the plumes. In the transect from the Williams Flats fire on 7 Aug. 2019

(Figure 3-12a), the highest CO mixing ratio was ~5600 ppbv, and the lowest was ~1500 ppbv near where two plumes had intersected, but still sampling in smoke (i.e., CO still significantly above background levels). This corresponds to a dilution ratio (the ratio of highest CO enhancement to the CO enhancement at a location of interest) of about 4. If only considering the effect of dilution-driven evaporation, the $NEMR_{PASBrC}$ profile would be similar to the CO profile (the CO change indicates degree of dilution between two regions). But the profile of $NEMR_{PASBrC}$ was opposite of this, which means other processes, such as O_3 oxidation in this case, drove the change in BrC absorption. This opposite pattern between CO and $NEMR_{PASBrC}$ also occurred in the transects of the Williams Flats fire on 3 Aug. 2019 (Figure 3-12c, 12f, 12i), but in this case a possible reason for the observed $NEMR_{BrC}$ shape was due to bleaching, or oxidation of BrC by O_3. In the Castle fire transect (Figure 3-12b, 12e, 12h), the dilution effect was superimposed on the enhancement by O_3 oxidation. From the analysis above, we conclude that the effect of O_3 oxidation was stronger than dilution and our finding of low BrC volatility is consistent with this $NEMR_{BrC}$ – O_3 analysis.

3.4.4.5 Search for other factors causing BrC changes with plume age

As noted in the Introduction, there are a host of factors that can affect BrC levels in an evolving smoke plume. We examined the FIREX-AQ dataset for other potential factors that might alter the optical properties of BrC, including relative humidity (RH) and aerosol liquid water content (LWC) for evidence of heterogeneous reactions, OH exposure (product of OH concentration and time), NH_4 associated with Ammonium- or Amine-containing BrC production, optical thickness of the plumes (j_{NO2} values), and type of material burning, but no evidence was found for a consistent relationship with BrC

evolution. Direct photolysis may also change the optical properties of BrC, however, the wildfire flight transects were made in the late afternoon or in the evening. Additionally, j_{NO2} in the center of the plumes was typically less than 5% of the j_{NO2} level outside of the plume, so direct photolysis may not be a significant factor causing BrC bleaching within these plumes. Late afternoon measurements and dense optically thick smoke plumes could also depress OH oxidation, except in the upper levels and sides of the plume where photochemical OH production would be more likely (Wang et al., 2021). Wildfire smoke generated at different times of day may evolve differently due to the type of oxidants involved and extent of photochemical bleaching in the first few hours (i.e., emissions late in the day or at night versus emissions in the morning or early afternoon). The DC-8 rarely continuously flew at the top or edges of plumes, limiting investigating the effect of OH on BrC aerosol in these more dilute regions. It is also possible that multiple simultaneous processes limited our ability to resolve individual ones. A positive matrix factorization (PMF) analysis did not show any consistent factors, which could be either due to lack of clear processes or that many were highly non-linear and not captured by the PMF analysis.

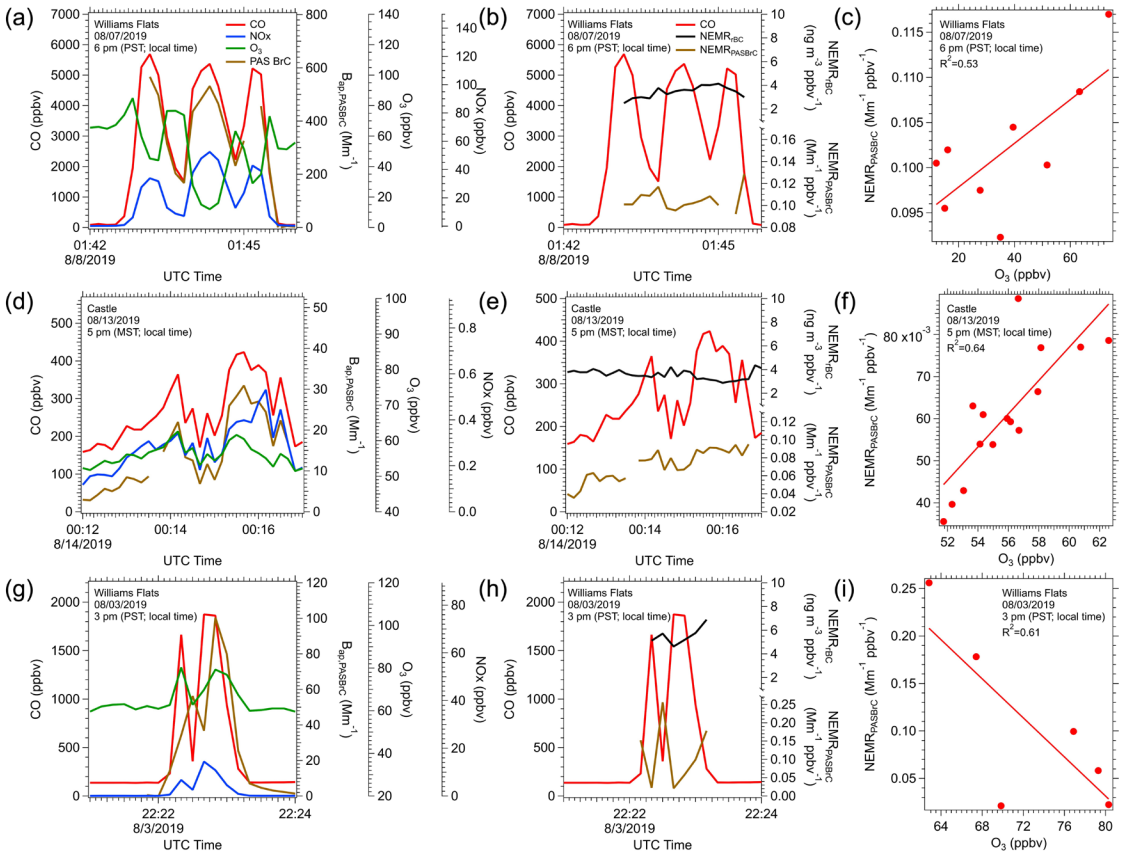

Figure 3-12 Time series for the concentration of CO (red), BrC from th PAS (brown), O_3 (green), and NOx (blue) in three example plume-transects in plots (a), (d), and (g). Corresponding time series for $NEMR_{BC}$ (black) and $NEMR_{BrC}$ (brown) for these transects, plots (b), (e), and (h), and the relationship between $NEMR_{BrC}$ and O_3 for each of these periods of in-plume sampling, plots (c), (f) and (i).

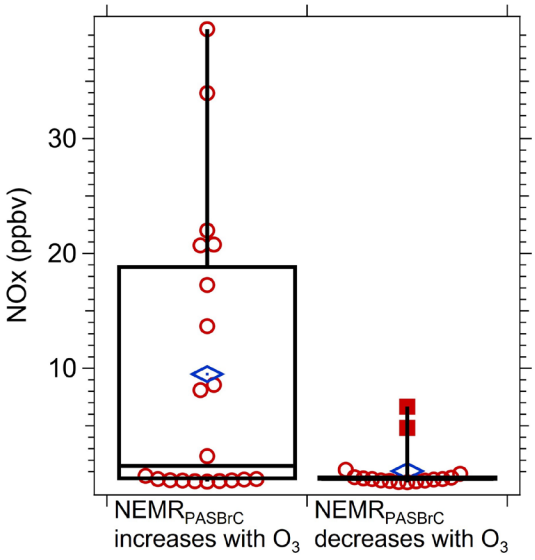

Figure 3-13 Comparison between the average NOx level across the transect for two groups of data segregated by the NEMR$_{PASBrC}$ having either a positive or negative relationship with O_3, such as shown in Figure 3-12.

3.5 Summary

Measurements of BrC based on absorption of aerosol particle chromophores in liquid solvent extracts from particles collected onto filters and BrC inferred from online measurements of total light absorption by particles in their native state with a PAS were conducted as a part of the NASA/NOAA FIREX-AQ campaign targeting wildfires burning in the western US in the summer of 2019. The emission ratio of BrC at 405 nm relative to CO is estimated to be 0.131 Mm^{-1} $ppbv^{-1}$ at 405 nm, and 0.071 Mm^{-1} $ppbv^{-1}$ for water soluble BrC and 0.163 Mm^{-1} $ppbv^{-1}$ for total soluble BrC, both at 365 nm and for light absorption in the extract solution (to convert to aerosol absorption multiply by ~1.75). The unique data set and high levels of BrC in these smoke plumes allowed detailed comparison between solvent and PAS BrC measurements. There is considerable uncertainty in the

comparison since it requires estimating the contribution of coated refractory black carbon (rBC) as a function of wavelength to the total PAS-measured absorption and a conversion factor to estimate aerosol particle BrC from measurements of BrC in a solvent extract. Considering these factors, we found that at about ~400 nm, the two methods provide similar estimates of BrC absorption. However, soluble BrC was consistently higher than the PAS BrC, with the difference increasing with decreasing wavelength from 400 to 300 nm, suggesting extrapolating the PAS-inferred BrC to below the lowest measurement wavelength of 405 nm may significantly under estimate BrC light absorption. In contrast, at wavelengths higher than roughly 400 nm, the PAS-inferred BrC was higher than the soluble BrC, but the difference was highly variable. This difference may be due to chromophores that were insoluble in the solvents utilized (water and methanol) and these insoluble chromophores absorb light more strongly at higher wavelengths than soluble species. These types of BrC species may have properties closer to BC, and are referred to as S-BrC, (strongly absorbing BrC), by Saleh (2020). Overall, the BrC aerosol in smoke observed during FIREX-AQ are in the class of M-BrC, (moderately absorbing), consistent with most emissions encountered in the campaign having a MCE of around 0.9, the boundary between smoldering and flaming burning conditions.

The evolution of BrC in the smoke plumes was also investigated. No consistent pattern of BrC evolution in the first eight hours following emission was observed. Enhancement, depletion and nearly constant $NEMR_{BrC}$ (Normalized Excess Mixing Ration of BrC, $\Delta BrC/\Delta CO$), were observed in various plumes. 4-nitrocatechol (4-NC, a known BrC chromophore) was highly depleted in more aged plumes relative to bulk BrC; after roughly 8 hours most 4-NC was gone indicating that the bulk BrC was much more stable.

Temperature-driven evaporation (T increase of 15 K) resulted in depletion of 4-NC, but had little effect on bulk BrC. Evidence was found that oxidation by O_3 in the presence of NOx might be an important pathway for BrC enhancement, while BrC was more likely to be bleached by O_3 when NOx levels were low. No other factor was found to be consistently related to $NEMR_{BrC}$.

Although the evolution of smoke in the first few hours following emission is highly complex, a few studies show that over larger time scales there tends to be a consistent loss of BrC, and there was some evidence for this in these plumes. Additional work focusing on the optical impacts of these aged species is essential, given they can impact radiative forcing over global scales (Zeng et al., 2020) on time scales of days to weeks. Similar arguments may apply to smoke toxicity, where human exposures may be dominated by highly aged smoke transported far from the fires (O'dell et al., 2021). The toxicity of very aged smoke may have substantially changed since emission.

CHAPTER 4. ASSESSMENT OF ONLINE WATER-SOLUBLE BROWN CARBON MEASURING SYSTEMS FOR AIRCRAFT SAMPLING

4.1 Abstract

Brown carbon (BrC) consists of particulate organic species that preferentially absorb light at visible and ultraviolet wavelengths. Ambient studies show that as a component of aerosol particles, BrC affects photochemical reaction rates and regional to global climate. Some organic chromophores are especially toxic linking BrC to adverse health effects. The lack of direct measurements of BrC has limited our understanding of its prevalence, sources, evolution, and impacts. We describe the first direct, online measurements of water-soluble BrC on research aircraft by three separate instruments. Each instrument measured light absorption over a broad wavelength range using a liquid waveguide capillary cell (LWCC) and grating spectrometer, with particles collected into water by a Particle-into-Liquid Sampler (CSU PILS-LWCC and NOAA PILS-LWCC) or a mist chamber (MC-LWCC). The instruments were deployed on the NSF C-130 aircraft during WE-CAN 2018 as well as the NASA DC-8 and the NOAA Twin Otter aircraft during FIREX-AQ 2019, where they sampled fresh and moderately aged wildfire plumes. Here, we describe the instruments, calibrations, data analysis, and corrections for baseline drift and hysteresis. Detection limits (3σ) at 365 nm were 1.53 Mm^{-1} (MC-LWCC; 2.5 min sampling time), 0.89 Mm^{-1} (CSU PILS-LWCC; 30 s sampling time), and 0.03 Mm^{-1} (NOAA PILS-LWCC; 30 s sampling time). Measurement uncertainties were 28% (MC-LWCC), 12% (CSU PILS-LWCC), and 11% (NOAA PILS-LWCC). The MC-LWCC

system agreed well with offline measurements from filter samples, with a slope of 0.91 and R^2=0.89. Overall, these instruments provide soluble BrC measurements with specificity and geographical coverage that is unavailable by other methods, but their sensitivity and time resolution can be challenging for aircraft studies where large and rapid changes in BrC concentrations may be encountered.

4.2 Introduction

4.2.1 Importance of Brown Carbon

Organic compounds are a major component of ambient aerosol that affect atmospheric visibility, Earth's radiation balance and human health. In the past, all organic aerosol (OA) compounds were assumed to only scatter light and exert a cooling effect (Koch et al., 2007; Myhre et al., 2008). Recent studies have shown that a fraction of OA absorbs light with a strong wavelength dependence (Andreae and Gelencsér, 2006; Lack and Cappa, 2010). These absorbing OA components are referred to as brown carbon (BrC) because they have a brown or yellow appearance when concentrated, resulting from higher absorption at shorter visible and ultraviolet (UV) wavelengths. This absorption offsets some portion of the scattering by OA. Modelling studies have suggested a non-negligible influence by BrC (Feng et al., 2013; Saleh et al., 2015; Zhang et al., 2017; Zhang et al., 2020a). Actual global measurements of BrC, using the analytical methods discussed here, have shown that BrC can contribute up to 48% of the overall warming effect globally by absorbing carbonaceous aerosols (i.e., BrC + black carbon (BC)) (Zeng et al., 2020). Due to its absorption at UV wavelengths, BrC may also suppress photolysis rates of some chemical reactions, such as decreasing surface ozone concentrations in certain locations

(Jo et al., 2016). A fraction of BrC chromophores are composed of nitro- or oxy-aromatic species (Desyaterik et al., 2013; Zhang et al., 2013), which are known toxins (Bandowe and Meusel, 2017; Tian et al., 2020), making measurements of BrC chromophores a useful tool for assessing aerosol health impacts from specific emissions (Verma et al., 2015; Gao et al., 2020a; Gao et al., 2020b). Unfortunately, ambient observations of BrC have been sparse, limiting an assessment of its impacts and the refinement of model simulations.

4.2.2 Methods of Brown Carbon Measurement

Methods to determine BrC in suspended aerosol particles can be challenging. BrC and BC are often co-emitted, and must be distinguished by their unique properties, including (1) the wavelength-dependence of their absorption; (2) volatility; or (3) solubility.

Brown Carbon Determined from Wavelength-Dependence of Absorption

The strong wavelength-dependence of BrC absorption allows it to be determined from total absorption measurements (BC + BrC) at multiple wavelengths in some cases. This requires the assumption that BrC does not absorb at mid-visible and longer wavelengths and that the absorption Ångström exponent (AAE; Absorption~λ^{-AAE}) for BC is known and constant with wavelength. AAE for BC is commonly calculated by fitting the absorption measurement based on two wavelengths in the visible wavelength range or it is simply assumed to be one. BrC absorption at shorter wavelengths is then found by difference from the extrapolated BC AAE (Lack and Langridge, 2013; Mohr et al., 2013). This approach can be applied to any technique that measures total absorption or absorption aerosol optical depth (AAOD) at multiple wavelengths, including filter-based methods,

photoacoustic spectroscopy, and remote sensing, although what is measured as BrC is operationally defined by the measurement method. Filter-based absorption measurements have existed for some time (Lin et al., 1973), and may suffer from artifacts (Bond et al., 1999; Subramanian et al., 2007; Lack et al., 2008), although correction methods have been proposed (Weingartner et al., 2003; Virkkula, 2010; Olson et al., 2015). Photoacoustic absorption spectroscopy measures aerosol light absorption at near-ambient conditions by heating particles with a controlled light source and detecting the soundwave, but is subject to interference by gaseous absorbers and sensitive to variations in temperature, pressure, and relative humidity (Arnott et al., 1999; Langridge et al., 2013). Ground-based remote sensing can determine AAOD at multiple wavelengths (Aerosol Robotic Network, AERONET; (Holben et al., 1998; Wang et al., 2016)). For each of these approaches, the AAE fitting and extrapolation introduce uncertainties, including the calculation of AAE from only a few wavelengths (typically two) and the extrapolation to shorter wavelengths to determine a relatively small BrC contribution by difference. Studies that use an assumed AAE value introduce even greater uncertainty into the determination of BrC, since a range of values for BC from 0.6-1.9 has been observed due to the coating effect (Bergstrom et al., 2007; Lack and Cappa, 2010; Lack et al., 2012a; Bond et al., 2013; Lan et al., 2013; Liu et al., 2015c; Li et al., 2016). Another BrC separation method employing an Integrating Sphere Method introduced by Wonaschütz et al. (2009) first assumes all absorption at long wavelength (660 nm) is due solely to BC, then an iterative technique is used to obtain BrC absorption based on calibration curves from simulated BC and BrC (carbon black and humic acid salt). The iteration can account for BrC absorption at longer wavelength, but there is difficulty in obtaining a calibration line for real ambient samples.

Brown Carbon Determined from Volatility

BrC may also be determined from total absorption measurements of thermally denuded and ambient samples (Cappa et al., 2012; Lack et al., 2012a). The low volatility of BC means that it remains after thermodenuding, and the difference between the total absorption and denuded absorption can be used to determined BrC absorption. Separating BrC and BC absorption using either thermodenuding or wavelength-dependence can be complicated by morphological conditions, particularly the coating of BrC onto BC that results in increased absorption through lensing (Jacobson, 2001; Schnaiter et al., 2005; Bond and Bergstrom, 2006). BC absorption can be enhanced due to a lensing effect involving an absorbing core covered by a scattering or slightly absorbing shell (Bond and Bergstrom, 2006; Cappa et al., 2012; Lack and Langridge, 2013), but a simple core-shell structure may not accurately represent the actual particle morphology, leading to further uncertainty (Sedlacek III et al., 2012). Other studies suggest this enhancement is small in certain regions (Cappa et al., 2012; Cappa et al., 2019).

Brown Carbon Determined from Solubility

Finally, BrC may be determined by extracting BrC chromophores in solvents to separate them from insoluble BC, and measuring light absorption caused by the soluble organic chromophores (Hecobian et al., 2010). This is the only method to directly separate and quantify BrC. A spectrophotometer with a UV-Vis light source and long-path liquid waveguide capillary cell (LWCC) provide high spectral resolution and high sensitivity absorption measurements over a broad wavelength range through the use of long optical pathlengths. Direct measurement of organic chromophores is also useful for studying the

prevalence and fundamental properties of BrC, such as the impact of aging on optical properties and the toxicity of chromophoric species. However there are major limitations when using this method to determine aerosol optical effects since all particle size and morphological information are lost (Liu et al., 2013) and any BrC species insoluble in the selected solvents are not included. Other limitations include pH dependent absorption, blank stability, especially when using organic solvents, and artifacts which may be introduced by extensive dilution, resulting in changes in chemical properties of chromophores relative to those of the ambient aerosol (Hinrichs et al., 2016; Phillips et al., 2017; Teich et al., 2017).

Spectrophotometric measurements of chromophores in solutions can be utilized in both offline and online systems (Hecobian et al., 2010; Liu et al., 2013; Zhang et al., 2013; Liu et al., 2015a). For offline systems, atmospheric particles are usually collected by filtration, and then extracted with a solvent, such as water, methanol, or acetonitrile (Chen and Bond, 2010), and absorptions of solvent and solute are quantified. Particle collection over a period of time onto a filter, followed by offline analyses at a later date, can lead to artifacts through filter sampling biases and changes during storage. Low time resolution and the resulting fewer data points can limit data interpretation. Among these weaknesses, poor time resolution is the most serious, especially when sampling fire plumes using a fast-moving aircraft. Online measurements can improve this, but these have only been used to measure water-soluble BrC due to the particle collection methods utilized. An online water-soluble BrC measuring system with a Particle-into-Liquid Sampler (PILS)-liquid waveguide capillary cell (LWCC), has been used in previous ground-based studies

(Hecobian et al., 2010; Washenfelder et al., 2015). Other systems can be used to collect the aerosol into water for subsequent BrC analysis, such as mist chambers (Cofer et al., 1985).

Complications Due to Intermediate Compounds

Separating BrC and BC by the wavelength-dependence of their absorption, their volatility, or their solubility is complicated by the possible existence of compounds with intermediate properties of absorption, volatility, or solubility. Some studies show evidence for the existence of intermediate BrC species, with properties between BC and BrC with a range of AAE values (Saleh et al., 2018). This intermediate BrC has been suggested to be an incompletely pyrolyzed precursor to BC that shows characteristics of both BC and BrC (Adler et al., 2019), much like what has been referred to as tar balls (Pósfai et al., 2004; Chakrabarty et al., 2010; Adachi et al., 2019) and consistent with the idea that carbonaceous light absorbing aerosol is comprised of a continuum of species from brown to black light absorbers (Cheng et al., 2021).

4.2.3 This Work

Here, we assess three systems for measuring the light absorption of water-soluble BrC (WS BrC) using either a mist chamber (MC) or PILS as the aerosol sampling system, followed by a LWCC and spectrometer (MC-LWCC and PILS-LWCC). These instruments were deployed in three separate aircraft studies of wildfire smoke. MC sampling has been used in past NASA aircraft studies (Talbot et al., 1999; Dibb et al., 2003; Scheuer et al., 2003), whereas this paper describes the first deployment of the MC-LWCC system. Similarly, PILS-LWCC instruments have been developed and used in ground-based studies (Hecobian et al., 2010; Washenfelder et al., 2015) and PILS systems have been deployed

on aircraft to measure aerosol composition (Sullivan et al., 2006; Sullivan et al., 2014; Sullivan et al., 2019), but this paper describes the first aircraft deployment of PILS-LWCC. BrC is reported in the form of light attenuation (unit of Mm^{-1}) and not converted to a mass concentration because there is no constant BrC mass absorption cross-section (MAC) value at a given wavelength as BrC is composed of multiple chromophores that change with emissions and atmospheric evolution.

4.3 Method

4.3.1 Overview of aircraft studies and brown carbon instruments

The Fire Influence on Regional to Global Environments Experiment - Air Quality (FIREX-AQ 2019; https://doi.org/10.5067/suborbital/firexaq2019/data001) and the Western Wildfire Experiment For Cloud Chemistry, Aerosol Absorption And Nitrogen (WE-CAN 2018; https://www.eol.ucar.edu/field_projects/we-can) field studies investigated the emissions and evolution of gases and aerosols from wildfires and prescribed burning to better understand fire impacts on air quality and climate. FIREX-AQ included the NASA DC-8 research aircraft (average aircraft speed of 200 m/s), which was deployed from Boise, ID and Salina, KS, USA during 22 Jul. 2019 – 5 Sep. 2019 and the NOAA Twin Otter research aircraft (average aircraft speed of 75 m/s), which was deployed from Boise, ID and Cedar City, UT, USA during 3 Aug. 2019 – 5 Sep. 2019. WE-CAN included the NSF C-130 research aircraft (average aircraft speed of 100 m/s), which was deployed from Boise, ID, USA during 22 Jul. 2018 – 14 Sep. 2018. For each campaign, large wildfires in the western United States were identified and flight plans included repeated plume intercepts to measure the smoke evolution.

The NASA DC-8, NOAA Twin Otter, and NSF C-130 payloads each included an instrument to measure the light absorption of WS BrC. These instruments employed similar approaches, but were developed separately. Briefly, ambient air was sampled through an aircraft inlet and then collected in aqueous solution using either a MC or PILS. The visible and ultraviolet absorption by the aqueous solution was determined using a deuterium/halogen lamp, LWCC, and grating spectrometer. All of the BrC measurements described in this work, including offline filter sample measurements, represent water-soluble BrC absorption coefficient. Any intermediate species that exist between BrC and BC are likely to be insoluble in water, and we treat the water-soluble BrC measurements here as being solely attributable to BrC. The three instruments are summarized in Table 4-1, and described in greater detail below.

Table 4-1 Overview of BrC instruments deployed during WE-CAN 2018 and FIREX-AQ 2019

	MC-LWCC	CSU PILS-LWCC	NOAA PILS-LWCC
Research Institution	University of New Hampshire Georgia Institute of Technology	Colorado State University	NOAA Chemical Sciences Laboratory
Field Campaign	FIREX-AQ 2019	WE-CAN 2018	FIREX-AQ 2019
Aircraft	NASA DC-8	NSF C-130	NOAA Twin Otter
Aircraft Altitude	200 – 1000 hPa	430 – 1000 hPa	630 – 1000 hPa
Inlet Pressure Control	None	None	620 hPa
Aerosol Collection	Mist chamber (Scheuer et al., 2003)	Particle-into-Liquid Sampler	Particle-into-Liquid Sampler (PILS-4001, Brechtel)
Liquid Transfer	Two syringe pumps	Syringe pumps and a peristaltic pump	Peristaltic pump
Solvent	Water	Water	Water
Aerosol Collection Efficiency and System Dilution	Standard addition of trifluoracetic acid to determine evaporative loss in mist chamber	Dilution ratio due to condensation was obtained from previous measurements	aerosol collection efficiency of 0.8 for $D_p < 1$ μm from calibration with aerosolized sucrose particles post-campaign
Removal of Gas-Phase VOCs	N.A.	Parallel plate carbon filter denuder	Parallel plate carbon filter denuder (DN-100, Sunset Laboratory)
Light Source	Deuterium and halogen lamps (DH-Mini, Ocean Optics)	Deuterium and halogen lamps (DH-Mini, Ocean Optics)	Deuterium and halogen lamps (DH-Mini, Ocean Optics)
Liquid Waveguide	2.5 m (LWCC-3250, World Precision Inst.)	2.5 m (LWCC-3250, World Precision Inst.)	2.5 m (LWCC-3250, World Precision Inst.)
Spectrometer	Ocean Optics FLAME-T-UV-VIS	Ocean Optics FLAME-T-UV-VIS	Ocean Optics QE Pro
Spectral Range	300 - 700 nm	300 - 700 nm	309 - 682 nm
Spectral Resolution	1.4 nm	1.4 nm	3.3 nm
Zero Measurement	N.A.	Filtered air measured for 10 min manually twice per flight	Filtered air measured for 6 min every 1.5 h
Detection Limit (3σ) at 365 nm	1.53 Mm^{-1}	0.89 Mm^{-1}	0.03 Mm^{-1}
Uncertainty	28%	12%	11%

4.3.2 Online Mist Chamber measurements on the DC-8 aircraft during FIREX-AQ 2019

A mist chamber-ion chromatograph (MC-IC) system has been deployed on the NASA DC-8 research aircraft in many previous missions for measurement of nitric acid and ionic particle species for all particles with sizes up to nominally 1 μm (Scheuer et al., 2003). We used the existing MC as an aerosol collection method and added a spectrophotometer for online measurement of BrC, without altering the existing MC-IC measurement capabilities. An instrument schematic is shown in Figure 4-1. The mist chamber (or Cofer Scrubber) has been extensively used to collect water-soluble gases or particles (Cofer et al., 1985; Cofer and Edahl, 1986; Spaulding et al., 2002). It must be operated vertically with the top of the mist chamber connected to a vacuum pump. Sample air flows in from the bottom and enters the mist chamber through a tube with a nozzle at the tube exit that is situated near the center of the mist chamber and then air exits the chamber at the top. Within this air jet, created by the nozzle, is a capillary that extends to near the bottom of the mist chamber. The low pressure near the air jet draws water sitting in the bottom of the chamber up the capillary, which breaks up the water into many small droplets within the air jet. The droplets and jet create a fine and uniform mist throughout the chamber, which is maintained in the chamber by a hydrophobic Teflon filter at the top of the mist chamber that limits most of the water from leaving with the sample air that is continually being drawn through the chamber (Cofer et al., 1985). Droplets impact on this filter and the walls, keeping all internal surfaces wet and draining to the liquid reservoir at the bottom, where it is continuously recycled through the jet during the sample collection period. After the sample collection period, liquid is removed from the chamber and analyzed. For the BrC measurement, this involves transferring the liquid sample via a

syringe pump with an associated multiport selection valve to a 2.5 m long liquid waveguide capillary cell (LWCC-3250; World Precision Instruments, Sarasota, FL, USA, internal volume of 0.625 mL). The LWCC was coupled to a deuterium/halogen light source with spectral output from 200–2500 nm (DH-mini Light Source, Ocean Optics, Dunedin, FL, USA) and spectrometer (FLAME-T-UV-VIS, Ocean Optics, Dunedin, FL, USA). Light absorption was measured and recorded between nominally 300 nm and 900 nm. A particle filter with 0.22 μm pore size (Polypropylene, Tisch Scientific, North Bend, OH, USA) was installed in front of the LWCC to prevent the long capillary from becoming clogged and to limit contributions of insoluble particles larger than 0.22 μm to the liquid absorption measurement. During the FIREX-AQ study, the liquid particle filter was replaced and rinsed with water at the beginning of every flight. The LWCC system was connected to the MC through a single channel on a multiport selection valve downstream of the syringe pump. A portion of the MC liquid sample was analyzed with an IC and the remaining liquid in the chamber was directed to the LWCC through this separate channel. In this configuration, it did not affect the performance of the pre-existing IC system for water-soluble ion quantification. Since the particle collection with the mist chamber was operated in batch mode, two MCs with identical corresponding syringe pumps operated alternatively, one sampling while the other was offline and the liquid sample was undergoing analysis. For example, a typical sampling sequence was as follows. The first MC (MC1 in Figure 4-1) was filled with 12 mL of water via the syringe pump, and then the valve before the vacuum pump switched to allow sampling of ambient air at ~50 SLPM in that chamber. After 150 s of sampling, this valve was switched to sample from MC2 which had been flushed and contained 12 mL of water in preparation for sample collection.

Now offline, the syringe pump for MC1 withdrew 6 mL of water and directed 3 mL through the 2.5 m LWCC. Absorbance spectra were recorded when sample pumping was completed, meaning that the liquid tubing/filter (green path in Figure 4-1) and the LWCC had been flushed by about 3 volumes prior to the absorption measurement and the flow was stopped. After analysis and removal of any remaining sample liquid from the offline chamber, MC1 was then cleaned by flushing with 10 mL of water, but with no air flow. MC1 was inactive until the start of the next sampling cycle of sampling. Once air sampling had begun by MC1, the liquid in MC2 was injected into the LWCC and IC, then MC2 was cleaned. Liquid sample lines were 0.76 mm ID peek tubing and the volume between the MC and LWCC was 0.5 mL. There was a 166 s total time lag between the beginning of the actual sampling and the time the light absorbance spectrum was recorded.

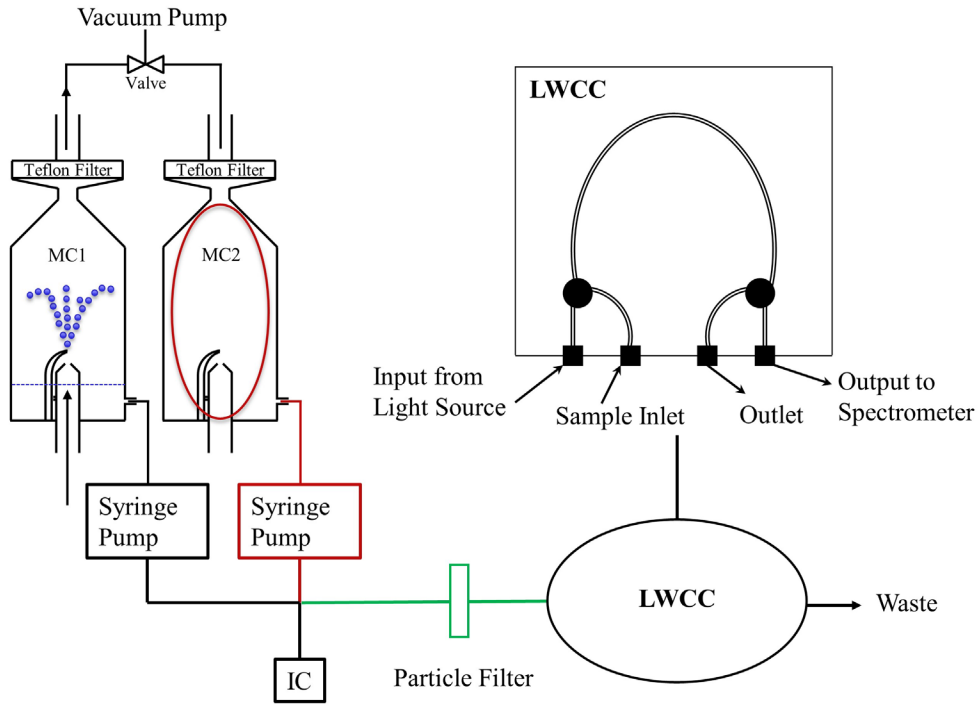

Figure 4-1 Flow diagram of the MC-LWCC instrument for WS BrC. Blue dots represent the mist generated in the scrubber. Red lines are the first hysteresis components described in Section 4.4.3, and green lines are the second components.

A reference spectrum of pure solvent (water) was generated at the beginning of every flight at every wavelength ($I_0(\lambda)$ in Eqn (4)), and the light absorbance ($log_{10}\left(\frac{I_0(\lambda)}{I(\lambda)}\right)$) was quantified by the spectrometer over the full spectrum. The integration time of the spectrometer was usually less than 0.1 s to keep the intensity at 365 nm in the range of 25,000 to 30,000 counts (i.e., below saturation). An internal standard of known aqueous concentration of trifluoroacetic acid (7.5 ppbm TFA) was added to the water supplied to the MC to track any evaporative loss of water from the MC during sampling, which was monitored with the MC-IC system. TFA did not interfere with the absorption measurement in the 300 nm to 700 nm wavelength range.

4.3.3 Online PILS measurements on the NSF C-130 aircraft during WE-CAN 2018

Unlike the mist chamber system, the PILS is run in a continuous sampling mode. The instrument operates by condensing water vapor onto particles with a saturated steam flow, and then using a single jet inertial impactor to collect the droplets onto a vertical impaction plate that is continually washed with a constant diluent flow (Weber et al., 2001; Orsini et al., 2003). Compared to a mist chamber, the PILS uses smaller liquid volumes, a smaller sampling flow rate, and produces a continuous liquid sample flow. The Colorado State University (CSU) PILS-LWCC system was similar to the one used in previous ground-based studies (Hecobian et al., 2010), and the schematic is shown in Figure 4-2a. Ambient air was sampled with a Submicron Aerosol Inlet (SMAI) (Craig et al., 2013a; Craig et al., 2013b; Craig et al., 2014; Moharreri et al., 2014) and passed through a nonrotating Micro-orifice Uniform Deposit Impactor (MOUDI) with a 50% transmission efficiency at 1 μm (aerodynamic diameter) at 1 atmosphere ambient pressure (Marple et al., 1991). The total airflow of the PILS was 15 SLPM (volumetric flow was controlled by a critical orifice). An activated carbon parallel plate denuder (Eatough et al., 1993) was placed upstream of the PILS to remove organic gases. The sample air then mixed with saturated water vapor (steam) in the growth chamber, and all particles in the sample air nominally larger than 40 nm grew to a few microns in size, and were then collected by impaction. The impaction plate was continually washed with a pure water transport flow of 1.3 mL/min dictated by the needs of the Total Organic Carbon Analyzer (Sievers M9 Portable TOC Analyzer; SUEZ Water Technologies & Solutions, Trevose, PA, USA) that was placed after the LWCC to quantify water-soluble organic carbon (WSOC). The liquid sample obtained from the PILS was then passed through a blown-glass debubbler, resulting

in a liquid sample free of air bubbles at a flowrate of 1.2 mL/min, which was then filtered by a 0.2 μm pore size PTFE liquid particle filter (Whatman plc, Maidstone, UK) to remove larger insoluble particles. The flow was then directed through a 2.5 m liquid waveguide capillary cell (LWCC-3250, World Precision Instruments, Sarasota, FL, USA) and TOC Analyzer for near real-time measurement of WS BrC and WSOC, respectively. The LWCC was coupled to a deuterium/halogen light source (DH-mini Light Source, Ocean Optics, Dunedin, FL, USA) and spectrometer (FLAME-T-UV-VIS, Ocean Optics, Dunedin, FL, USA), the same model LWCC and spectrophotometer as used with the MC-LWCC and offline filter sampling system discussed below.

All liquid sample lines were 0.51 mm ID PEEK tubing. The liquid handling for the flows to and from the impactor used two pairs of syringe pumps with 1 mL syringes operating in handshaking mode. This minimized contamination observed by peristaltic pumps in previous ground-based studies, and provided more precise flow control for aircraft sampling with rapid changes in ambient pressure. One pair of syringe pumps delivered the transport flow to the top of the PILS impactor and the other pair withdrew the sample out of the PILS and pushed it through the liquid filter and to the LWCC and TOC Analyzer. A peristaltic pump handled other liquid flows to operate the PILS (see Figure 4-2a). Using syringe pumps to move sample liquid to the LWCC has a major disadvantage because it alters the relationship between sample collection and analysis in each syringe stroke; the first liquid into the syringe is the last out (and last sample in is the first out), assuming minimal mixing in the syringe. This results in a roughly 1-minute (50 s) loss in sample time resolution (volume of syringe is 1 mL, flowrate 1.2 mL/min). The LWCC internal volume of 0.625 mL and liquid flow rate of 1.2 mL/min means the light

absorption measurement is also averaged over a 32 s interval. The absorbance spectrum was saved every 16 s. Because of these effects, the time resolution of this method was roughly 1 minute. Periodic background measurements were made by manually switching a valve upstream of the PILS to direct sample air through a Teflon filter for 10 min. A dilution factor of 1.33 was used to account for dilution from steam condensation.

4.3.4 Online PILS measurements by NOAA on the NOAA Twin Otter aircraft during FIREX-AQ 2019

The NOAA PILS-LWCC instrument was developed separately, but followed the approach first described in Hecobian et al. (2010) and is similar to the CSU PILS-LWCC system. The key differences of the NOAA PILS-LWCC system included: (1) a pressure-controlled aerosol inlet with constant PILS gas flow; (2) an automated valve and aerosol filter to record aerosol-free background measurements in flight; (3) a five-channel peristaltic pump for all liquid flow transfer, including the sample lines in and out of the PILS impactor. These details and the full system are described below. The schematic of the NOAA PILS-LWCC is shown in Figure 4-2b.

During FIREX-AQ, the NOAA PILS-LWCC sampled from a forward-facing, near-isokinetic inlet (Schwarz et al., 2006; Perring et al., 2013) on the NOAA Twin Otter aircraft. The inlet flow was actively pressure-controlled at 620 hPa using a flow restriction, pressure controller, and scroll pump. The total inlet sample flow of 8.13 SLPM passed through an impactor (TE296, Tisch Environmental, Cleves, OH, USA) with a measured 50% cut point at 0.95 μm, and was then distributed to the aerosol instruments onboard the NOAA Twin Otter. The PILS-LWCC sampled the incoming aerosol flow through an automated valve

(MDM-060DT; Hanbay Laboratory Automation, Pointe Claire, QC, CAN) with filter (116IL; Headline Filters Limited, Aylesford, Kent, UK) for periodic, automated measurements of the aerosol-free background that were performed for 6 min every 1.5 h. A parallel-plate carbon filter denuder (DN-100; Sunset Laboratory, Tigard, OR, USA) removed gas-phase volatile organic compounds (VOCs). Pressure and temperature of the flow were recorded at 1 Hz.

The PILS (PILS 4001; Brechtel Manufacturing Inc., Hayward, CA, USA) collected aerosol in solution using a steam generator, droplet impactor, and five-channel peristaltic pump, with an average liquid output flow from the impactor of 1.53 mL/min. The sample air flow into the PILS was maintained at a constant 6.0 SLPM using a 1.35 mm diameter critical orifice (Lenox Laser, Glen Arm, MD, USA) between the PILS and the scroll pump. The pressure-controlled inlet and constant gas flow had two advantages for the PILS-LWCC: (1) The steam temperature within the PILS varies with pressure according to the Clausius-Clapeyron equation, and maintaining a constant gas pressure within the PILS allowed more stable behavior and better characterization of the PILS collection efficiency; (2) The liquid flow from the peristaltic pumps was found to vary with the system pressure, and maintaining constant upstream pressure improved the system stability and accuracy. Bubbles were removed using a commercially-available flow-through debubbler (Omnifit 006BT; Diba Industries, Inc., Danbury, CT; modified by Brechtel Manufacturing Inc) consisting of a porous PTFE membrane under vacuum.

Following the PILS, a particle filter with 0.2 μm pore size (Puradisc 25 TF; GE Healthcare Life Sciences, Pittsburgh, PA, USA) removed insoluble components from the liquid sample stream before it entered the 2.5 m-long LWCC, which is the same model

used in the other instruments (LWCC-3250, World Precision Instruments, Sarasota, FL, USA). Subsequently, 1.1 mL/min was sampled by a TOC analyzer (M9 Portable TOC Analyzer; GE Analytical Instruments Inc., Boulder, CO, USA) for measurement of WSOC and the excess flow (~0.43 mL/min) was directed by an automated 14-port valve (C25Z; Vici Valco Instruments, Houston, TX, USA) to a series of 12 polypropylene sample tubes for offline analysis or to a waste container.

Similar to the CSU PILS-LWCC, the optical system consisted of a deuterium/halogen light source nm (DH-mini; Ocean Optics Inc., Dunedin, FL, USA) coupled to the LWCC, however in this case, the exiting light was coupled to a 101 mm focal length symmetrical cross Czerny-Turner spectrometer with a 18-bit back-thinned 1024 × 58 pixel CCD array detector cooled to -5 deg C (QE Pro; Ocean Optics Inc., Dunedin, FL, USA). The spectrometer contained a 600 groove/mm grating (300 nm blaze wavelength) rotated to give a useful spectral range from 309 to 682 nm. The entrance slit was 200 μm wide × 1000 μm tall, and was illuminated by a fiber bundle containing a linear array of 200 μm diameter UV/Vis fibers. 50 spectra with 0.02 s integration time were averaged to 1 Hz and saved. Following the field campaign, the collection efficiency of the PILS system at 620 hPa was measured using atomized sucrose aerosol, and the BrC absorption and WSOC concentrations were subsequently corrected by a factor of 1.25. Since this system used a peristaltic pump (in contrast to the syringe pump of the CSU PILS-LWCC system) to move liquid sample from the PILS to the LWCC, the time resolution should be improved. At a liquid sample flow rate of 1.53 mL/min through the LWCC of internal volume 0.625, the maximum possible time resolution would be 25 s, assuming no

other interferences. The observed time resolution is 60 s, likely due to sample mixing at the PILS impaction plate, liquid fittings, and other instrument components.

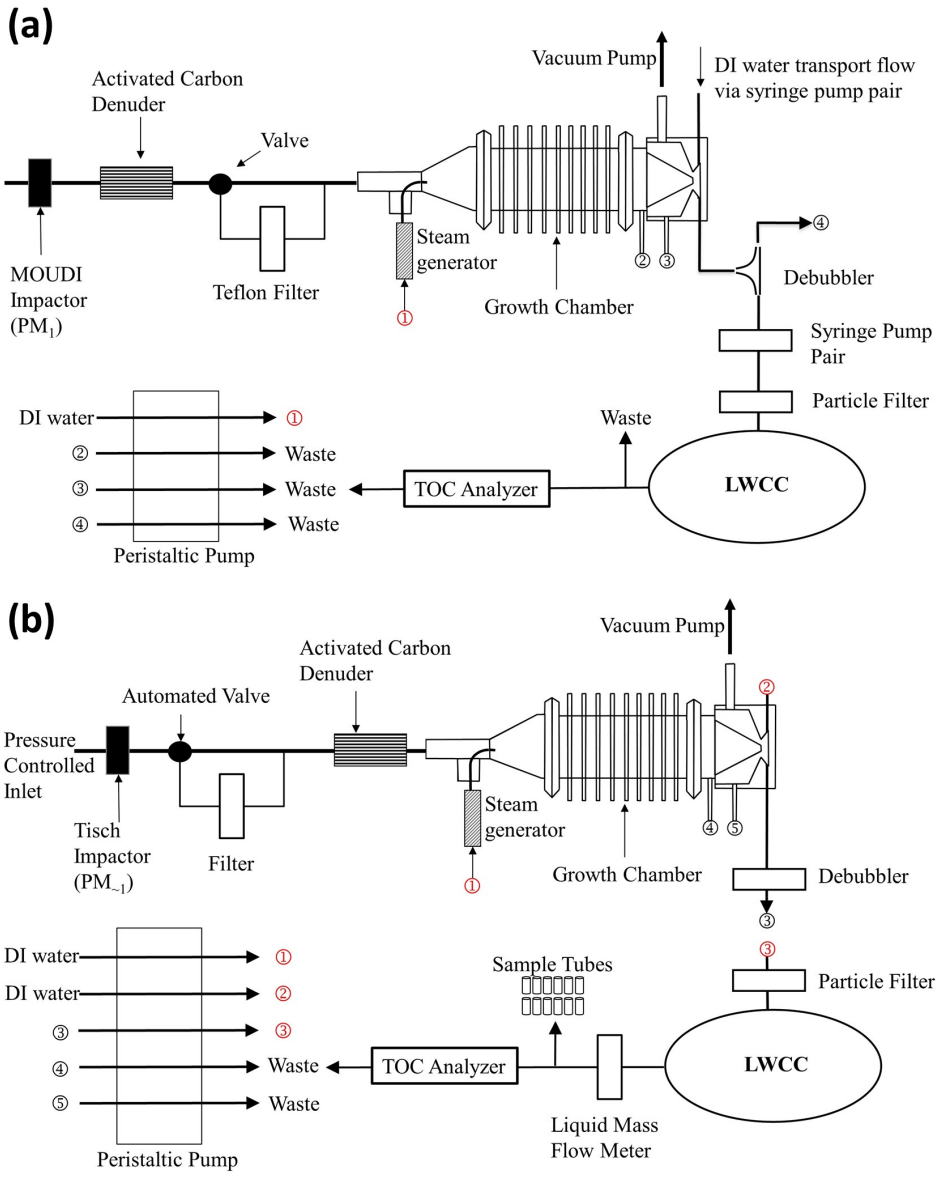

Figure 4-2 Flow diagrams of the (a) CSU PILS-LWCC and (b) NOAA PILS-LWCC instruments for WS BrC. For the CSU PILS-LWCC, a combination of syringe and peristaltic pumps was used for handling the liquid flows. For the NOAA PILS-LWCC, a peristaltic pump was used for all flows.

4.3.5 *Offline measurements from filter samples on the DC-8 aircraft during FIREX-AQ 2019*

Filters were also collected as part of the FIREX-AQ NASA DC-8 measurement suite and BrC was determined offline with the same analytical method used in previous missions (i.e., NASA SEAC^{4}RS, DC3, and ATom, which are described in detail elsewhere (Liu et al., 2014; Liu et al., 2015a; Zhang et al., 2017; Zeng et al., 2020)). Atmospheric particles with aerodynamic diameters less than nominally 4.1 μm were collected onto 90 mm diameter Teflon filters with 1 μm pore size (MilliporeSigma, Burlington, MA, USA) (McNaughton et al., 2007). During plume sampling, each filter sample was timed to (as best as possible) coincide with a transect through a single smoke plume. During other periods, sampling times were generally 5 min or less when sampling at altitudes below 3 km and increased to a maximum of 15 min for higher altitudes. Subsequently, the filters were extracted first into 15 mL of water via 30 min of sonication and then using a syringe pump, extracts were filtered and injected into a 2.5m LWCC (LWCC-3250, World Precision Instruments, Sarasota, FL, USA), coupled with the same light source and spectrometer (USB-4000, similar to FLAME-T-UV-VIS, Ocean Optics, Dunedin, FL, USA). The air filters were dried passively and then extracted again in 15 mL of methanol, and this extraction liquid was filtered and injected with the syringe pump into the LWCC. Only the water extracts are discussed here for comparison to the MC-LWCC. The same type of 0.22 μm pore size particle filter as the online system was installed in front of the LWCC to filter out insoluble particles for both the water and methanol extracts, and the particle filter was changed every 5 to 20 samples depending on the sample concentration. Overall, the spectrometer was operated in the same way as the online MC system. Some

samples collected in thick fire plumes were diluted to prevent saturation of the raw absorbance signal. Due to high organic concentrations in the filter extracts, the waveguide required periodic cleaning. Contamination was observed as the signal intensity for pure solvent, $I_0(\lambda)$, decreasing as contaminates accumulated in the waveguide. Flushing the waveguide with a large volume (50 mL) of water was generally sufficient to clean it, but occasionally a stronger cleanser (10% of Contrad-NF, Decon Labs, King of Prussia, PA, USA) was used, as recommended by the manufacturer.

4.3.6 Calculation of light absorption for PILS-LWCC, MC-LWCC, and filter samples

Light absorption by the liquid in the LWCC is described by Beer's Law:

$$Abs_{solution}(\lambda) = c_{solution} \cdot \sigma_{solution}(\lambda) = \frac{1}{l} \cdot log_{10}\left(\frac{I_0(\lambda)}{I(\lambda)}\right) \quad (5)$$

where $Abs_{solution}(\lambda)$ is the absorption of the solution, c is concentration, $\sigma_{solution}(\lambda)$ is the mass absorption efficiency, l is the LWCC cell length, $I_0(\lambda)$ is light intensity in the absence of the absorber, which is the spectrum of pure water, and $I(\lambda)$ is light intensity with the absorber present. This can be converted to an absorption coefficient for the aerosol:

$$Abs_{aerosol}(\lambda) = \frac{V_{solution} \times log_{10}\left(\frac{I_0(\lambda)}{I(\lambda)}\right)}{V_{air} \times l} \times ln(10) \quad (6)$$

For online PILS-LWCC measurements, $V_{solution}$ is the liquid sample flow rate and V_{air} is the air flow rate. For the MC-LWCC and offline filter measurements, $V_{solution}$ is the liquid sample volume for extraction and V_{air} is the sampled volume of air. The light absorption determined from Eqn (6) is not directly equivalent to the ambient particle light absorption coefficient due to Mie effects. To determine the absorption that would be observed in the particle phase, the solution-phase absorption must be corrected as described previously (Liu et al., 2013; Zeng et al., 2020). The correction can be calculated from the imaginary part (k) of the aerosol complex refractive index, m = n + ki, and the measured size distribution. In this work, we report only the light absorption from water-soluble chromophores, calculated from Eqn (6).

The absorption coefficient at 365 nm (Abs_{365nm}) is used to represent WS BrC absorption in the analysis and figures, and is determined by averaging from 360 nm to 370 nm. Abs_{675nm} (670–680 nm average) or Abs_{700nm} (695–705 nm average) is used as a baseline to monitor any air bubbles or insoluble BC passing through the liquid particle filter (pore -size: 0.22 μm for MC and filter; 0.2 μm for PILS) with the assumption BrC does not absorb light in these wavelength ranges. All absorption coefficient data have been blank corrected by water blanks for MC-LWCC and field blanks for PILS-LWCC by switching the upstream valve. Data from the MC-LWCC and PILS-LWCC instruments were time-corrected due to delays in the liquid flow system between sampling and analysis.

4.3.7 Other Measurements

Carbon monoxide (CO) is emitted by biomass burning and is relatively chemically inert. It is often used as a marker for smoke and as a tracer for determining plume dilution.

For the NASA DC-8 during FIREX-AQ, CO was measured with a diode laser spectrometer method (Differential Absorption Carbon Monoxide Measurements; DACOM; (Warner et al., 2010)). For the NSF C-130 during WE-CAN, CO was measured by a quantum cascade laser instrument (CS-108 miniQCL, Aerodyne Research Inc., Billerica, MA, USA). For the NOAA Twin Otter during FIREX-AQ, CO was measured by cavity ringdown spectroscopy (G2401-m; Picarro Inc., Santa Clara, CA, USA; (Crosson, 2008; Karion et al., 2013)).

Refractory Black Carbon (rBC, or just BC) was measured by a single particle soot photometer (SP2) on the DC-8 and the C-130 aircraft. The SP2 measures the incandescent signal generated from single particles heated by a laser source, which is proportional to their mass (Schwarz et al., 2008). The SP2 measured rBC particles with mass equivalent diameters between ~90 – 550 nm on the DC-8 during FIREX-AQ and ~90 – 500 nm on the C-130 during WE-CAN. Higher frequency CO and BC data were merged to the MC-LWCC, PILS-LWCC or filter collection times as needed. BC was not measured on the NOAA Twin Otter.

4.4 Results and Discussion

4.4.1 Brown Carbon Measurements in Smoke Plumes

Example flight tracks downwind of wildfires are shown in Figure 4-3 for the three aircraft. Each of these flights sampled a single fire complex, with initial transects close to the source, followed by a pattern of downwind transects ideally perpendicular to the dominant wind direction. This type of sampling was repeated for numerous fires

throughout each field study. The corresponding time series of Abs_{365nm} and baseline Abs_{700nm} (Abs_{675nm} for NOAA PILS-LWCC) for these flights are shown in Figure 4-4. One Hz CO concentrations are plotted to identify when the aircraft was in smoke and indicate smoke concentrations. The peak CO values decreased downwind as the plumes dispersed and diluted with cleaner background air as they advected away from the fire.

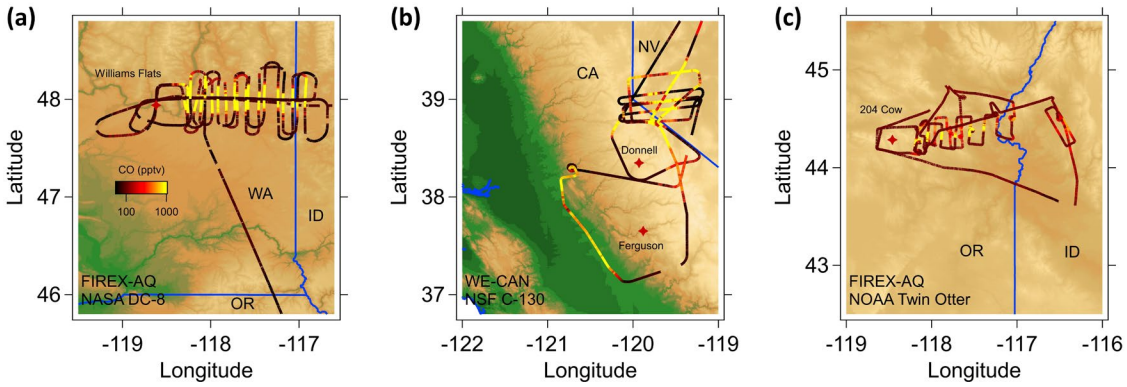

Figure 4-3 Examples of flight tracks for measurements made near and downwind of fires in the western USA for (a) the NASA DC-8 on 7 Aug. 2019 in FIREX-AQ (MC-LWCC); (b) the NSF C-130 on 6 Aug. 2018 in WE-CAN (CSU PILS-LWCC); (c) the NOAA Twin Otter on 24 Aug. 2019 in FIREX-AQ (NOAA PILS-LWCC). Each flight is color coded by the CO mixing ratio. Fires are labelled as red stars.

For these methods, in general, Abs_{365nm} has a similar trend with CO, but there are discrepancies. For the NASA DC-8 sampling during FIREX-AQ, the typical transit time through the plume was ~3 min; the MC-LWCC sample time was 2.5 min, thus the sampling frequency with this instrument was not sufficient to resolve structure within the plume during one transect. In contrast, the PILS-LWCC on the NSF C-130 and NOAA Twin Otter provided better time resolution. The average time for both the NSF C-130 and NOAA Twin Otter to transit a plume was ~4 min since their air speeds were lower than the DC-8. The

data for all three systems show an increase in baseline (Abs_{700nm} or Abs_{675nm}) within the plumes and there is evidence of hysteresis in the BrC measurements. Both of these issues are discussed next.

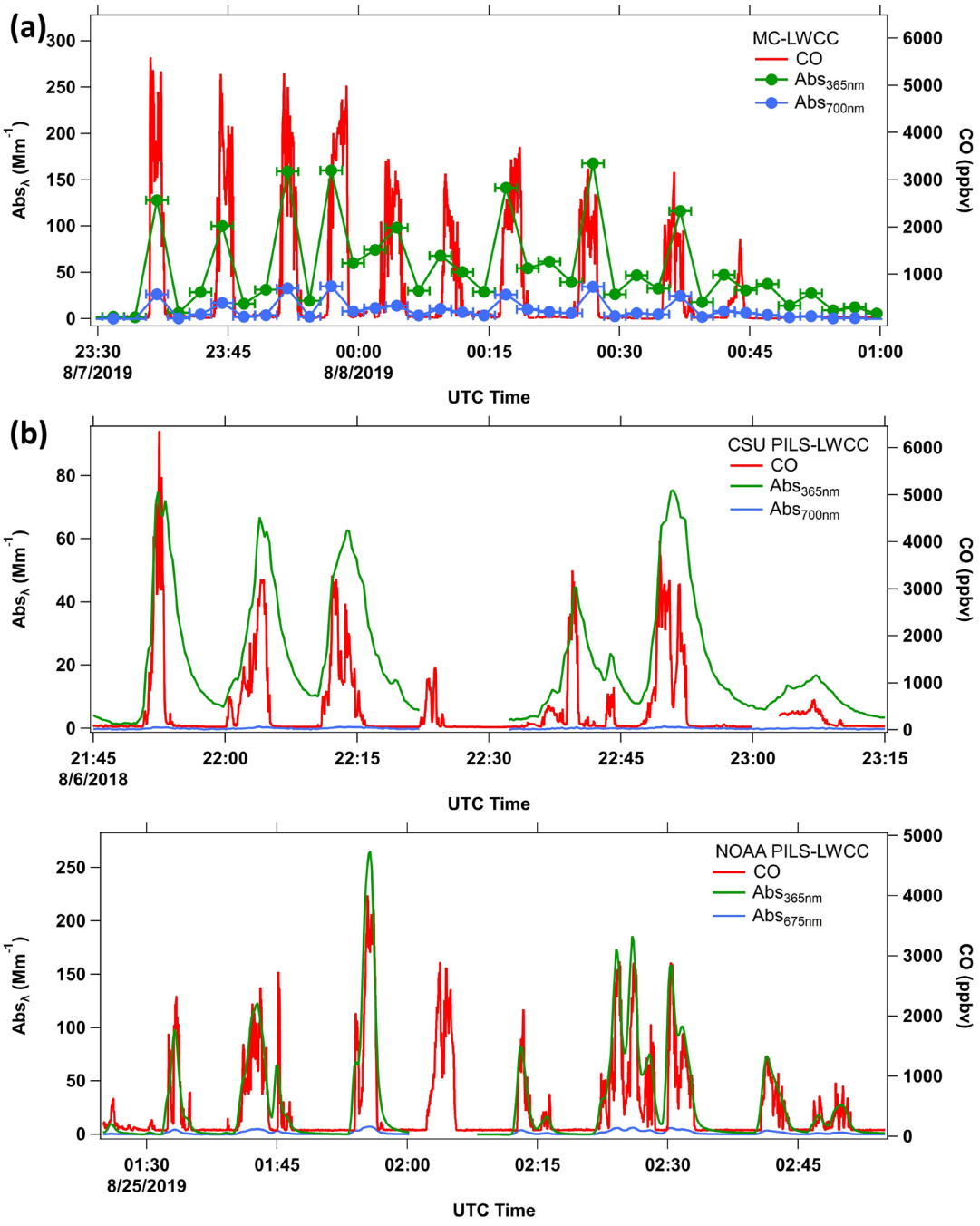

Figure 4-4 Example data from sampling in smoke plumes by MC-LWCC and PILS-LWCC (CSU and NOAA) systems for the flights shown in Figure 4-3. Time series of Abs_{365nm} (green), Abs_{700nm} or Abs_{675nm} (blue), and CO (red) for the (a) FIREX-AQ NASA DC-8 flight on 7 Aug. 2019, (b) WE-CAN NSF C-130 flight on 6 Aug. 2018, and (c) FIREX-AQ NOAA Twin Otter flight on 24 Aug. 2019. The sampling frequencies were (a) MC-LWCC 2.5 min; (b) CSU PILS-LWCC 16 s; (c) NOAA PILS-LWCC 10s; and CO 1 s. Horizontal error bars in (a) represent the MC sampling interval.

4.4.2 Baseline drift correction using long-wavelength absorption

The accuracy of $Abs(\lambda)$ calculated from Eqn (6) may be limited by drift in $I(\lambda)$. Potential sources of drift in $I(\lambda)$ include air bubbles in the LWCC, variable levels of insoluble BC that passed through the particle filter, or changes in the light source intensity. Measured absorption at visible wavelengths can be used as a correction for air bubbles or insoluble BC in the LWCC. The presence of insoluble BC has been reported by Phillips and Smith (2017) for methanol extracts. They observed that the long-wavelength absorption decreased when filtering the liquid extract with smaller pore size particle filters. We use Abs_{675nm} or Abs_{700nm} for corrections here. This requires the assumption that WS BrC does not absorb at 675 or 700 nm.

MC-LWCC: Figure 4-4a shows that Abs_{365nm} is correlated with CO, with some differences. Abs_{700nm} is generally less than ~0.5 Mm^{-1} when sampling background air, but increases with Abs_{365nm} in smoke plumes. Air bubbles or small insoluble black carbon particles that pass through the particle filter may lead to elevation of Abs_{700nm}as well as Abs_{365nm}. The scatter plot between Abs_{365nm} and Abs_{700nm} for all samples is shown in Figure 4-5a. There are two groups of data. Red data points are typical BrC measurements that have high absorption at short wavelength but insignificant absorption at long wavelength, and Abs_{700nm} is possibly due to the penetration of small BC particles through the liquid filter. Blue data points are interpreted to be small air bubbles in the sample liquid that were introduced during the syringe pump valve switching or due to leaks at liquid sample-line joints. The result is an upward shift of the complete absorption spectrum,

which is consistent with a regression slope between Abs_{365nm} and Abs_{700nm} of approximately 1, and this error can be corrected by subtracting Abs_{700nm} from $Abs(\lambda)$.

In most cases, however, the presence of Abs_{700nm} is likely due to a fraction of BC, which absorbs light at higher wavelengths (e.g., 700 nm), that passed through the 0.22 μm particle filter. Abs_{700nm} is found to have a good correlation (Figure 4-5e, R^2=0.65) with BC mass concentration consistent with BC as a potential contributor of long wavelength absorption. These data suggest the MC-LWCC is at least somewhat effective at collection of insoluble species into water.

Filters: In contrast to the MC system, when using a filter as the particle collection method Abs_{700nm} does not have any correlation with Abs_{365nm}, and the magnitude of Abs_{700nm} is much smaller compared to that for the MC. The random interference at Abs_{700nm} is not likely due to BC as $\mathrm{Abs}_{700\mathrm{nm}}$ is independent of the BC mass concentration, as shown in Figure 4-5f. The filter collects insoluble particles, but apparently the water extraction process does not efficiently move these particles from the filter to the extraction water in comparison to the MC-LWCC.

CSU and NOAA PILS-LWCC: A slight, but much smaller increase in the light absorption at high wavelengths is seen in the CSU (Figure 4-4b) and NOAA PILS-LWCC data (Figure 4-4c). Similar scatter plots, Figure 4-5c and 5d, were made for data from the CSU PILS-LWCC and the NOAA PILS-LWCC, where the data were classified by flight using different colors. For the CSU PILS-LWCC, the slope of Abs_{365nm} to Abs_{700nm} varies between flights, whereas for the NOAA PILS-LWCC a similar relationship was seen for different flights. Comparing the CSU PILS-LWCC Abs_{700nm}light absorption in Figure

4-5g shows in most flights some relationship to BC, or no relationship for a few flights. (A similar plot is not included for the NOAA PILS since no BC data were available). The results suggest that some BC contributed to the PILS-LWCC measurement, but it was minor compared to the MC-LWCC (note, difference in axis scales). Previous studies have indicated that the PILS is not a good collector for water-insoluble species (Peltier et al., 2007). Since this analysis suggests it is largely due to some fraction of BC being included in the BrC measurement, this BC interference can be removed.

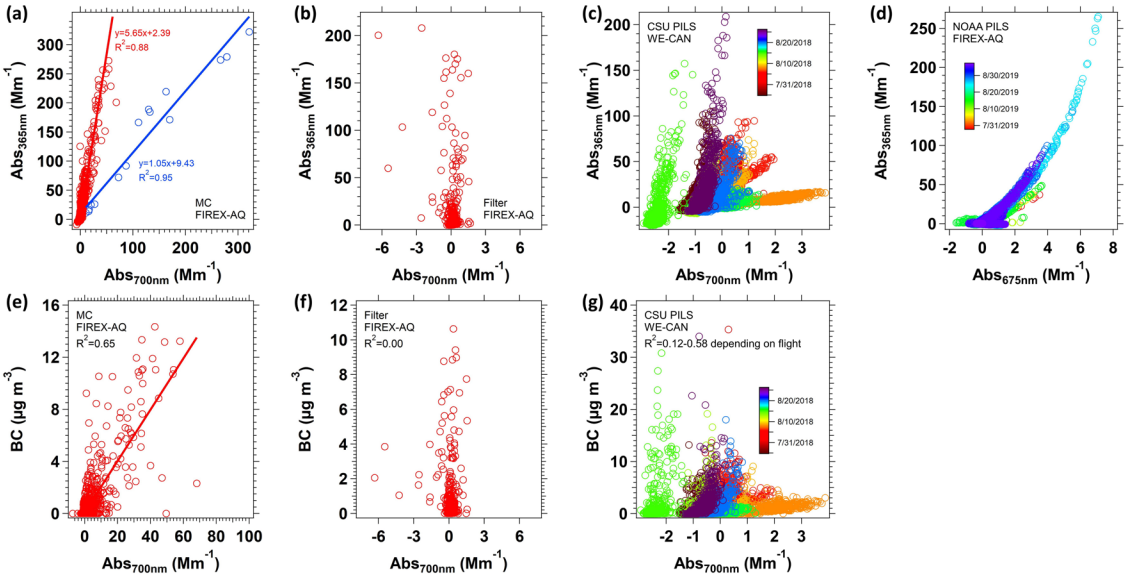

Figure 4-5 Scatter plots between Abs_{365nm} and baseline (Abs_{700nm}; Abs_{675nm} for NOAA PILS) with (a) MC, (b) filter, (c) CSU PILS, and (d) NOAA PILS. The corresponding scatter plots between Abs_{700nm} and BC are shown in (e, f, and g). For the (a) MC-LWCC system, two groups of data are classified visually and fit with an orthogonal distance regression. Red data is the baseline drift due to BC passing the particle filter, and blue data is because of small air bubbles in the LWCC. For PILS-LWCC (c and d), data are color coded by sampling date.

Baseline Correction: $Abs(\lambda)$ can be corrected for absorption by insoluble BC by assuming that AAE_{BC} = 1 and Abs_{700nm} is due to BC with no contribution from BrC. These are the same assumptions that other optical instruments use to infer BrC from total light absorption, as described in the introduction. With the assumption that $\mathrm{Abs}_{700\mathrm{nm}}$ is solely due to BC, $\mathrm{Abs}_{365\mathrm{nm}}$ due to BC can be estimated to be equal to $(365/700)^{-1} \times Abs_{700nm}$. According to the slope of the red line in Figure 4-5a, BC contributes to about one third of $\mathrm{Abs}_{365\mathrm{nm}}$ measured with the MC. Alternatively, one can simply subtract the measured absorption at all wavelengths, including (Abs_{365nm}) by $\mathrm{Abs}_{700\mathrm{nm}}$ (BrC, or corrected $Abs_{365nm} = Abs_{365nm} - Abs_{700nm}$). This simplified method results in 25% overestimation of BrC for the MC data compared to estimating the contribution of BC as a function of wavelength (BC AAE=1). Therefore, in the following analysis for the MC-LWCC system, WS BrC was calculated by $WS\ BrC = Abs_{365nm} - (365/700)^{-1} \times Abs_{700nm}$. For the CSU PILS-LWCC, the overestimation is between 2 and 5% as BC is not as efficiently collected and transported to the LWCC. Thus, in the following only the simplified method is used to correct for BC interference, that is CSU $WS\ BrC = Abs_{365nm} - Abs_{700nm}$. The same approach was used for the filter data. No correction for BC in the NOAA PILS data is made because of an observed slow baseline drift for 365 nm and 675 nm absorption, possibly caused by independent drifts in the output of the deuterium lamp (~200 - 400 nm) and halogen lamp (~400 -1600 nm) within the DH Mini light source. In any case, as noted above, the correction would be small (<5%).

4.4.3 Hysteresis

An effect of retention of liquid on the internal wetted components (Gomes et al., 1993) or within dead volumes (i.e., poorly flushed volumes within fittings or components) in the instrument is an observed hysteresis, which appears as a tail or asymmetry in measurement peaks toward larger times. As seen in Figure 4-4, WS BrC (Abs_{365nm}) demonstrates hysteresis when the aircraft exited a smoke plume for both the MC-LWCC and PILS-LWCC systems, whereas the CO mixing ratio decreases sharply (i.e., any hysteresis associated with the CO measurement is much less). The hysteresis in WS BrC results in it being overestimated when the aircraft moves out of a polluted region to a cleaner environment due to high residual concentrations from the previous run. Conversely, when moving from a region of low to high concentration, such as entering the smoke plume, cleaner sample liquid from the previous airmass sampled can dilute the current measurement, resulting in an underestimation of the BrC levels. The hysteresis effect is most obvious when the plume concentration changes significantly during a short period. These large hysteresis effects can to some extent be removed.

MC-LWCC: For the MC BrC measurement system, liquid remains in the MC, syringe, and liquid lines associated with a specific MC (red in Figure 4-1, this whole group is referred to as just the MC) and in the common sample line and liquid filter shared by both MCs (green in Figure 4-1) from the previous sample, although these common lines are flushed with sample prior to the measurement to minimize some of the latter hysteresis effect. Some fraction of the hysteresis can be removed by estimating its contribution based on comparison to a measurement that is not as affected by hysteresis, such as the CO measurement. The approach is based on two assumptions: (1) The volume fraction due to residues from the previous run does not change, making a constant hysteresis effect, no

matter dilution or enrichment; (2) The WS BrC level is zero (or at least much lower compared to in the plume) when the CO concentration is at background concentrations, in this case we assume this occurs if CO < 80 ppbv. For i-th MC sample, we decompose the hysteresis into two components: (1) residue from a previous run of the same MC used to collect the currently analyzed sample, which, since there are two MCs running alternatively, is sample from the (i-2)-th sample (i.e., red components in Figure 4-1) and (2) residue from the tubing transporting the liquid from the MC to the LWCC (including the particle filter) which comes from the (i-1)-th (i.e., immediately preceding) sample (green components in Figure 4-1). We pick time periods when the DC-8 was exiting fire plumes, in which case the observed WS BrC signals following the smoke plumes were ideally all due to contribution from the previous airmass sampled.

We assume the observed WS BrC absorption at the i-th sample is due to $a\%$ of the real WS BrC during the time period of the i-th sample, $b\%$ due to (i-1)-th sample from the tubing, and $c\%$ due to (i-2)-th sample from the MC. Based on mass conservation, the relationship between the coefficients and absorption can be described by the following equations.

$$a + b + c = 100 \tag{7}$$

$$Abs_{i,observed} = a\% \times Abs_{i,real} + b\% \times Abs_{i-1,observed} + c\% \times Abs_{i-2,observed} \tag{8}$$

Rearranging Eqn (8),

$$a\% \times Abs_{i,real} = Abs_{i,observed} - b\% \times Abs_{i-1,observed} - c\% \times Abs_{i-2,observed} \quad (9)$$

Using the sample immediately after the DC-8 had just exited the plume and labelling the last WS BrC measurement within the plume as $\mathrm{Abs}_{0,\mathrm{observed}}$ the series of measurements can be described as:

$$a\% \times Abs_{2,real} = Abs_{2,observed} - b\% \times Abs_{1,observed} - c\% \times Abs_{0,observed} \quad (10)$$

$$a\% \times Abs_{3,real} = Abs_{3,observed} - b\% \times Abs_{2,observed} - c\% \times Abs_{1,observed} \quad (11)$$

$$a\% \times Abs_{4,real} = Abs_{4,observed} - b\% \times Abs_{3,observed} - c\% \times Abs_{2,observed} \quad (12)$$

…etc.

The left side of the equations are zero due to the second assumption that WS BrC absorption is negligible outside the plume. These equations can be solved by least squares for an overdetermined system to obtain the coefficients, which as noted, we assume are constant. For our MC setup we find: $a = 56 \pm 13$, $b = 7 \pm 4$, and $c = 37 \pm 12$ based on integrating the result from nine cases of plume exits, where the uncertainties are the standard deviations from multiple plume exit analyses. In other words, for one measurement of WS BrC absorption, about 56% of absorption is from the current i-th sample, and 7% from residue in the tubing due to (i-1)-th sample and 37% from MC residue due to (i-2)-th sample. The largest source is residue in the MC. Although 10 mL of water was used to clean the chamber, since there was no airflow during the cleaning, no mist was generated and so the walls, nozzle and water-refluxing filter of the MC were not rinsed. As for hysteresis in the sample lines and LWCC, the length of the tubing between the MCs

and LWCC was as short as possible (about 1 m long), but there was still 0.5 mL of liquid volume (with 0.76 mm ID tubing) for the instrument arrangement on the DC-8. The internal volume of the 2.5 m LWCC was 0.625 mL. In our setup, the maximum liquid available for the BrC measurement with the LWCC was 3 mL (the IC analysis required most of the MC liquid sample), thus based on the volume of the sample line and LWCC combined, these components were roughly flushed twice with the sample and the third volume was used for the analysis (internal volume of tubing and LWCC was approximately 1 mL and volume of liquid sent through the system in each MC analysis was 3 mL). Flushing with more sample (i.e., use more water in the MC) would reduce the hysteresis, but the under-measurement of the peak BrC levels within the plume will remain and it will also reduce the sensitivity of the overall BrC measurement if all other factors, such as sampling time, remain the same. From these analyses, the greatest improvement in the sampling system could be gained by minimizing hysteresis from residue in the MC from the previous sample.

Figure 4-6a shows the time series plot of WS BrC ($Abs_{365nm} - (365/700)^{-1} \times Abs_{700nm}$) with CO before and after applying the hysteresis correction. This figure shows that corrected WS BrC is higher within the plumes and lower outside the plumes and in better agreement with the CO trend, which is not affected by hysteresis. However, this method does not completely remove all hysteresis as some disagreement still exists. The uncertainties of the measurements also increased as the hysteresis is not a constant; the uncertainties of the three factors *a*, *b*, and *c* are not insignificant, as assumed.

The effect of this correction can also be assessed through scatter plots of measured WS BrC and CO before and after the correction, as shown in Figure 4-7a and 7b,

respectively. A better correlation is observed when the hysteresis correction is applied; R^2 increases from 0.75 to 0.86.

CSU and NOAA PILS-LWCC: A similar hysteresis of WS BrC is seen in the continuously flowing liquid system of the CSU PILS-LWCC relative to the CO data in Figure 4-4b. Here we attempt to remove some of this effect by applying a similar analysis method used for the MC using the raw higher time resolution BrC data. Unlike the dual MC system, the hysteresis could occur from hang-up of liquid in the internal wetted components encompassing the PILS impaction plate to the LWCC, along with the mixing caused by using a syringe pump (i.e., first liquid in is last out, discussed above). To correct the hysteresis effect, similar assumptions noted for the MC also apply here. In this case, we assume $d\%$ of the current absorbance observation ($Abs_{j,observed}$) is due to current j-th sample ($Abs_{j,real}$), and (1- $d\%$) absorbance is due to hysteresis ($Abs_{j-1,observed}$). The relationship can be described as:

$$Abs_{j,observed} = d\% \times Abs_{j,real} + (1 - d\%) \times Abs_{j-1,observed} \quad (13)$$

We also assume that WS BrC is nearly zero when the CO mixing ratio is less than 80 ppbv, which means the first term on the right side of Eqn (13) vanishes. Again, using data when the C-130 just exited the plume and then following with ten background samples (CO<80 ppbv, but where WS BrC is not zero due to the hysteresis effect), the overdetermined system was also solved with the least square method, but this time only with one unknown, *d*. The mean and standard deviation of the factor *d* with data from 10 plumes analyzed is 11 ± 2 (again, ± is the standard deviation in d determined from multiple

plumes). Figure 4-6b shows the result. The trend of the corrected WS BrC corresponds better with the CO trend, but is noisier than the original data due to the corrected WS BrC being derived by dividing by a small number, i.e., *d%*. The noise data may also be due to an overcorrection. The data shown in Figure 4-6b is the most exaggerated case of hysteresis encountered during WE-CAN. In lower concentration smoke plumes, generally when CO was less than 2000 ppbv, the hysteresis effect was not apparent, indicating a correction may not be necessary in all cases. To remove the added noise, the data could be smoothed (over longer time intervals, 150 s was found to be optimal), but that will reduce the time resolution of the measurement. Similar to the MC results, better correlation is seen in the scatter plots between WS BrC vs. CO, shown in Figure 4-7c and 7d, where the R^2 increases from 0.49 to 0.58. The greater scatter for the PILS data compared to the MC is likely due to the C-130 in WE-CAN flying over more fires that were relatively small while the DC-8 focused on larger stronger plumes in FIREX-AQ. Therefore, the WE-CAN data was more influenced by variability in the WS BrC vs. CO between different smoke plumes. The hysteresis phenomenon (Figure 4-3c) is not obvious for the NOAA PILS-LWCC compared with CSU PILS-LWCC (Figure 4-3b), possibly due to the smaller dead volume throughout the system (e.g., use of a inline bubble trap with PTFE membrane versus glass bulb debubbler), the use of a peristaltic pump versus syringe pump to move sample liquid, avoiding the syringe pump sample mixing issues, and overall lower concentrated plumes being sampled by the Twin Otter (most smoke plumes had CO below 2000 ppbv compared to typical CO of more than 3000 ppbv for the plumes encountered in WE-CAN mission). Because of this, no overall hysteresis correction was performed for the NOAA PILS-LWCC.

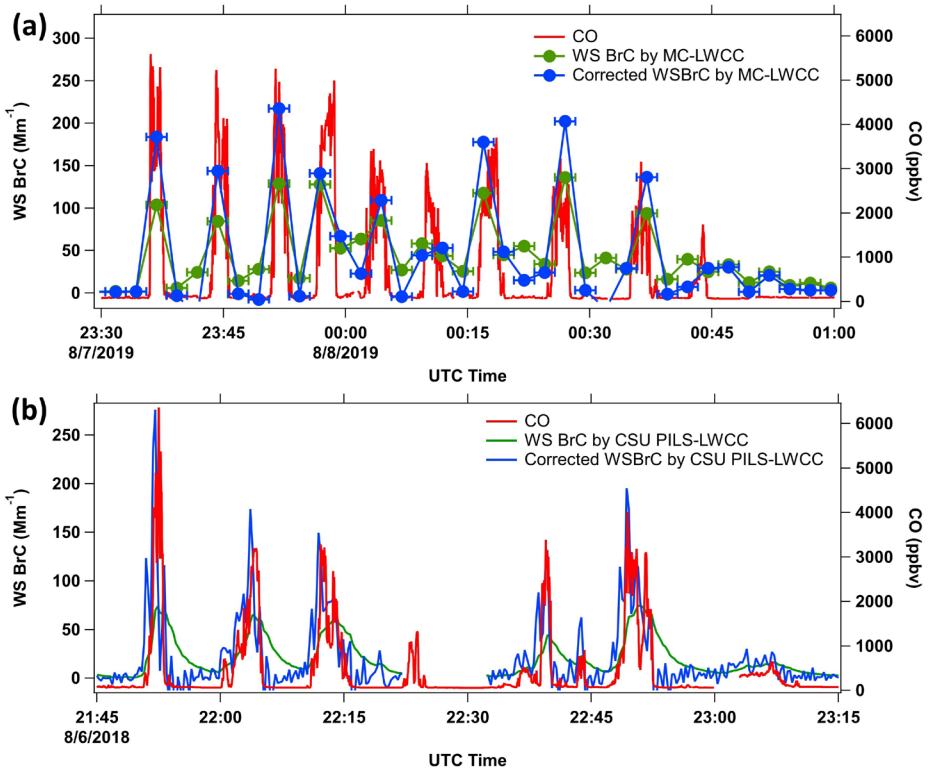

Figure 4-6 Time series of water-soluble BrC (WS BrC) corrected for baseline drift and hysteresis (blue) compared to original data (green) and CO concentrations (red) for (a) the MC-LWCC measurement and (b) the CSU PILS-LWCC measurement for the same flights shown in Figure 4-4a and b, respectively. Horizontal error bars in (a) represent the MC-LWCC interval.

4.4.4 Comparison between MC and Filter Measurements of BrC

We also compare the online WS BrC measurements to filter sample results, noting that the filter does not have this liquid hysteresis issue. This can only be done for the MC measurements of WS BrC since of the three aircraft, only the DC-8 included a particle filter sampling system allowing for off-line BrC aerosol particle analysis.

The MC-LWCC BrC data with 2.5 min resolution were averaged to the lower time resolved offline filter data. Figure 4-8 shows the comparison between these two methods.

In the comparisons that follow, all the MC-LWCC data have been corrected for the baseline drift likely due to BC, as discussed in Sect. 3.2. Fairly good agreement is found between the online and offline BrC measuring systems when not corrected for the hysteresis associated with the online data, with a slope of 0.74 and R^2=0.84. However, the agreement is better once the hysteresis correction is applied, with slope of 0.91 and R^2=0.89. The improvement in R^2 is less than that seen for the comparison with CO in Figure 4-7 and is likely due to averaging the MC WS BrC data to the longer filter sampling times and that most filter sampling times where restricted to periods within the smoke plumes (i.e., less data for periods of transition from within to outside of plumes). Overall, the agreement suggests that the filter measurement of BrC is not biased by possible sampling artifacts associated with absorption of gases or evaporative loss of BrC components from the filter, which is common for filter sampling of semi-volatile species, but not as significant an issue for online sampling systems, such as the MC-LWCC.

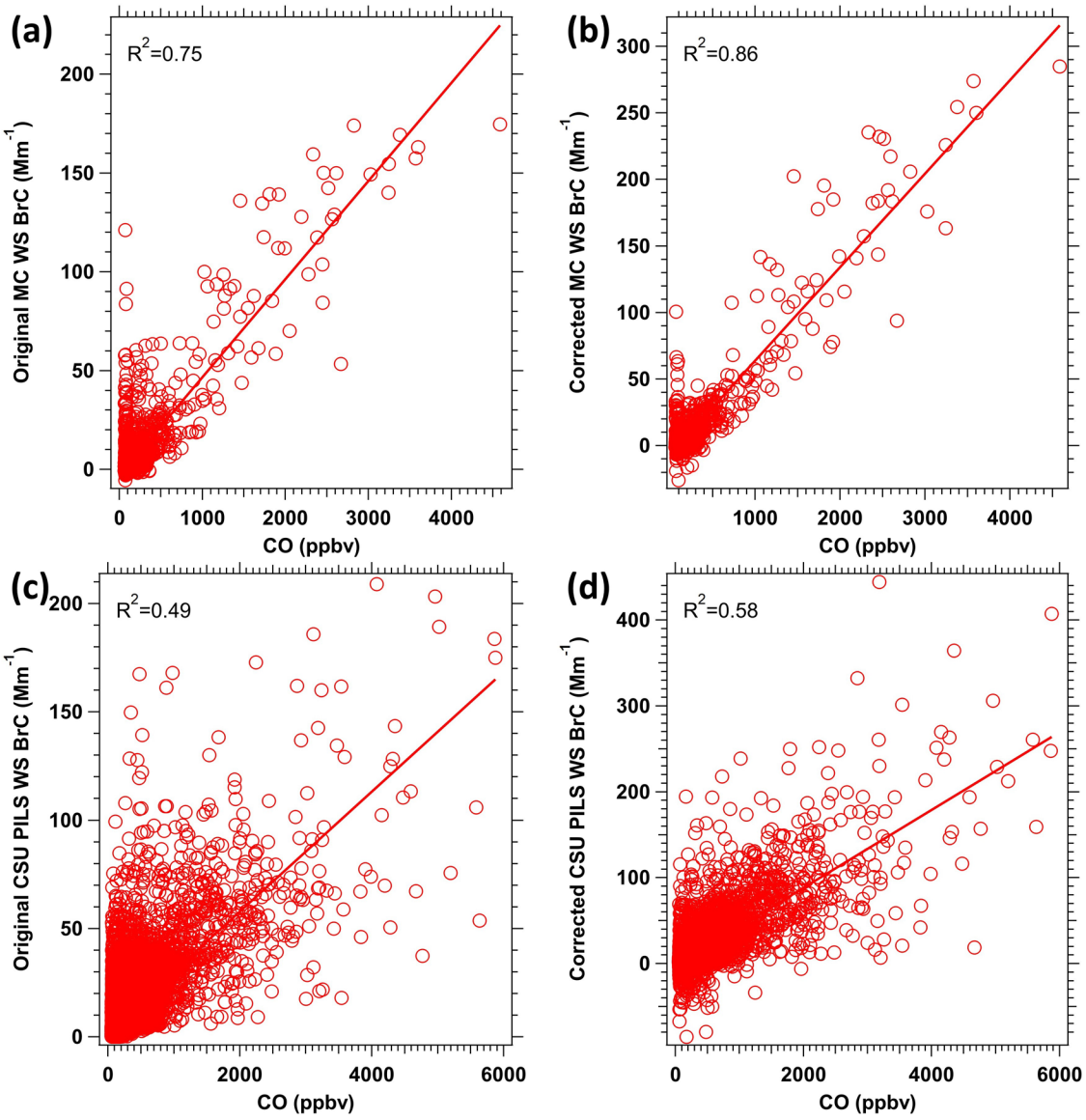

Figure 4-7 Scatter plots of WS BrC versus CO concentration for the MC-LWCC before (a) and after the (b) hysteresis correction, and for the CSU PILS-LWCC before (c) and after the (d) hysteresis correction.

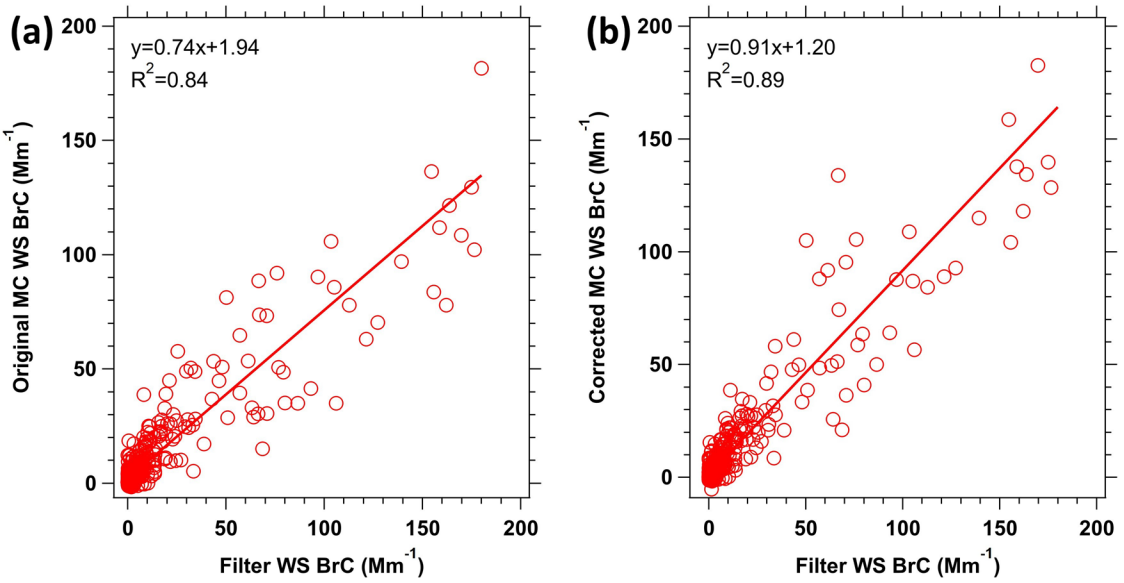

Figure 4-8 Comparison of the WS BrC determined online using the MC-LWCC vs. offline from extraction of filters. (a) shows the original MC-LWCC WS BrC data, and (b) shows the MC data with the hysteresis correction applied. The data is fitted by orthogonal distance regression.

4.4.5 Detection limits and measurement uncertainty

The limit of detection (LOD) and measurement uncertainty of the three instruments are presented below. The detection limits depend on the spectral integration time, sample air flow rate, volume of extraction water, and also the optical path length of the waveguide.

MC-LWCC: The air sample flow rate directly affects the detection limit and thereby the sensitivity of the MC-LWCC for measuring BrC. The nominal flow rate of the MC-LWCC was set to ~50 SLPM. For a given MC-LWCC design, a sufficient flow rate is necessary so that particles are efficiently scrubbed, and all internal surfaces are wetted and continually flushed. The highest flow rates possible are also limited by the pressure drop across the Teflon water-refluxing filter and vacuum pump size. Longer sampling times will

have larger volumes of air sampled as well as cause more evaporation of the water in the MC-LWCC, both increase the sample concentration, but reduce the time resolution. The water level in the MC-LWCC should be kept as low as possible to have the highest concentration, but must be sufficient to maintain a reservoir in the bottom at all times while operating so that a mist is continually maintained and all surfaces are wetted and drained during sampling. Also, there must be sufficient sample for the various measurements. Insufficient sample can lead to drawing in air bubbles into the analytical instruments, which, depending on the amount, can invalidate the measurement or as seen, cause extensive baseline drift.

Based on experiments, the optimal sampling time and water injection volume were found to be 150 s and 12 mL for this MC and analytical system. Approximately 10 mL of liquid remained in the chamber after sampling was completed. 3 mL of ambient sample was the maximum volume that could be injected into the waveguide without interference to the IC system. Occasionally, some air bubbles were introduced into the waveguide due to insufficient liquid volume left in the MC or the system leaking, as discussed above. Two cycles of liquid injection were found to be enough in most cases to remove the resulting absorption baseline drift caused by air bubbles.

Limits of detection (LOD) are typically calculated by three times the standard deviation of the blank measurement; however, we did not have any blank measurements involving filtering out aerosol in the MC-LWCC during the FIREX-AQ campaign. Instead, a water blank at the beginning of each flight was used, where pure water was injected into the MC and then removed and injected into the waveguide. Based on these water blanks, the LOD of the method was 0.69 Mm^{-1}, mainly due to the uncertainty associated with the

spectrometer measurement. The MC-LWCC LOD was higher than the LOD for the offline filter method at 0.10 Mm^{-1} due to a smaller volume of air sampled by the MC. Alternatively, MC-LWCC blank variability can be estimated when sampling in clean background air when BrC levels are expected to be low. For example, the flight on 19 Aug. 2019 did not encounter any smoke plumes, and the WS BrC was very low, together with other smoke tracers CO and BC. Using the time period from 19 Aug. 2019 18:20:00 – 19:29:59 (CO =73 ppb and BC=0.5 ng/m^3) as the blank, the LOD ($3*\sigma$) is calculated to be 1.53 Mm^{-1}. With this LOD, only ~40% of the data was above the LOD for the whole FIREX-AQ study period, below LOD periods were primarily when not sampling in smoke plumes (e.g., traveling to and from the fires and between fires). When the DC-8 was sampling smoke plumes (CO>300 ppbv), which was the main focus in FIREX-AQ, more than 90% of the MC data was above the LOD, implying that this system was mainly useful for in-plume sampling.

The uncertainty of the MC-LWCC WS BrC system was calculated by propagating the uncertainties from air sampling volume, liquid extraction volume, the spectrometer absorption measurement, baseline drift correction, and hysteresis correction. Besides the hysteresis correction, the relative uncertainty for other components was approximately 5%. The combined overall estimated uncertainty based on these variables was roughly 28%.

PILS-LWCC: Each PILS-LWCC system acquired continuous data at 10 s (NOAA PILS-LWCC) or 16 s resolution (CSU PILS-LWCC). The measurement precision can be determined for in-flight measurements of ambient air with no detectable BrC absorption. Figure 4-9 shows an Allan deviation (Werle et al., 1993; Allan, 2016) plot for Abs_{365nm} calculated for the CSU PILS-LWCC (1 h 38 m period on 13 Aug. 2018) and NOAA PILS-

LWCC (2 h 3 m period on 11 Aug. 2019), during measurements in background air. The 1σ Allan Deviation for 30 s averaging is 0.29 Mm^{-1} and 0.008 Mm^{-1} for CSU and NOAA PILS-LWCC respectively, equivalent to 3σ LODs of 0.89 Mm^{-1} and 0.03 Mm^{-1}, respectively. Although the NOAA PILS-LWCC shows high precision over short intervals, the Allan deviation plot indicates instrumental drift at all time scales.

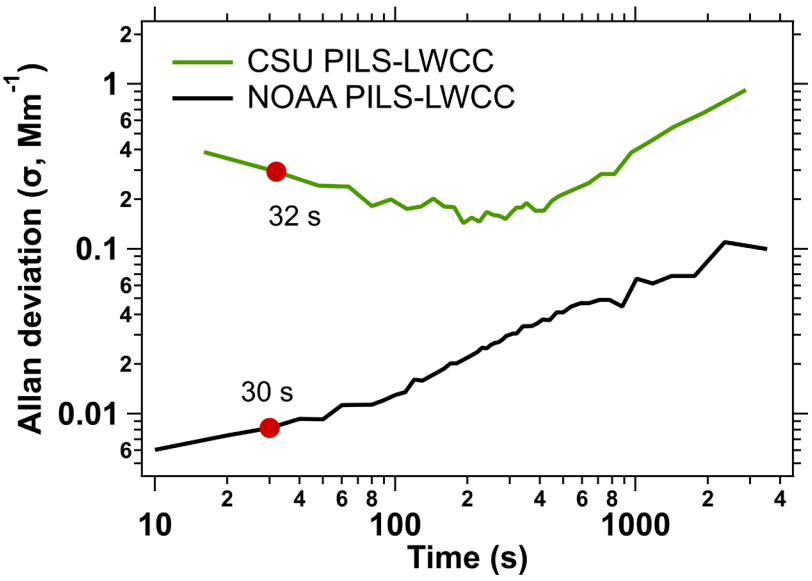

Figure 4-9 Allan Deviation plot calculated for all WE-CAN data without plumes on Flight 10 (1:38h from 13 Aug. 2018 19:16:29-20:54:58) and FIREX-AQ NOAA Twin Otter flight data 11 Aug. 2019 flight (2:03h from 11 Aug. 2019 22:46:04 - 12 Aug. 2019 00:49:54). There were no plumes during either of these periods. Data in red dots are used to determined LODs for both systems.

The uncertainty of the CSU PILS-LWCC system was estimated to be 12% based on the uncertainties in the air and liquid flow rates and the ambient and background

absorption measurement. The uncertainty of the NOAA PILS-LWCC system was calculated to be 11%.

4.4.6 Recommendations for further improvements

The MC-LWCC and PILS-LWCC instruments successfully measured WS BrC throughout the WE-CAN and FIREX-AQ aircraft deployments. However, future improvements have the potential to improve the detection limits and time response of these instruments.

For the MC-LWCC, the cleaning procedure between consecutive samples was not sufficient and resulted in a large hysteresis effect (44%) when moving in and out of smoke plumes. This could be improved by introducing a clean air flow through the MC to wash the interior wetted surfaces between samples. Shortening the tubing running between the MC and LWCC could reduce the dead volume, improving the time response and hysteresis. Arranging the MC with a minimal distance between the sample extraction port and the MC bottom would decrease the residual liquid sample within the MC (or by placing the MC sample port on the bottom of the MC body). The addition of an automated filter at the sample inlet would allow repeated blank measurements of filtered air, and a better assessment of the LOD. This would also be useful in quantifying measurement hysteresis.

Increasing the sensitivity of the MC system would allow obtaining more data, especially outside of the smoke plumes. The extraction volume and sampling flow rate cannot be significantly altered. The most effective way to increase sensitivity is to increase the sampling time, but the time resolution would decrease. Although not ideal for this study due to the fast speed of the DC-8, this could be a viable solution for ground-based studies,

where decreasing the time resolution from 2.5 min to 30 or 60 min may still produce acceptable time resolved data, with 12 to 24 times improvement in the sensitivity (lower LOD). This higher sensitivity could also reduce measurement uncertainty.

For the PILS-LWCC time response could be improved and hysteresis reduced by using a peristaltic pump instead of syringe pumps to move the liquid sample from the PILS to the LWCC, and by decreasing the volume between the impaction plate to the LWCC and any places where liquid gets stalled in the system. This would entail use of short small-bore tubing, and the smallest internal volume possible for the debubbler (e.g., use of a inline bubble trap with PTFE membrane with vacuum assist) and liquid filter, and reducing the dead volume in the syringe pumps (i.e. using a cone tip instead of a flat tip on the piston).

For all liquid systems, adding surfactants to the water to reduce the water surface tension can reduce hysteresis (Rastogi et al., 2009), but must be selected so as not to interfere with the analytical systems. It is known that introduction of air bubbles in the sample line, that are completely removed just upstream of the LWCC, can reduce hysteresis by "wiping" the walls of the wetted surfaces as they pass through the liquid system.

Drift in the light source intensity may contribute to instrument drift, seen in the Allan Deviation plot in Figure 4-9. This could be improved by temperature-controlling the light source and monitoring its output intensity. The pressure-controlled inlet system for the NOAA-PILS also seems to have distinct advantages since it allowed the use of the peristaltic pumping system instead of syringe pumps and likely dampens other variability

in the complete PILS-LWCC due to changes in ambient pressure with aircraft altitude changes and possible turbulence in the inlet and air sample lines.

4.5 Conclusion

We present a comparison of three WS BrC measuring systems, including two PILS-LWCC and a newly developed MC-LWCC. The new system was based on expanding the analytical capabilities of a mist chamber (MC) sampling system on the NASA DC-8 research aircraft which had been extensively used in past studies for measuring inorganic gases and aerosol particles. The new system was deployed during the NASA FIREX-AQ and contrasted with the performance of the PILS-LWCC systems for measuring WS BrC on the NSF C-130 aircraft as part of WE-CAN and on the NOAA Twin Otter during FIREX-AQ. These three systems used almost identical BrC analytical methods (LWCCs and spectrophotometers) to determine levels of light absorbing chromophores in liquid water samples, whereas the particle collection and liquid handling systems differed. Using a dual MC system operating in batch mode, the MC-LWCC measurement time resolution was 2.5 min. Sampling air at 50 SLPM with 12 mL of collection water and a 2.5 m long LWCC, the LOD of the system for measuring WS BrC was 1.53 Mm^{-1} with an estimated 28% uncertainty. For comparison the filter sampling system with offline analysis of BrC using an identical LWCC and spectrophotometer had a LOD of 0.10 Mm^{-1} and uncertainty of 16%. The CSU PILS-LWCC system sampling at an air flow rate of 15 SLPM had a LOD of 0.89 Mm^{-1} and uncertainty of 12%, and NOAA PILS-LWCC with 6 SLPM had a LOD of 0.03 Mm^{-1} and uncertainty of 11%, both operating as continuous samplers. Spectral drift due to air bubbles in the sample line and BC that passed the liquid particle filter was an issue with the MC-LWCC, but not as apparent in the PILS-LWCC systems,

and had no effect on the filter sampling method. Hysteresis (smearing) of samples between consecutive measurements was a major artifact in this study for the MC-LWCC and on many occasions for the CSU PILS-LWCC, which was clearly seen in this study of smoke plumes measured near the fires. For the MC-LWCC, the hysteresis was largely due to not completely flushing the MC with clean water and not generating a mist to wash all internal surfaces, with a minor contribution from hysteresis in the sample lines. For the CSU PILS-LWCC, hysteresis issues were due to the size of the wetted area of the impaction plate (which was small, a specific design feature of the system) and the liquid flow system that included the debubbler, liquid filter, syringe pumps, and sample lines. A hysteresis correction results in sharper changes in concentrations, that more closely track changes in CO when transitioning from sampling in and out of wildfire smoke plumes with the aircraft (average aircraft speed for NASA DC-8=200 m/s and for NSF C-130=100 m/s), and increases the in-plume BrC levels, but produced more variability (noise) in the CSU PILS-LWCC dataset. The NOAA PILS-LWCC showed very little evidence of sample hysteresis possibly due to the different liquid sample flow system that used a peristaltic versus syringe pumps (e.g., for each stroke first liquid into pump is last out) to move the sample liquid, and the overall lower concentrated plumes encountered. For the MC-LWCC, the online WS BrC data was in good agreement with the offline WS BrC measured with filters with a regression slope of 0.91 and R^2=0.89. Since the MC-LWCC should not be susceptible to WS BrC volatility artifacts known to occur in filter sampling, the good agreement suggests that there are few artifacts associated with the filter method and that much of the BrC was likely not highly volatile. In this study, the MC-LWCC was only of sufficient sensitivity to measure BrC levels in smoke plumes, the filter sampling system with much higher mass

loading (~20 times higher) could measure WS BrC even in continental background conditions. As this was the first attempt at WS BrC measurements with a mist chamber, possible improvements to the MC-LWCC system were proposed.

CHAPTER 5. CONCLUSIONS AND FUTURE WORK

5.1 Summary of findings

This thesis improves the understanding of BrC sources, evolution, and radiative impact by measuring BrC and then analyzing the data, along with results from an extensive suite of instruments for measuring gas and aerosol particles from two multi-investigator airborne campaigns (ATom and FIREX-AQ). The objective of the ATom mission was to characterize BrC aerosol over the most remote regions globally, and the goal of the FIREX-AQ is to gain a better understanding of BrC properties near wildfire sources. In these two campaigns, the light absorption of BrC aerosol was measured in aerosol liquid extracts from filters or online instruments or was calculated from overall aerosol absorption measurements.

In the ATom mission, BrC aerosol was measured from filter samples collected from aircraft flights that extended from pole to pole over three seasons providing the first direct measurement for BrC on a global scale. The distribution of BrC aerosol was found to be highly heterogeneous. In most regions of the remote atmosphere, the BrC level was too low to be detected. However, a substantial level of BrC was observed in the mid-Atlantic region, and back-trajectory analysis suggests that the air masses had been transported from Africa or South America with extensive burning events. A radiative transfer model suggested DRE due to BrC accounted for 7-48% of total DRE due to all carbonaceous aerosol (BrC+BC) absorption.

The same filter collection system was also deployed on the same aircraft in another airborne study FIREX-AQ, and BrC were measured with the same approach. We provide the first comparison of BrC measurements with two methods: BrC absorption in aerosol liquid extracts with filters and BrC inferred from a photoacoustic spectrometer (PAS). The results showed two methods agreed at ~400 nm, the typical wavelength used to represent BrC absorption. However, discrepancies were found at other wavelengths, possibly due to poorly constrained extrapolation of absorption from visible wavelength to UV range for the PAS and the existence of low-solubility S-BrC at higher wavelengths. BrC aerosol emitted from wildfires belonged to M-BrC, in accordance with the definition of this classification framework proposed by a recent study (Saleh, 2020). The evolution of BrC was highly complex, both enhancement and depletion were observed in the first few hours after emission. BrC was not observed to be volatile over 15 K temperature rise, in contrast to the bulk OA and individual BrC chromophore 4-Nitrocatechol. The relationship between BrC and O_3 suggests that O_3 is an important species in the evolution of BrC: BrC was more likely formed under high-NOx condition with O_3 oxidation, while BrC was bleached under low-NOx condition. Other factors, including aqueous reaction, reaction with NH_4, and direct photolysis, did not significantly affect BrC evolution in this campaign.

Besides the filter collection system and the PAS instrument, we have developed an online measuring system for WS BrC and deployed it on the NASA DC-8 in FIREX-AQ. We compared the performance of the newly built system with the other two similar WS BrC measuring systems, which were developed separately and deployed on the NSF C-130 in WE-CAN and NOAA Twin Otter in FIREX-AQ. In general, WS BrC measured by these three instruments tracked CO on a time series plot, where CO can be used as a tracer for

biomass burning plumes and BrC is expected to follow the same profile if there were no measurement artifacts. However, baseline drift and signal hysteresis were observed. Correction methods for both of these issues and future improvements of these three methods are proposed.

5.2 Future work

5.2.1 BrC measurements

BrC measurements in aerosol liquid extracts were widely used in this dissertation and have been in other studies. However, there are some shortcomings that must be acknowledged and may be improved in future work. In most cases, BrC measurements in liquid extracts were obtained from filters and BrC levels determined offline. This method is suitable for studies that do not require high time resolution data. However, it is necessary to have a fast response instrument to characterize BrC in some special cases, for example monitoring emission changes or tracing the evolution of BrC in plumes when sampling from a fast-moving platform. This thesis compares three online WS BrC measuring systems and provides some feasible solutions in Chapter 4. Other than that, in Chapter 3, we have observed we may miss some BrC with low solubility in the solvent we used (water and methanol). Therefore, it may be worth extracting aerosols in a less polar solvent, for example, acetonitrile or even acetone. As mentioned in the previous chapter, aerosol morphology information is lost during the disolution process, and a conversion factor K needs to be applied to convert the absorption in liquid phase to the absorption in aerosol phase. In this dissertation, we applied Mie theory with a series of simplified assumptions. However, a comprehensive study of Mie theory is needed.

As BrC and BC are always emitted together from combustion processes, it is essential to correctly separate BC and BrC physically or mathematically from measurement of total aerosol particle absorption to quantify just the BrC component. However, the absorption by BC is not well constrained, considering its complex morphology and mixing state. In addition to this, intermediate BrC, which is also called tar balls or S-BrC, have very similar properties with BC hindering the separation between them. In Chapter 4 we have seen the light absorption at 664 nm measured by the PAS cannot be explained by the rBC mass reported by the SP2, which means assuming all absorption at that wavelength is due to BC absorption can underestimate the contribution of BrC. The missed absorption can be due to intermediate BrC. Future work should be carried out on characterizing optical properties of BC or intermediate BrC.

5.2.2 Radiative impact of BrC aerosol

In this dissertation, we have used ATom data to estimate the DRE of BrC. However, it is not a true "global" effect as Chapter 2 focuses only on the regions sampled by the aircraft, which may bias the result. An alternative approach to estimate the radiative impact of BrC is to use a global model to simulate the distribution and abundance of BrC aerosol, and then use the observation from the ATom (global scale) to constrain the simulation result. This is, however, difficult since the emission and evolution of BrC has not been fully determined. BrC emission in current modelling studies is often parameterized based on the BC/OA or MCE, however, their relationship is rarely reported in field observations. Adding to this, the evolution of BrC has not been presented correctly in models. More evidence has shown that BrC level can be enhanced after emission, and therefore simplified decay scheme may not be enough to characterize the BrC change close to fire.

5.2.3 Health impact of BrC aerosol

Although the chemical structure of BrC aerosol has not been completely deciphered, current known BrC compounds, such as nitroaromatics and PAHs, have been found to be carcinogenic (Lewtas, 2007; Shen et al., 2014). Verma et al. (2015) have linked BrC to oxidative potential with the dithiothreitol (DTT) assay, which is often used to assess the generation of reactive oxygen species (ROS) via catalytical reactions by ambient aerosols. BrC might be more representative of ambient aerosol toxicity than the typical used PM mass concentration. Given that a fraction of BrC is recalcitrant and widespread in the atmosphere, the health impact of BrC aerosol needs further evaluation. Moreover, BrC can act as a shell coating on other cancerogenic compounds, hindering atmospheric oxidation. Future work should also investigate how BrC affects the atmospheric scavenging of toxic pollutants.

A. APPENDIX A. SUPPORTING MATERIALS FOR CHAPTER 2

A.1 Methods Details

Ambient particles were collected on a filter sampling system and then analyzed offline identical to that used in our previous studies. Based on earlier characterization studies, it was estimated that the inlet and transport system allowed sampling of particles with aerodynamic diameter less than nominally 4.1 μm (McNaughton et al., 2007). Particles were collected onto 1-μm pore size, 90 mm diameter, Teflon filters (MilliporeSigma, Burlington, MA), which were maintained at low temperatures (typically less than 0 °C) by refrigerating following each flight and during shipment to the Georgia Institute of Technology (Atlanta, GA, USA) in coolers with blue ice. 15 mL opaque polypropylene tubes (Argos Technologies, Vernon Hills, IL) were used in ATom-2 and 15 mL glass centrifuge tubes with Teflon lined caps (DWK Life Sciences, Rockwood, TN) were used for ATom-3 and ATom-4. The glass vials were baked at 500 °C for 24 hours to remove organic residue. Figure A-1 illustrates the analytical system for the filter analyses.

Filters were first extracted in 15 mL of deionized water (DI water, >18.2 MΩ·cm) in its storage vial by 30 min sonication (FS60H Ultrasonic Cleaner, Fisher Scientific, Hampton, NH). For the analysis, the sample was injected via a programmable syringe pump (Kloehn Inc., Las Vegas, NV) through a pre-cleaned (flushed with extraction solvent) polypropylene syringe filter of 0.45 μm pore size (Tisch Scientific, North Bend, OH) and then into a 2.5 m long (total internal volume with 625 μL) liquid waveguide capillary cell (LWCC-3250, World Precision Instruments, Sarasota, FL). After the waveguide, the liquid sample was drawn into a total organic carbon analyzer (TOC analyzer, Sievers 900 Series, GE Analytical Instruments, Boulder, CO) to measure WSOC (Hecobian et al., 2010). (WSOC is not discussed in this paper). The LWCC was coupled to a dual deuterium and tungsten halogen light source (DH-mini Light Source, Ocean Optics, Dunedin, FL) and absorption spectrometer (USB4000 Miniature Fiber Optic Spectrometer, Ocean Optics, Dunedin, FL) via fiber optic cables. The spectrometer provided wavelength-resolved absorption spectra from 200 nm to 850 nm. These spectra

were recorded by data acquisition software, SpectraSuite, every two seconds and were saved three times for each filter, which were then averaged to determine the final absorption spectra. After water extraction, filters and extraction vials were drained and passively dried for roughly 3-6 hours at room temperature. Then, the filters were extracted again using 15 ml of methanol by 30 minutes of sonication following the same method used for the water extracts (i.e., sample filtered and passed through LWCC), but without TOC analysis. Only light spectra were analyzed since the use of organic solvent prohibited the extract carbon mass quantification.

Light absorption coefficient of chromophores in solution (Abs_λ, units m^{-1}) was calculated using Eqn (S1) (Hecobian et al., 2010).

$$Abs_\lambda = \frac{V_{liquid} \times \log_{10} \frac{I_{\lambda,0}}{I_\lambda}}{V_{air} \times l} \times \ln(10), \quad \text{(S1)}$$

where $I_{\lambda,0}/I_\lambda$ is the ratio of the measured intensity of incident to transmitted light through the waveguide at a given wavelength, V_{liquid} is the solvent volume used in the extraction, V_{air} is the sampling air volume passed through the filter and l is the waveguide optical path length (2.5 m). Exclusive measurements of chromophores require subtracting out any absorbance by the solvent, buildup of contamination in the LWCC, or contribution of BC (if any). Daily, absorption reference spectra were produced by injecting pure DI water or methanol, depending on which extraction solvent was used. Then, during the subsequent sample analysis, prior to each filter analysis, pure solvent was injected into the analyzing system to monitor if a LWCC cleaning procedure was necessary. A routine cleaning procedure was done before and after daily experiments by injecting pure solvent into the LWCC. If necessary, but seldom for this study, 5 mL of 0.6N HCl solution was used to thoroughly clean the LWCC, and then at least 50 mL of DI water was flushed through the LWCC. Ideally, the result is that the absorption spectrum would be near zero at all wavelengths for pure solvent in the LWCC.

The light absorption coefficient determined by Eqn (S1) at 700 nm ($\mathrm{Abs}_{700\mathrm{nm}}$) was subtracted from measured Abs_{λ} (all wavelengths) to account for any baseline drift or any insoluble components (e.g., BC) that passed the liquid flow system and syringe filter, under the assumption that there is no BrC absorption at 700 nm. For ATom, $\mathrm{Abs}_{700\mathrm{nm}}$ was typically very small meaning that few interferences from insoluble particles were present in the LWCC and baseline drift was minimal; in the worst case, strong smoke plumes, $\mathrm{Abs}_{700\mathrm{nm}}$ was less than 20% of $\mathrm{Abs}_{365\mathrm{nm}}$.

The blank meausrement for Methanol-soluble BrC (MS BrC) data were higher for all ATom missions, and therefore less data were available. Nonetheless, there were very limited data available for both WS BrC and MS BrC greater than LOD to determine the ratio of WS fraction. ATom-2 high blanks were thought to be due to the use of plastic extraction vials. Glass vials were than used for ATom-3 and 4. After this change, MS BrC still showed little contrast to the blank filter signal, and so in the following analysis we focus on only water-soluble BrC (WS BrC) in most cases.

The data used in the following analysis are available in the ORNL DAAC ATom data archive (Wofsy et al., 2018). In these datasets, absorption coefficient data were averaged every 20 nm between 300 nm and 700 nm. The absorption coefficient at 365 nm, which is used here to represents the absorption by BrC, was determined by averaging from 360 nm to 370 nm (averaged to minimize noise). All data discussed below and uploaded in the data achieve were blank corrected by subtracting the average of the filter blank for each deployment and reported at standard temperature and pressure (273K & 1013 mb). It is important to note that the absorption measured in this study, discussed in this paper (unless otherwise indicated), and reported in the data achieve is the absorption by individual chromophores (molecules) dissolved in solution, not the absorption of suspended aerosols. Past studies, based on measured BrC aerosol size distributions and Mie theory, indicate that a multiplication factor of 1.8 to 2 can be used to estimate the light absorption by aerosol particles based on measurements of chromophores in the bulk liquid extracts (Liu et al., 2013; Zhang et al., 2017).

A.2 Back Trajectories and Fire Events

Airmass back trajectories were computed using the Hybrid Single-Particle Lagrangian Integrated Trajectory (HYSPLIT) analysis method were calculated starting from the aircraft GPS location at the middle of the filter collection interval and traced back for up to 72 hours. Locations and fire radiative power (FRP) of large biomass burning regions for each ATom deployment were obtained from the Fire Information for Resource Management System (FIRMS). Although each mission lasted for approximately one month, no significant variation in regions strongly associated with FIRMS-derived fire events was observed throughout a given mission. The MODIS FRP retrieval, which was performed using the Wooster et al. (2005) approach, was used as a proxy for biomass burning emission rates.

A.3 Radiative Transfer Model

For each altitude layer in the model, the particle single scattering albedo (SSA) and aerosol optical depth (AOD) were calculated using the following equations:

$$\mathrm{SSA}(\lambda) = \frac{b_{scat}(\lambda)}{b_{scat}(\lambda) + b_{BC}(\lambda) + b_{BrC}(\lambda)} \tag{S2}$$

$$\mathrm{AOD} = \sum_{i=1}^{n} Ext(\lambda)\,\tau_i = \sum_{i=1}^{n} (b_{scat}(\lambda) + b_{BC}(\lambda) + b_{BrC}(\lambda))\,\tau_i \tag{S3}$$

where Ext is the extinction coefficient averaged in the i-th altitude bin with a thickness of τ_i. Vertically resolved data were binned every 3 km. An asymmetry parameter (g) of 0.65 (Andrews et al., 2006) was used and the global direct radiative effect (DRE) was calculated under the condition of clear sky and a mean solar zenith angle computed from the specified date and geographic coordinates using an internal solar ephemeris algorithm. For a

complete ATom deployment, the mean zenith angle used was ~60°. In all cases, the surface albedo was that of seawater since most flights were conducted over the ocean.

A.4 Calculation of Biomass Burning Potassium (K^+_{BB})

Water soluble potassium, (K^+) has been widely used as a biomass burning tracer, however its application is complicated because of additional sources of K^+, such as mineral dust and sea salt (Zhang et al., 2010). Biomass burning K^+ (K^+_{BB}) was calculated by $K^+_{BB}=K^+ -0.036*Na^+ -0.12*(Ca^{2+}_{NSS}-Ca^{2+}_{BB})$ (Pio et al., 2008) to exclude K^+ contributed from sea salt and mineral dust. All ions were measured by ion chromatography from filters extracts (Dibb et al., 1999). The factor of 0.036 is the ratio of K^+ to Na^+ in sea water and 0.12 is a mean crustal K^+ to crustal Ca^{2+} mass ratio proposed by Pio et al. (2007). Biomass burning Ca^{2+} (Ca^{2+}_{BB}) can be estimated by 10 times biomass burning K^+ (K^+_{BB}), and non-sea-salt Ca^{2+} (Ca^{2+}_{NSS}) can be calculated from the difference between overall measured Ca^{2+} and Ca^{2+} related with sea salt (Pio et al., 2008).

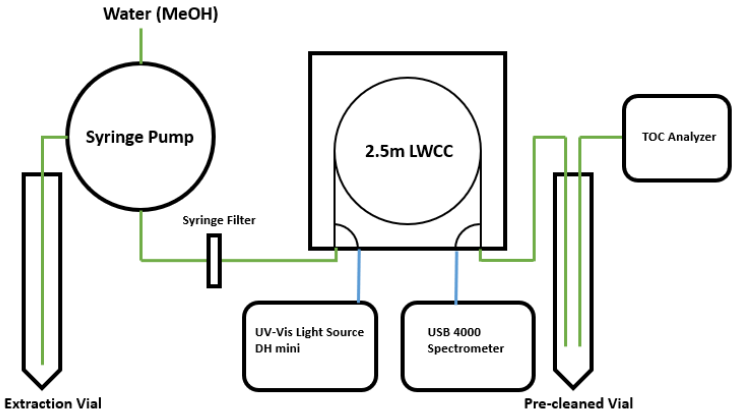

Figure A-1 Schematic of the bench top laboratory instrument to measure aerosol Brown Carbon (BrC) and Water-Soluble Organic Carbon (WSOC) from filter extracts. The syringe filter is 0.45 µm pore size polypropylene (Tisch Scientific, North Bend, OH). An identical system was used for measuring BrC from the extraction of the filter in methanol, but without the TOC analysis (sample discarded after LWCC). WSOC data are not discussed in this paper.

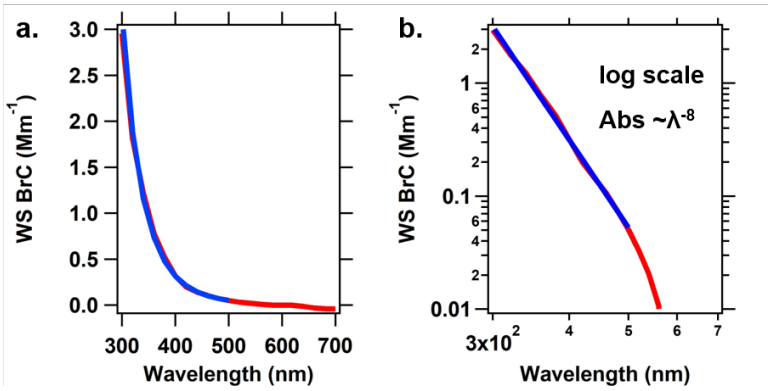

Figure A-2 Example absorption spectrum (red) of filter extracts. Blue line is the fit line from 300 nm to 500 nm and resulting predicted Angstrom exponent of 8 based on linear regression of the log-transformed variables. Plot (a) is on a linear scale and (b) log-log scale.

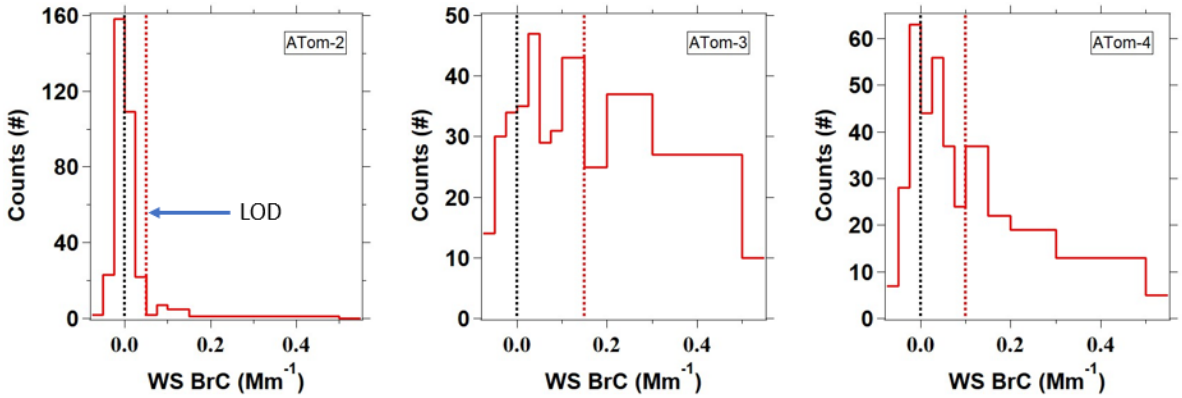

Figure A-3 Frequency distribution of water-soluble BrC measurements (absorption coefficient at 365nm, see Eqn (S1)) with filter blank correction. The vertical red dotted line is the estimated LOD for each mission based on three times the standard deviation of the blanks, and vertical black dotted line is the zero line. Negative values are when the ambient measurement is less than the filter blank.

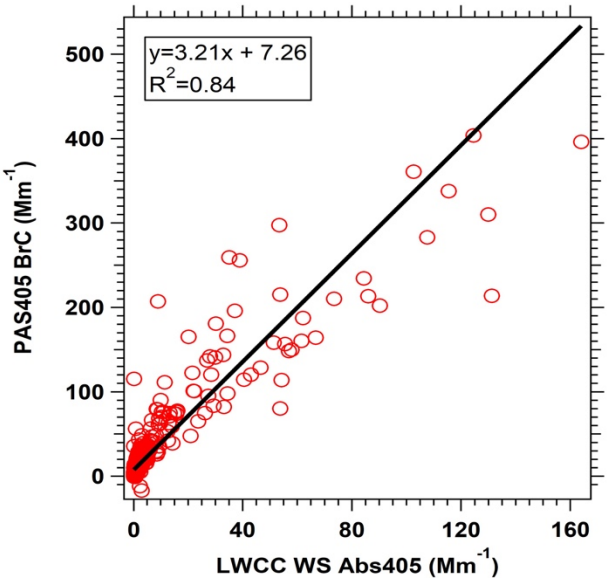

Figure A-4 Comparison of aerosol total BrC light absorption coefficients measured at a wavelength of 405 nm by a photoacoustic aerosol absorption spectrometer (PAS405 BrC) and water-soluble BrC in solution measured with the filter/liquid wave guide capillary cell (LWCC WS BrC Abs405) photospectrometer deployed in this study. Data are from the recent NASA FIREX-AQ study of smoke plumes in the western USA utilizing the same aircraft and identical filter sampling system, and same BrC analysis and data processing as that used for ATom. The PAS lowest measurement wavelength was 405 nm, which was used in this direct comparison. BrC was determined from the PAS aerosol absorption data (PAS405 BrC) by assuming a BC AAE of 1, a MAC of 10 m^2/g at 660 nm and using the measured SP2 BC mass, the same parameters used for determining the wavelength dependent BC absorption coefficients in the ATom radiative model. (This results in a BC MAC of 16.3 m2/g at 405 nm; from $10m^2/g \times \frac{660nm}{405nm}$). Then, PAS405 BrC = (PAS measured absorption at 405 nm) – (16.3 m2/g) (SP2 BC mass). WS-BrC was determined from spectrophotometer measurements at 405 nm and converted to absorption coefficient by Eqn (S1). The slope in the plot, which is the conversion factor between WS BrC and actual BrC at 405 nm, was determined by orthogonal regression.

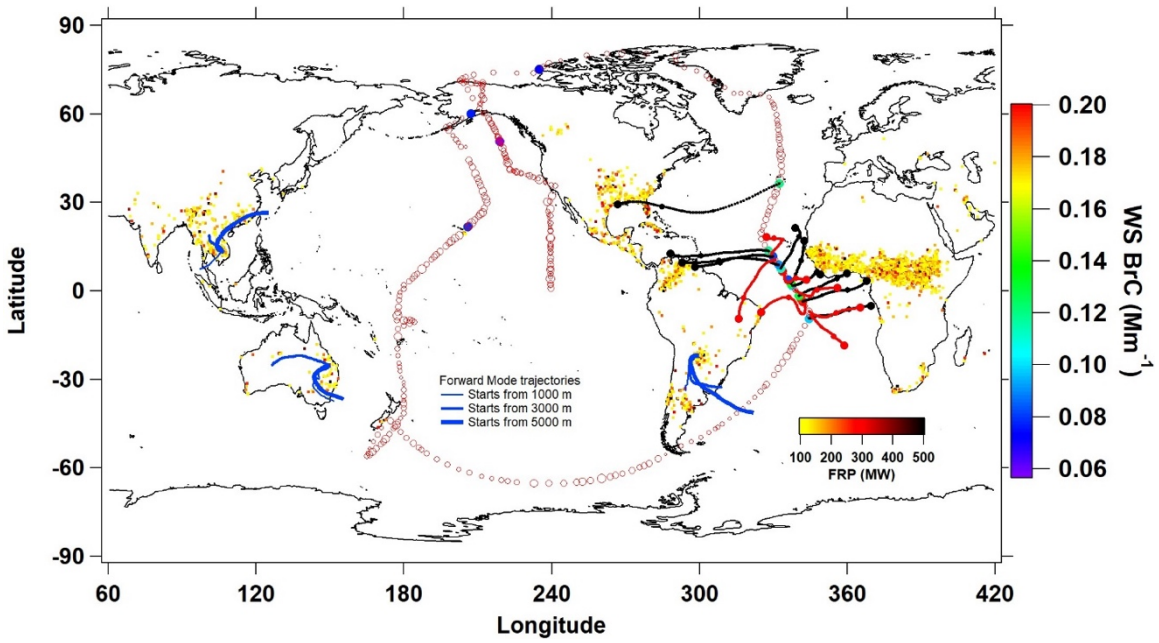

Figure A-5 Forward trajectories (blue) at various altitudes for regions of burning at times when the plume could be intercepted by the DC8 aircraft during ATom-2. For example, the fires in Southeast Asia and Australia did not reach or were not transported in the direction of the aircraft during roughly the time the DC8 was in the southern Pacific Ocean. For the fires in southern Africa that passed over the aircraft sampling path within 3 days of emission, the altitude did not intersect with the aircraft sampling location.

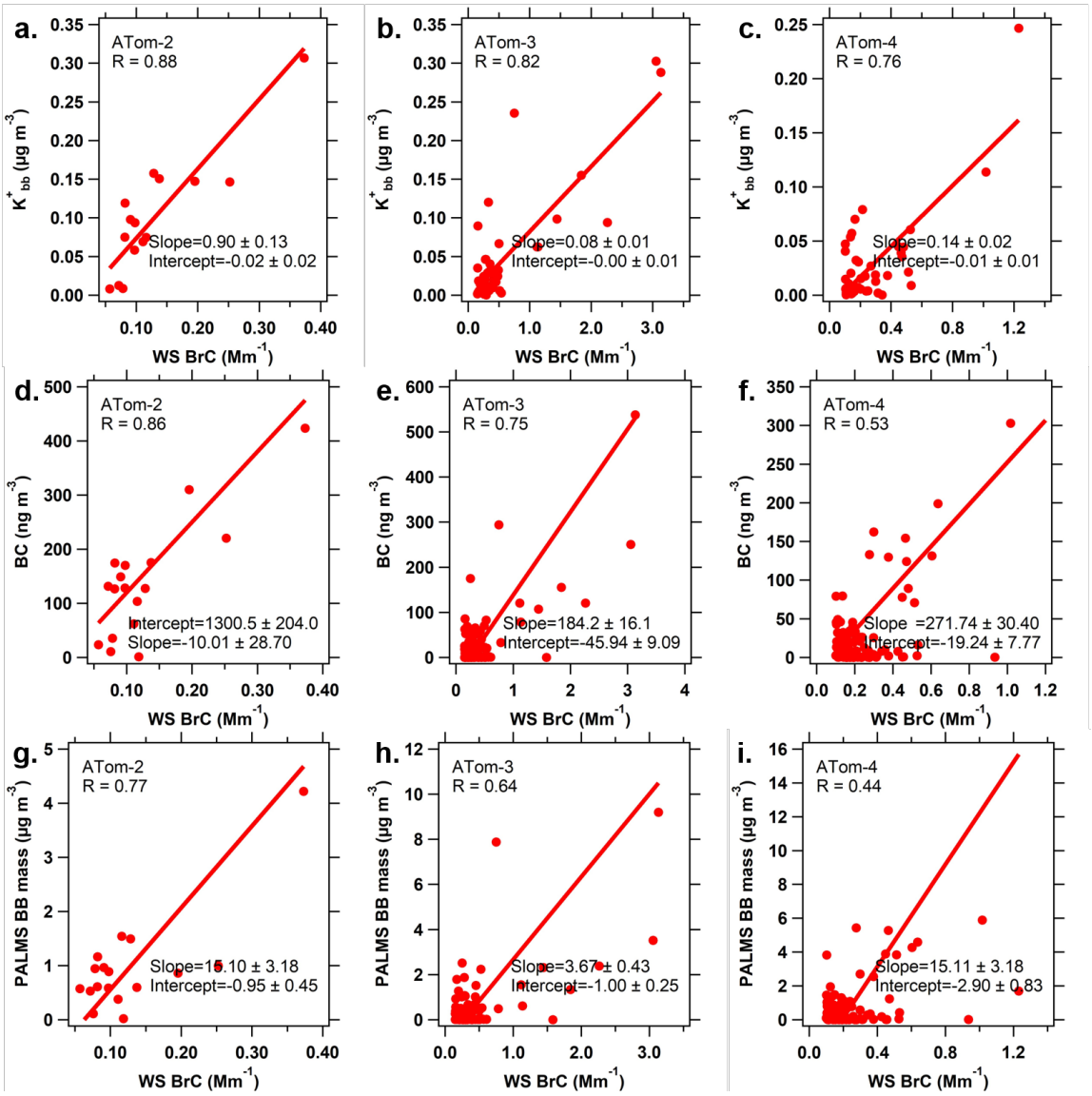

Figure A-6 Relationship between WS BrC, biomass burning potassium (K^+_{BB}), BC, and PALMS tracer analysis of biomass burning aerosol mass. Only data above the LOD are included. All plots have a p-value less than 0.01. WS BrC is the absorption coefficient at 365 nm determined from the LWCC by Eqn (S1).

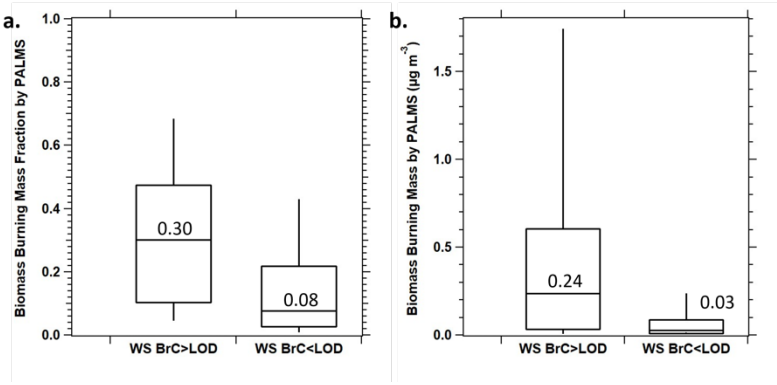

Figure A-7 Summary of single particle tracer analysis of biomass burning contribution to aerosols 0.1 to 4.8 μm diameter for periods when WS BrC > LOD and and WS BrC < LOD; (a) biomass burning percent mass fraction, and (b) biomass burning mass concentration. Data are for combined ATom 2, 3 and 4 missions. Middle line in box is median, with the value given above the line, the lower and upper edges of the box are the lower (25%) and upper (75%) quartiles and the line extend to the lower and upper extremes (10 and 90%).

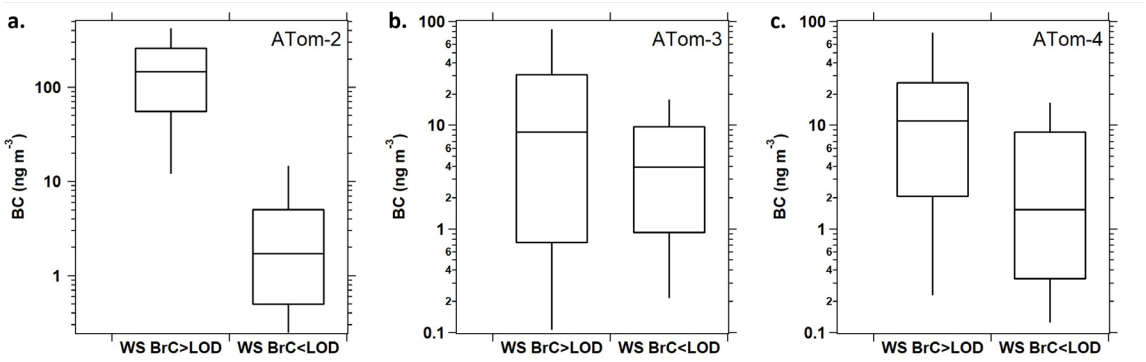

Figure A-8 Comparison for each ATom mission of BC mass measured by the SP2 for data when BrC was greater than LOD and when BrC was less than the LOD. BC was always higher when BrC>LOD, and was substantially higher for ATom mission 2. The results are consistent with high levels of BC being associated with incomplete combustion, such as biomass burning, a known strong source for BrC. In the plots the middle line in the box is the median, the lower and upper edges of the box are the lower (25%) and upper (75%) quartiles and the line extend to the lower and upper extremes (10 and 90%).

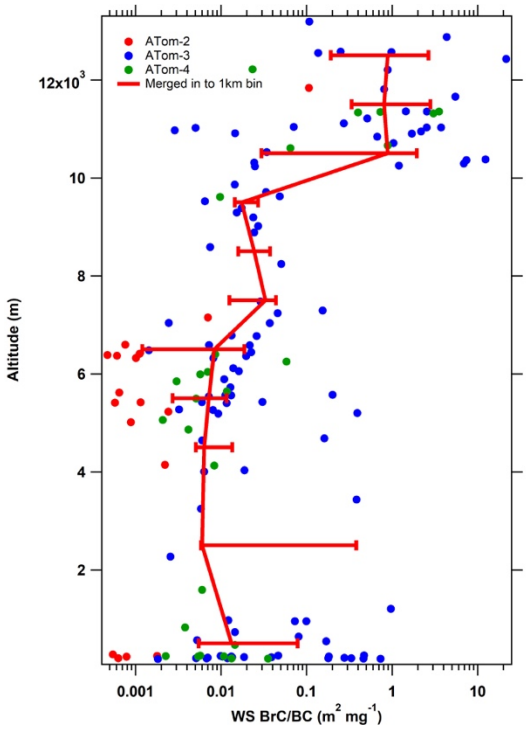

Figure A-9 Vertical profiles of WS BrC to BC (ratio). Data are averaged over 1 km altitude bins. Data for 2.5 km are merged from 1 km to 4 km due to fewer data points. Error bars are the interquartile range of the ratio.

Table A-1 Pearson correlations (r).

	ATom-2	ATom-3	ATom-4
WS BrC and BC	0.86	0.75	0.53
WS BrC and K^+_{BB}	0.88	0.82	0.76
WS BrC and PALMS BB mass	0.77	0.64	0.44
BC and K^+_{BB}	0.92	0.85	0.45

Table A-2 Mean DRE due to absorption by BrC and BC, and dry particle scattering by longitude range for combined ATom-2, 3 and 4. Numbers in parentheses are results from using zero as the WS BrC data less than LOD.

		DRE due to absorption by BrC (W m^{-2})	DRE due to absorption by BC (W m^{-2})	Scattering (W m^{-2})	The fraction of total carbonaceous aerosol DRE by BrC
Arctic	ATom-2	0.013 (0.002)	0.063	-6.013	17% (3%)
60N – 90N	ATom-3	0.040 (0.031)	0.092	-4.633	30% (25%)
	ATom-4	0.085 (0.058)	0.102	-4.277	46% (36%)
N Subtropical	ATom-2	0.029 (0.005)	0.126	-6.184	19% (4%)
20N – 60N	ATom-3	0.147 (0.097)	0.064	-11.675	70% (60%)
	ATom-4	0.179 (0.138)	0.371	-13.166	33% (27%)
Tropical	ATom-2	0.051 (0.023)	0.188	-9.196	21% (11%)
20S – 20N	ATom-3	1.204 (1.404)	1.664	-42.474	42% (46%)
	ATom-4	0.185 (0.152)	0.141	-9.648	57% (52%)
S Subtropical	ATom-2	0.029 (0)	0.017	-10.680	63% (0)
60S – 20S	ATom-3	0.151 (0.098)	0.220	-12.261	41% (31%)
	ATom-4	0.103 (0.049)	0.041	-8.376	71% (54%)
Antarctic	ATom-2	0.012 (0)	0.003	-5.823	79% (0)
90S – 60S	ATom-3	0.037 (0.040)	0.030	-3.217	56% (58%)
	ATom-4	0.057 (0.023)	0.005	-3.681	93% (83%)

*Z. Angle is the mean solar Zenith Angle used in the radiative transfer calculation.

B. APPENDIX B. SUPPORTING MATERIALS FOR CHAPTER 3

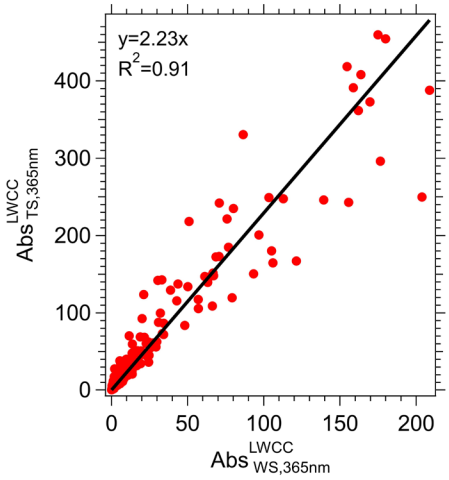

Figure B-1 Comparison of TS BrC ($Abs^{LWCC}_{TS,365nm}$) and WS BrC ($Abs^{LWCC}_{WS,365nm}$) at 365 nm (total soluble=water soluble + methanol soluble) for all FIREX-AQ identified smoke plumes. The intercept is forced to zero and regression line is fitted with ODR.

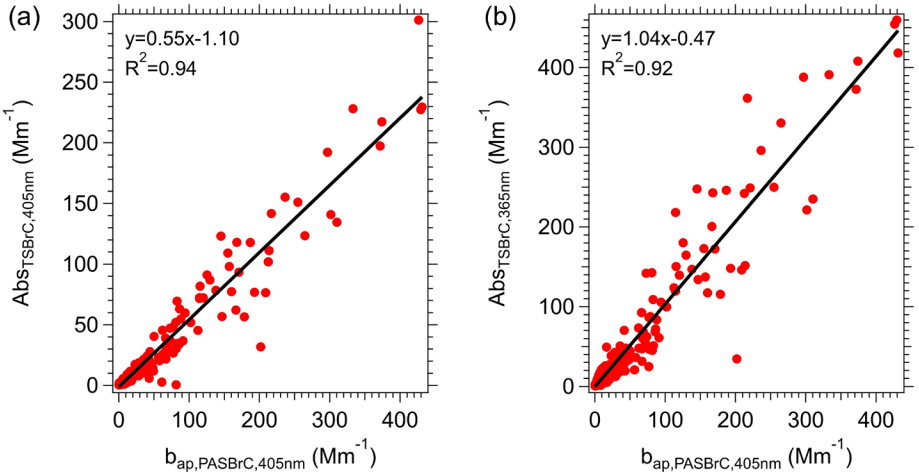

Figure B-2 Comparison of BrC absorption in liquid (without applying the conversion factor K) at (a) 405 nm and at (b) 365 nm with BrC absorption inferred from the PAS at 405 nm.

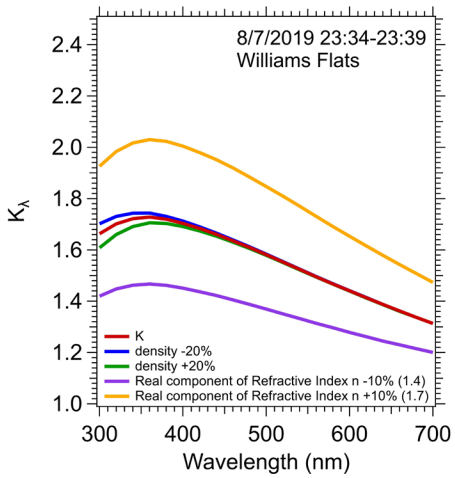

Figure B-3 Sensitivity analysis of the conversion factor from absorption in liquid to aerosol based on Mie theory. The red curve, which is the same as the one in Figure 3-4, with assumptions that n=1.55, and density is 1.4 g cm^{-3}. Tuning the particle density by up (green) or down (blue) by 20% only results in less than 5% change. Altering the real component of the refractive index (n) by up (yellow) or down (purple) by 10% can lead to ~20% of variation.

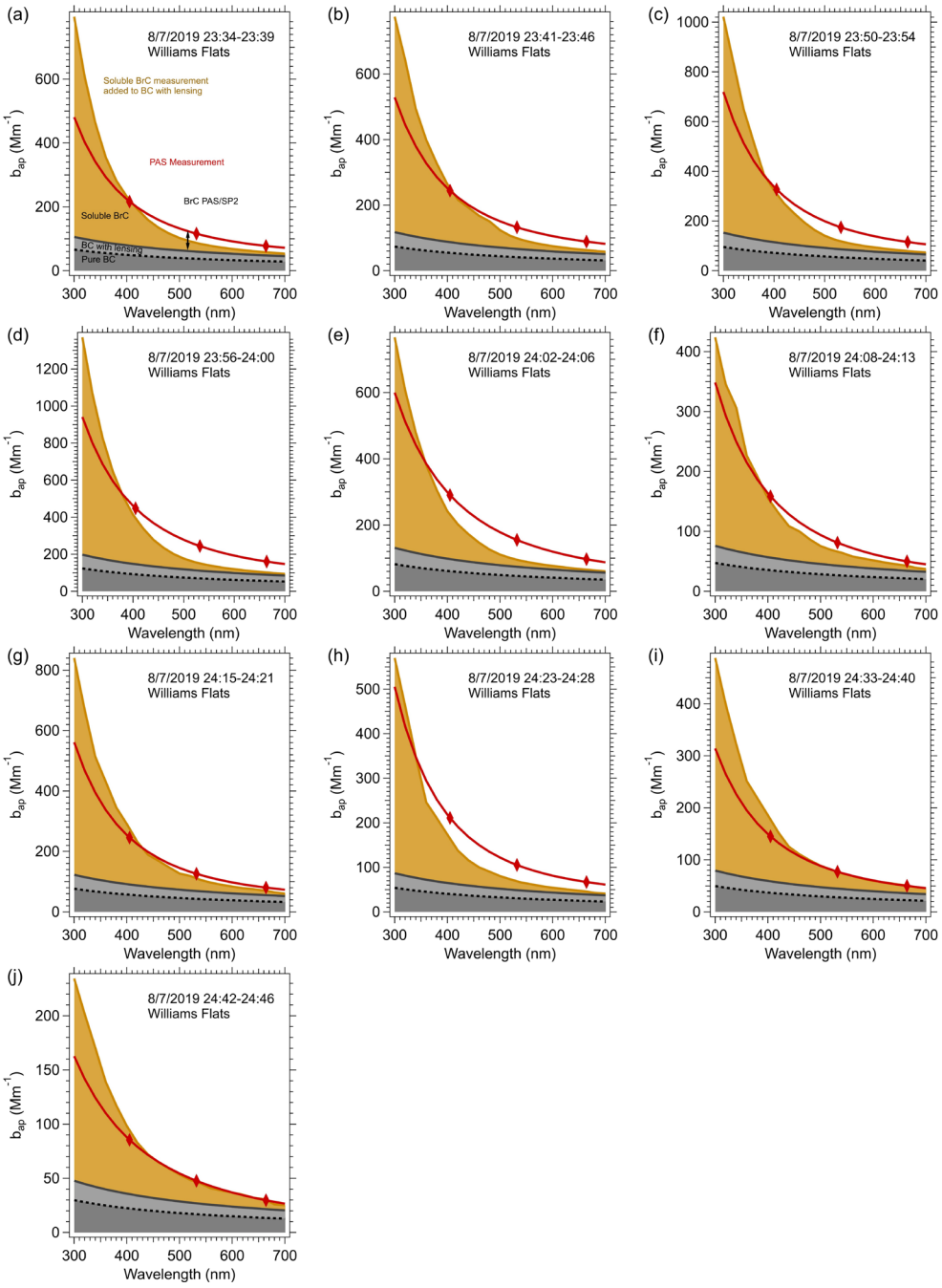

Figure B-4 Closure analysis of aerosol absorption measurements for the Williams Flats fire airborne measurements starting on 7 Aug. 2019. Each plot is the average of a plume transect starting from near to further from the fire. This fire had high BC concentrations relative to BrC.

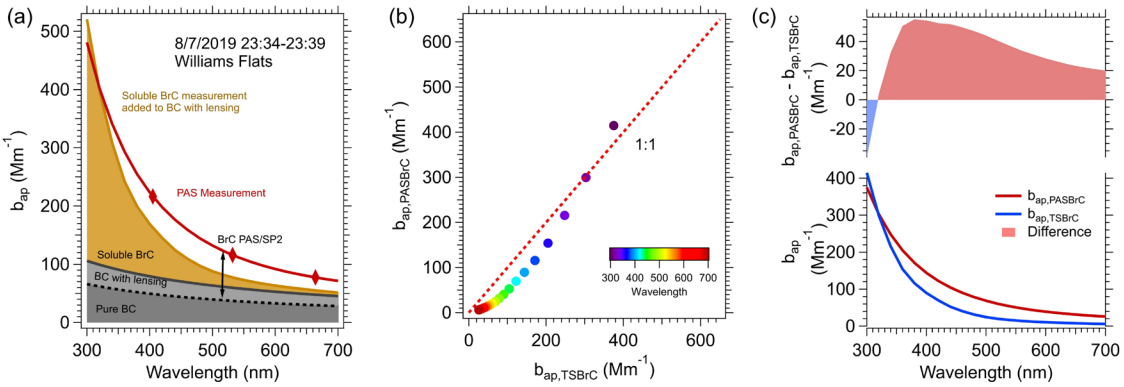

Figure B-5 Similar plots shown in Figure 3-5, but with K=1 (without applying the conversion from liquid to aerosol).

REFERENCES

Adachi, K., Sedlacek, A. J., Kleinman, L., Springston, S. R., Wang, J., Chand, D., Hubbe, J. M., Shilling, J. E., Onasch, T. B., Kinase, T., Sakata, K., Takahashi, Y., and Buseck, P. R.: Spherical tarball particles form through rapid chemical and physical changes of organic matter in biomass-burning smoke, Proceedings of the National Academy of Sciences, 116, 19336, 10.1073/pnas.1900129116, 2019.

Adler, G., Wagner, N. L., Lamb, K. D., Manfred, K. M., Schwarz, J. P., Franchin, A., Middlebrook, A. M., Washenfelder, R. A., Womack, C. C., Yokelson, R. J., and Murphy, D. M.: Evidence in biomass burning smoke for a light-absorbing aerosol with properties intermediate between brown and black carbon, Aerosol Science and Technology, 59, 976-989, 10.1080/02786826.2019.1617832, 2019.

Aguilera, R., Corringham, T., Gershunov, A., and Benmarhnia, T.: Wildfire smoke impacts respiratory health more than fine particles from other sources: observational evidence from Southern California, Nature Communications, 12, 1493, 10.1038/s41467-021-21708-0, 2021.

Aiona, P. K., Luek, J. L., Timko, S. A., Powers, L. C., Gonsior, M., and Nizkorodov, S. A.: Effect of Photolysis on Absorption and Fluorescence Spectra of Light-Absorbing Secondary Organic Aerosols, ACS Earth and Space Chemistry, 2, 235-245, 10.1021/acsearthspacechem.7b00153, 2018.

Akimoto, H.: Global Air Quality and Pollution, Science, 302, 1716, 10.1126/science.1092666, 2003.

Allan, D. W.: Historicity, strengths, and weaknesses of Allan variances and their general applications, Gyroscopy and Navigation, 7, 1-17, 10.1134/S2075108716010028, 2016.

Andreae, M. O., and Gelencsér, A.: Black carbon or brown carbon? The nature of light-absorbing carbonaceous aerosols, Atmos. Chem. Phys., 6, 3131-3148, 10.5194/acp-6-3131-2006, 2006.

Andreae, M. O.: Emission of trace gases and aerosols from biomass burning – an updated assessment, Atmos. Chem. Phys., 19, 8523-8546, 10.5194/acp-19-8523-2019, 2019.

Andrews, E., Sheridan, P. J., Fiebig, M., McComiskey, A., Ogren, J. A., Arnott, P., Covert, D., Elleman, R., Gasparini, R., Collins, D., Jonsson, H., Schmid, B., and Wang, J.: Comparison of methods for deriving aerosol asymmetry parameter, Journal of Geophysical Research: Atmospheres, 111, 10.1029/2004jd005734, 2006.

Appel, B. R., Tokiwa, Y., Hsu, J., Kothny, E. L., and Hahn, E.: Visibility as related to atmospheric aerosol constituents, Atmospheric Environment (1967), 19, 1525-1534, https://doi.org/10.1016/0004-6981(85)90290-2, 1985.

Arnott, W. P., Moosmüller, H., Rogers, C. F., Jin, T., and Bruch, R.: Photoacoustic spectrometer for measuring light absorption by aerosol: instrument description, Atmospheric Environment, 33, 2845-2852, https://doi.org/10.1016/S1352-2310(98)00361-6, 1999.

Bahreini, R., Ervens, B., Middlebrook, A. M., Warneke, C., de Gouw, J. A., DeCarlo, P. F., Jimenez, J. L., Brock, C. A., Neuman, J. A., Ryerson, T. B., Stark, H., Atlas, E., Brioude, J., Fried, A., Holloway, J. S., Peischl, J., Richter, D., Walega, J., Weibring, P., Wollny, A. G., and Fehsenfeld, F. C.: Organic aerosol formation in urban and industrial plumes near Houston and Dallas, Texas, Journal of Geophysical Research: Atmospheres, 114, https://doi.org/10.1029/2008JD011493, 2009.

Bandowe, B. A. M., and Meusel, H.: Nitrated polycyclic aromatic hydrocarbons (nitro-PAHs) in the environment – A review, Science of The Total Environment, 581-582, 237-257, https://doi.org/10.1016/j.scitotenv.2016.12.115, 2017.

Bates, J. T., Fang, T., Verma, V., Zeng, L., Weber, R. J., Tolbert, P. E., Abrams, J. Y., Sarnat, S. E., Klein, M., Mulholland, J. A., and Russell, A. G.: Review of Acellular Assays of Ambient Particulate Matter Oxidative Potential: Methods and Relationships with Composition, Sources, and Health Effects, Environmental Science & Technology, 53, 4003-4019, 10.1021/acs.est.8b03430, 2019.

Bellouin, N., Boucher, O., Haywood, J., and Reddy, M. S.: Global estimate of aerosol direct radiative forcing from satellite measurements, Nature, 438, 1138-1141, 10.1038/nature04348, 2005.

Bergstrom, R. W., Pilewskie, P., Russell, P. B., Redemann, J., Bond, T. C., Quinn, P. K., and Sierau, B.: Spectral absorption properties of atmospheric aerosols, Atmos. Chem. Phys., 7, 5937-5943, 10.5194/acp-7-5937-2007, 2007.

Bluvshtein, N., Lin, P., Flores, J. M., Segev, L., Mazar, Y., Tas, E., Snider, G., Weagle, C., Brown, S. S., Laskin, A., and Rudich, Y.: Broadband optical properties of biomass-burning aerosol and identification of brown carbon chromophores, Journal of Geophysical Research: Atmospheres, 122, 5441-5456, https://doi.org/10.1002/2016JD026230, 2017.

Bond, T. C., Anderson, T. L., and Campbell, D.: Calibration and Intercomparison of Filter-Based Measurements of Visible Light Absorption by Aerosols, Aerosol Science and Technology, 30, 582-600, 10.1080/027868299304435, 1999.

Bond, T. C., and Bergstrom, R. W.: Light Absorption by Carbonaceous Particles: An Investigative Review, Aerosol Science and Technology, 40, 27-67, 10.1080/02786820500421521, 2006.

Bond, T. C., Doherty, S. J., Fahey, D. W., Forster, P. M., Berntsen, T., DeAngelo, B. J., Flanner, M. G., Ghan, S., Kärcher, B., Koch, D., Kinne, S., Kondo, Y., Quinn, P. K., Sarofim, M. C., Schultz, M. G., Schulz, M., Venkataraman, C., Zhang, H., Zhang, S., Bellouin, N., Guttikunda, S. K., Hopke, P. K., Jacobson, M. Z., Kaiser, J. W., Klimont, Z., Lohmann, U., Schwarz, J. P., Shindell, D., Storelvmo, T., Warren, S. G., and Zender, C. S.: Bounding the role of black carbon in the climate system: A scientific assessment, Journal of Geophysical Research: Atmospheres, 118, 5380-5552, 10.1002/jgrd.50171, 2013.

Brock, C. A., Wagner, N. L., Anderson, B. E., Attwood, A. R., Beyersdorf, A., Campuzano-Jost, P., Carlton, A. G., Day, D. A., Diskin, G. S., Gordon, T. D., Jimenez, J. L., Lack, D. A., Liao, J., Markovic, M. Z., Middlebrook, A. M., Ng, N. L., Perring, A. E., Richardson, M. S., Schwarz, J. P., Washenfelder, R. A., Welti, A., Xu, L., Ziemba, L. D., and Murphy, D. M.: Aerosol optical properties in the southeastern United States in summer – Part 1: Hygroscopic growth, Atmos. Chem. Phys., 16, 4987-5007, 10.5194/acp-16-4987-2016, 2016.

Brock, C. A., Williamson, C., Kupc, A., Froyd, K. D., Erdesz, F., Wagner, N., Richardson, M., Schwarz, J. P., Gao, R. S., Katich, J. M., Campuzano-Jost, P., Nault, B. A., Schroder, J. C., Jimenez, J. L., Weinzierl, B., Dollner, M., Bui, T., and Murphy, D. M.: Aerosol size distributions during the Atmospheric Tomography Mission (ATom): methods, uncertainties, and data products, Atmos. Meas. Tech., 12, 3081-3099, 10.5194/amt-12-3081-2019, 2019.

Browne, E. C., Zhang, X., Franklin, J. P., Ridley, K. J., Kirchstetter, T. W., Wilson, K. R., Cappa, C. D., and Kroll, J. H.: Effect of heterogeneous oxidative aging on light absorption by biomass burning organic aerosol, Aerosol Science and Technology, 53, 663-674, 10.1080/02786826.2019.1599321, 2019.

Burke, M., Driscoll, A., Heft-Neal, S., Xue, J., Burney, J., and Wara, M.: The changing risk and burden of wildfire in the United States, Proceedings of the National Academy of Sciences, 118, e2011048118, 10.1073/pnas.2011048118, 2021.

Buseck, P. R., Adachi, K., Gelencsér, A., Tompa, É., and Pósfai, M.: Are black carbon and soot the same?, Atmos. Chem. Phys. Discuss., 2012, 24821-24846, 10.5194/acpd-12-24821-2012, 2012.

Cappa, C. D., Onasch, T. B., Massoli, P., Worsnop, D. R., Bates, T. S., Cross, E. S., Davidovits, P., Hakala, J., Hayden, K. L., Jobson, B. T., Kolesar, K. R., Lack, D. A., Lerner, B. M., Li, S.-M., Mellon, D., Nuaaman, I., Olfert, J. S., Petäjä, T., Quinn, P. K., Song, C., Subramanian, R., Williams, E. J., and Zaveri, R. A.: Radiative Absorption Enhancements Due to the Mixing State of Atmospheric Black Carbon, Science, 337, 1078, 10.1126/science.1223447, 2012.

Cappa, C. D., Zhang, X., Russell, L. M., Collier, S., Lee, A. K. Y., Chen, C.-L., Betha, R., Chen, S., Liu, J., Price, D. J., Sanchez, K. J., McMeeking, G. R., Williams, L. R., Onasch, T. B., Worsnop, D. R., Abbatt, J., and Zhang, Q.: Light Absorption by Ambient Black and Brown Carbon and its Dependence on Black Carbon Coating State for Two California, USA, Cities in Winter and Summer, Journal of Geophysical Research: Atmospheres, 124, 1550-1577, 10.1029/2018jd029501, 2019.

Chakrabarty, R. K., Moosmüller, H., Chen, L. W. A., Lewis, K., Arnott, W. P., Mazzoleni, C., Dubey, M. K., Wold, C. E., Hao, W. M., and Kreidenweis, S. M.: Brown carbon in tar balls from smoldering biomass combustion, Atmos. Chem. Phys., 10, 6363-6370, 10.5194/acp-10-6363-2010, 2010.

Chakrabarty, R. K., Gyawali, M., Yatavelli, R. L. N., Pandey, A., Watts, A. C., Knue, J., Chen, L. W. A., Pattison, R. R., Tsibart, A., Samburova, V., and Moosmüller, H.: Brown carbon aerosols from burning of boreal peatlands: microphysical properties, emission factors, and implications for direct radiative forcing, Atmos. Chem. Phys., 16, 3033-3040, 10.5194/acp-16-3033-2016, 2016.

Chakrabarty, R. K., and Heinson, W. R.: Scaling Laws for Light Absorption Enhancement Due to Nonrefractory Coating of Atmospheric Black Carbon Aerosol, Physical Review Letters, 121, 218701, 10.1103/PhysRevLett.121.218701, 2018.

Chen, J., Li, C., Ristovski, Z., Milic, A., Gu, Y., Islam, M. S., Wang, S., Hao, J., Zhang, H., He, C., Guo, H., Fu, H., Miljevic, B., Morawska, L., Thai, P., Lam, Y. F.,

Pereira, G., Ding, A., Huang, X., and Dumka, U. C.: A review of biomass burning: Emissions and impacts on air quality, health and climate in China, Science of The Total Environment, 579, 1000-1034, https://doi.org/10.1016/j.scitotenv.2016.11.025, 2017.

Chen, Y., and Bond, T. C.: Light absorption by organic carbon from wood combustion, Atmos. Chem. Phys., 10, 1773-1787, 10.5194/acp-10-1773-2010, 2010.

Cheng, Z., Atwi, K. M., Yu, Z., Avery, A., Fortner, E. C., Williams, L., Majluf, F., Krechmer, J. E., Lambe, A. T., and Saleh, R.: Evolution of the light-absorption properties of combustion brown carbon aerosols following reaction with nitrate radicals, Aerosol Science and Technology, 54, 849-863, 10.1080/02786826.2020.1726867, 2020.

Cheng, Z., Atwi, K., Hajj, O. E., Ijeli, I., Fischer, D. A., Smith, G., and Saleh, R.: Discrepancies between brown carbon light-absorption properties retrieved from online and offline measurements, Aerosol Science and Technology, 55, 92-103, 10.1080/02786826.2020.1820940, 2021.

Chýlek, P., and Coakley, J. A.: Aerosols and Climate, Science, 183, 75, 10.1126/science.183.4120.75, 1974.

Claeys, M., Vermeylen, R., Yasmeen, F., Gómez-González, Y., Chi, X., Maenhaut, W., Mészáros, T., and Salma, I.: Chemical characterisation of humic-like substances from urban, rural and tropical biomass burning environments using liquid chromatography with UV/vis photodiode array detection and electrospray ionisation mass spectrometry, Environmental Chemistry, 9, 273-284, 2012.

Cofer, W. R., Collins, V. G., and Talbot, R. W.: Improved aqueous scrubber for collection of soluble atmospheric trace gases, Environmental Science & Technology, 19, 557-560, 10.1021/es00136a012, 1985.

Cofer, W. R., and Edahl, R. A.: A new technique for collection, concentration and determination of gaseous tropospheric formaldehyde, Atmospheric Environment (1967), 20, 979-984, https://doi.org/10.1016/0004-6981(86)90282-9, 1986.

Cohen, A. J., Brauer, M., Burnett, R., Anderson, H. R., Frostad, J., Estep, K., Balakrishnan, K., Brunekreef, B., Dandona, L., Dandona, R., Feigin, V., Freedman, G., Hubbell, B., Jobling, A., Kan, H., Knibbs, L., Liu, Y., Martin, R., Morawska, L., Pope, C. A., III, Shin, H., Straif, K., Shaddick, G., Thomas, M., van Dingenen, R., van Donkelaar, A., Vos, T., Murray, C. J. L., and Forouzanfar,

M. H.: Estimates and 25-year trends of the global burden of disease attributable to ambient air pollution: an analysis of data from the Global Burden of Diseases Study 2015, The Lancet, 389, 1907-1918, 10.1016/S0140-6736(17)30505-6, 2017.

Cooke, W. F., and Wilson, J. J. N.: A global black carbon aerosol model, Journal of Geophysical Research: Atmospheres, 101, 19395-19409, 10.1029/96JD00671, 1996.

Corbin, J. C., Czech, H., Massabò, D., de Mongeot, F. B., Jakobi, G., Liu, F., Lobo, P., Mennucci, C., Mensah, A. A., Orasche, J., Pieber, S. M., Prévôt, A. S. H., Stengel, B., Tay, L. L., Zanatta, M., Zimmermann, R., El Haddad, I., and Gysel, M.: Infrared-absorbing carbonaceous tar can dominate light absorption by marine-engine exhaust, npj Climate and Atmospheric Science, 2, 12, 10.1038/s41612-019-0069-5, 2019.

Craig, L., Moharreri, A., Schanot, A., Rogers, D. C., Anderson, B., and Dhaniyala, S.: Characterizations of Cloud Droplet Shatter Artifacts in Two Airborne Aerosol Inlets, Aerosol Science and Technology, 47, 662-671, 10.1080/02786826.2013.780648, 2013a.

Craig, L., Schanot, A., Moharreri, A., Rogers, D. C., and Dhaniyala, S.: Design and Sampling Characteristics of a New Airborne Aerosol Inlet for Aerosol Measurements in Clouds, Journal of Atmospheric and Oceanic Technology, 30, 1123-1135, 10.1175/jtech-d-12-00168.1, 2013b.

Craig, L., Moharreri, A., Rogers, D. C., Anderson, B., and Dhaniyala, S.: Aircraft-Based Aerosol Sampling in Clouds: Performance Characterization of Flow-Restriction Aerosol Inlets, Journal of Atmospheric and Oceanic Technology, 31, 2512-2521, 10.1175/jtech-d-14-00022.1, 2014.

Crosson, E. R.: A cavity ring-down analyzer for measuring atmospheric levels of methane, carbon dioxide, and water vapor, Applied Physics B, 92, 403-408, 10.1007/s00340-008-3135-y, 2008.

Dasari, S., Andersson, A., Bikkina, S., Holmstrand, H., Budhavant, K., Satheesh, S., Asmi, E., Kesti, J., Backman, J., Salam, A., Bisht, D. S., Tiwari, S., Hameed, Z., and Gustafsson, Ö.: Photochemical degradation affects the light absorption of water-soluble brown carbon in the South Asian outflow, Science Advances, 5, eaau8066, 10.1126/sciadv.aau8066, 2019.

De Haan, D. O., Hawkins, L. N., Welsh, H. G., Pednekar, R., Casar, J. R., Pennington, E. A., de Loera, A., Jimenez, N. G., Symons, M. A., Zauscher, M., Pajunoja, A., Caponi, L., Cazaunau, M., Formenti, P., Gratien, A., Pangui, E., and Doussin, J.-F.: Brown Carbon Production in Ammonium- or Amine-Containing Aerosol Particles by Reactive Uptake of Methylglyoxal and Photolytic Cloud Cycling, Environmental Science & Technology, 51, 7458-7466, 10.1021/acs.est.7b00159, 2017.

DeCarlo, P. F., Kimmel, J. R., Trimborn, A., Northway, M. J., Jayne, J. T., Aiken, A. C., Gonin, M., Fuhrer, K., Horvath, T., Docherty, K. S., Worsnop, D. R., and Jimenez, J. L.: Field-Deployable, High-Resolution, Time-of-Flight Aerosol Mass Spectrometer, Analytical Chemistry, 78, 8281-8289, 10.1021/ac061249n, 2006.

DeCarlo, P. F., Dunlea, E. J., Kimmel, J. R., Aiken, A. C., Sueper, D., Crounse, J., Wennberg, P. O., Emmons, L., Shinozuka, Y., Clarke, A., Zhou, J., Tomlinson, J., Collins, D. R., Knapp, D., Weinheimer, A. J., Montzka, D. D., Campos, T., and Jimenez, J. L.: Fast airborne aerosol size and chemistry measurements above Mexico City and Central Mexico during the MILAGRO campaign, Atmos. Chem. Phys., 8, 4027-4048, 10.5194/acp-8-4027-2008, 2008.

Dentener, F. J., Carmichael, G. R., Zhang, Y., Lelieveld, J., and Crutzen, P. J.: Role of mineral aerosol as a reactive surface in the global troposphere, Journal of Geophysical Research: Atmospheres, 101, 22869-22889, https://doi.org/10.1029/96JD01818, 1996.

Desyaterik, Y., Sun, Y., Shen, X., Lee, T., Wang, X., Wang, T., and Collett Jr, J. L.: Speciation of "brown" carbon in cloud water impacted by agricultural biomass burning in eastern China, Journal of Geophysical Research: Atmospheres, 118, 7389-7399, 10.1002/jgrd.50561, 2013.

Di Lorenzo, R. A., and Young, C. J.: Size separation method for absorption characterization in brown carbon: Application to an aged biomass burning sample, Geophysical Research Letters, 43, 458-465, 10.1002/2015GL066954, 2016.

Di Lorenzo, R. A., Washenfelder, R. A., Attwood, A. R., Guo, H., Xu, L., Ng, N. L., Weber, R. J., Baumann, K., Edgerton, E., and Young, C. J.: Molecular-Size-Separated Brown Carbon Absorption for Biomass-Burning Aerosol at Multiple Field Sites, Environmental Science & Technology, 51, 3128-3137, 10.1021/acs.est.6b06160, 2017.

Dibb, J. E., Talbot, R. W., Scheuer, E. M., Blake, D. R., Blake, N. J., Gregory, G. L., Sachse, G. W., and Thornton, D. C.: Aerosol chemical composition and distribution during the Pacific Exploratory Mission (PEM) Tropics, Journal of Geophysical Research: Atmospheres, 104, 5785-5800, 10.1029/1998jd100001, 1999.

Dibb, J. E., Talbot, R. W., Scheuer, E., Seid, G., DeBell, L., Lefer, B., and Ridley, B.: Stratospheric influence on the northern North American free troposphere during TOPSE: 7Be as a stratospheric tracer, Journal of Geophysical Research: Atmospheres, 108, 8863, https://doi.org/10.1029/2001JD001347, 2003.

Duplissy, J., DeCarlo, P. F., Dommen, J., Alfarra, M. R., Metzger, A., Barmpadimos, I., Prevot, A. S. H., Weingartner, E., Tritscher, T., Gysel, M., Aiken, A. C., Jimenez, J. L., Canagaratna, M. R., Worsnop, D. R., Collins, D. R., Tomlinson, J., and Baltensperger, U.: Relating hygroscopicity and composition of organic aerosol particulate matter, Atmos. Chem. Phys., 11, 1155-1165, 10.5194/acp-11-1155-2011, 2011.

Eatough, D. J., Wadsworth, A., Eatough, D. A., Crawford, J. W., Hansen, L. D., and Lewis, E. A.: A multiple-system, multi-channel diffusion denuder sampler for the determination of fine-particulate organic material in the atmosphere, Atmospheric Environment. Part A. General Topics, 27, 1213-1219, https://doi.org/10.1016/0960-1686(93)90247-V, 1993.

Echalar, F., Gaudichet, A., Cachier, H., and Artaxo, P.: Aerosol emissions by tropical forest and savanna biomass burning: Characteristic trace elements and fluxes, Geophysical Research Letters, 22, 3039-3042, 10.1029/95GL03170, 1995.

Fan, X., Cao, T., Yu, X., Wang, Y., Xiao, X., Li, F., Xie, Y., Ji, W., Song, J., and Peng, P.: The evolutionary behavior of chromophoric brown carbon during ozone aging of fine particles from biomass burning, Atmos. Chem. Phys., 20, 4593-4605, 10.5194/acp-20-4593-2020, 2020.

Fang, T., Verma, V., Bates, J. T., Abrams, J., Klein, M., Strickland, M. J., Sarnat, S. E., Chang, H. H., Mulholland, J. A., Tolbert, P. E., Russell, A. G., and Weber, R. J.: Oxidative potential of ambient water-soluble PM2.5 in the southeastern United States: contrasts in sources and health associations between ascorbic acid (AA) and dithiothreitol (DTT) assays, Atmos. Chem. Phys., 16, 3865-3879, 10.5194/acp-16-3865-2016, 2016.

Feng, Y., Ramanathan, V., and Kotamarthi, V. R.: Brown carbon: a significant atmospheric absorber of solar radiation?, Atmos. Chem. Phys., 13, 8607-8621, 10.5194/acp-13-8607-2013, 2013.

Fierce, L., Onasch, T. B., Cappa, C. D., Mazzoleni, C., China, S., Bhandari, J., Davidovits, P., Fischer, D. A., Helgestad, T., Lambe, A. T., Sedlacek, A. J., Smith, G. D., and Wolff, L.: Radiative absorption enhancements by black carbon controlled by particle-to-particle heterogeneity in composition, Proceedings of the National Academy of Sciences, 117, 5196-5203, 10.1073/pnas.1919723117, 2020.

Fleming, L. T., Lin, P., Roberts, J. M., Selimovic, V., Yokelson, R., Laskin, J., Laskin, A., and Nizkorodov, S. A.: Molecular composition and photochemical lifetimes of brown carbon chromophores in biomass burning organic aerosol, Atmos. Chem. Phys., 20, 1105-1129, 10.5194/acp-20-1105-2020, 2020.

Forrister, H., Liu, J., Scheuer, E., Dibb, J., Ziemba, L., Thornhill, K. L., Anderson, B., Diskin, G., Perring, A. E., Schwarz, J. P., Campuzano-Jost, P., Day, D. A., Palm, B. B., Jimenez, J. L., Nenes, A., and Weber, R. J.: Evolution of brown carbon in wildfire plumes, Geophysical Research Letters, 42, 4623-4630, 10.1002/2015GL063897, 2015.

Friedlander, S. K.: Smoke, dust and haze: Fundamentals of aerosol behavior, 1977.

Froyd, K. D., Murphy, D. M., Brock, C. A., Campuzano-Jost, P., Dibb, J. E., Jimenez, J. L., Kupc, A., Middlebrook, A. M., Schill, G. P., Thornhill, K. L., Williamson, C. J., Wilson, J. C., and Ziemba, L. D.: A new method to quantify mineral dust and other aerosol species from aircraft platforms using single-particle mass spectrometry, Atmos. Meas. Tech., 12, 6209-6239, 10.5194/amt-12-6209-2019, 2019.

Gao, D., Godri Pollitt, K. J., Mulholland, J. A., Russell, A. G., and Weber, R. J.: Characterization and comparison of PM2.5 oxidative potential assessed by two acellular assays, Atmos. Chem. Phys., 20, 5197-5210, 10.5194/acp-20-5197-2020, 2020a.

Gao, D., Mulholland, J. A., Russell, A. G., and Weber, R. J.: Characterization of water-insoluble oxidative potential of PM2.5 using the dithiothreitol assay, Atmospheric Environment, 224, 117327, https://doi.org/10.1016/j.atmosenv.2020.117327, 2020b.

Garofalo, L. A., Pothier, M. A., Levin, E. J. T., Campos, T., Kreidenweis, S. M., and Farmer, D. K.: Emission and Evolution of Submicron Organic Aerosol in Smoke from Wildfires in the Western United States, ACS Earth and Space Chemistry, 3, 1237-1247, 10.1021/acsearthspacechem.9b00125, 2019.

Gomes, M. S. P., Pui, D. Y. H., Vincent, J. H., and Liu, B. Y. H.: Convective and diffusive dispersion of particles in laminar tube flow: Effects on time-dependent concentration measurements, Journal of Aerosol Science, 24, 643-654, https://doi.org/10.1016/0021-8502(93)90021-Z, 1993.

Haan, D. O. D., Corrigan, A. L., Smith, K. W., Stroik, D. R., Turley, J. J., Lee, F. E., Tolbert, M. A., Jimenez, J. L., Cordova, K. E., and Ferrell, G. R.: Secondary Organic Aerosol-Forming Reactions of Glyoxal with Amino Acids, Environmental Science & Technology, 43, 2818-2824, 10.1021/es803534f, 2009.

Harrison, A. W., Waterson, A. M., and De Bruyn, W. J.: Spectroscopic and Photochemical Properties of Secondary Brown Carbon from Aqueous Reactions of Methylglyoxal, ACS Earth and Space Chemistry, 4, 762-773, 10.1021/acsearthspacechem.0c00061, 2020.

Haynes, J. P., Miller, K. E., and Majestic, B. J.: Investigation into Photoinduced Auto-Oxidation of Polycyclic Aromatic Hydrocarbons Resulting in Brown Carbon Production, Environmental Science & Technology, 53, 682-691, 10.1021/acs.est.8b05704, 2019.

Haywood, J., and Boucher, O.: Estimates of the direct and indirect radiative forcing due to tropospheric aerosols: A review, Reviews of Geophysics, 38, 513-543, 10.1029/1999rg000078, 2000.

He, Q., Tomaz, S., Li, C., Zhu, M., Meidan, D., Riva, M., Laskin, A., Brown, S. S., George, C., Wang, X., and Rudich, Y.: Optical Properties of Secondary Organic Aerosol Produced by Nitrate Radical Oxidation of Biogenic Volatile Organic Compounds, Environmental Science & Technology, 55, 2878-2889, 10.1021/acs.est.0c06838, 2021.

Heald, C. L., Ridley, D. A., Kroll, J. H., Barrett, S. R. H., Cady-Pereira, K. E., Alvarado, M. J., and Holmes, C. D.: Contrasting the direct radiative effect and direct radiative forcing of aerosols, Atmos. Chem. Phys., 14, 5513-5527, 10.5194/acp-14-5513-2014, 2014.

Healy, R. M., Wang, J. M., Jeong, C.-H., Lee, A. K. Y., Willis, M. D., Jaroudi, E., Zimmerman, N., Hilker, N., Murphy, M., Eckhardt, S., Stohl, A., Abbatt, J. P. D., Wenger, J. C., and Evans, G. J.: Light-absorbing properties of ambient black carbon and brown carbon from fossil fuel and biomass burning sources, Journal of Geophysical Research: Atmospheres, 120, 6619-6633, https://doi.org/10.1002/2015JD023382, 2015.

Hecobian, A., Zhang, X., Zheng, M., Frank, N., Edgerton, E. S., and Weber, R. J.: Water-Soluble Organic Aerosol material and the light-absorption characteristics of aqueous extracts measured over the Southeastern United States, Atmos. Chem. Phys., 10, 5965-5977, 10.5194/acp-10-5965-2010, 2010.

Hems, R. F., and Abbatt, J. P. D.: Aqueous Phase Photo-oxidation of Brown Carbon Nitrophenols: Reaction Kinetics, Mechanism, and Evolution of Light Absorption, ACS Earth and Space Chemistry, 2, 225-234, 10.1021/acsearthspacechem.7b00123, 2018.

Hinrichs, R. Z., Buczek, P., and Trivedi, J. J.: Solar Absorption by Aerosol-Bound Nitrophenols Compared to Aqueous and Gaseous Nitrophenols, Environmental Science & Technology, 50, 5661-5667, 10.1021/acs.est.6b00302, 2016.

Hobbs, P. V., Sinha, P., Yokelson, R. J., Christian, T. J., Blake, D. R., Gao, S., Kirchstetter, T. W., Novakov, T., and Pilewskie, P.: Evolution of gases and particles from a savanna fire in South Africa, Journal of Geophysical Research: Atmospheres, 108, https://doi.org/10.1029/2002JD002352, 2003.

Hoffer, A., Gelencsér, A., Guyon, P., Kiss, G., Schmid, O., Frank, G. P., Artaxo, P., and Andreae, M. O.: Optical properties of humic-like substances (HULIS) in biomass-burning aerosols, Atmos. Chem. Phys., 6, 3563-3570, 10.5194/acp-6-3563-2006, 2006.

Holben, B. N., Eck, T. F., Slutsker, I., Tanré, D., Buis, J. P., Setzer, A., Vermote, E., Reagan, J. A., Kaufman, Y. J., Nakajima, T., Lavenu, F., Jankowiak, I., and Smirnov, A.: AERONET—A Federated Instrument Network and Data Archive for Aerosol Characterization, Remote Sensing of Environment, 66, 1-16, https://doi.org/10.1016/S0034-4257(98)00031-5, 1998.

Hook, S. J., Myers, J. J., Thome, K. J., Fitzgerald, M., and Kahle, A. B.: The MODIS/ASTER airborne simulator (MASTER) — a new instrument for earth science studies, Remote Sensing of Environment, 76, 93-102, https://doi.org/10.1016/S0034-4257(00)00195-4, 2001.

Horvath, H.: Atmospheric light absorption—A review, Atmospheric Environment. Part A. General Topics, 27, 293-317, https://doi.org/10.1016/0960-1686(93)90104-7, 1993.

Huffman, J. A., Docherty, K. S., Aiken, A. C., Cubison, M. J., Ulbrich, I. M., DeCarlo, P. F., Sueper, D., Jayne, J. T., Worsnop, D. R., Ziemann, P. J., and Jimenez, J. L.: Chemically-resolved aerosol volatility measurements from two megacity field studies, Atmos. Chem. Phys., 9, 7161-7182, 10.5194/acp-9-7161-2009, 2009a.

Huffman, J. A., Docherty, K. S., Mohr, C., Cubison, M. J., Ulbrich, I. M., Ziemann, P. J., Onasch, T. B., and Jimenez, J. L.: Chemically-Resolved Volatility Measurements of Organic Aerosol from Different Sources, Environmental Science & Technology, 43, 5351-5357, 10.1021/es803539d, 2009b.

Jacobson, M. Z.: Strong radiative heating due to the mixing state of black carbon in atmospheric aerosols, Nature, 409, 695-697, 10.1038/35055518, 2001.

Jiang, H., Frie, A. L., Lavi, A., Chen, J. Y., Zhang, H., Bahreini, R., and Lin, Y.-H.: Brown Carbon Formation from Nighttime Chemistry of Unsaturated Heterocyclic Volatile Organic Compounds, Environmental Science & Technology Letters, 6, 184-190, 10.1021/acs.estlett.9b00017, 2019.

Jo, D. S., Park, R. J., Lee, S., Kim, S. W., and Zhang, X.: A global simulation of brown carbon: implications for photochemistry and direct radiative effect, Atmos. Chem. Phys., 16, 3413-3432, 10.5194/acp-16-3413-2016, 2016.

Jordan, C. E., Stauffer, R. M., Lamb, B. T., Hudgins, C. H., Thornhill, K. L., Schuster, G. L., Moore, R. H., Crosbie, E. C., Winstead, E. L., Anderson, B. E., Martin, R. F., Shook, M. A., Ziemba, L. D., Beyersdorf, A. J., Robinson, C. E., Corr, C. A., and Tzortziou, M. A.: New in situ aerosol hyperspectral optical measurements over 300–700 nm – Part 1: Spectral Aerosol Extinction (SpEx) instrument field validation during the KORUS-OC cruise, Atmos. Meas. Tech., 14, 695-713, 10.5194/amt-14-695-2021, 2021.

Karion, A., Sweeney, C., Wolter, S., Newberger, T., Chen, H., Andrews, A., Kofler, J., Neff, D., and Tans, P.: Long-term greenhouse gas measurements from aircraft, Atmos. Meas. Tech., 6, 511-526, 10.5194/amt-6-511-2013, 2013.

Kasthuriarachchi, N. Y., Rivellini, L.-H., Chen, X., Li, Y. J., and Lee, A. K. Y.: Effect of Relative Humidity on Secondary Brown Carbon Formation in Aqueous Droplets,

Environmental Science & Technology, 54, 13207-13216, 10.1021/acs.est.0c01239, 2020.

Kieber, R. J., Whitehead, R. F., Reid, S. N., Willey, J. D., and Seaton, P. J.: Chromophoric Dissolved Organic Matter (CDOM) In Rainwater, Southeastern North Carolina, USA, Journal of Atmospheric Chemistry, 54, 21-41, 10.1007/s10874-005-9008-4, 2006.

Kleinman, L. I., Sedlacek Iii, A. J., Adachi, K., Buseck, P. R., Collier, S., Dubey, M. K., Hodshire, A. L., Lewis, E., Onasch, T. B., Pierce, J. R., Shilling, J., Springston, S. R., Wang, J., Zhang, Q., Zhou, S., and Yokelson, R. J.: Rapid evolution of aerosol particles and their optical properties downwind of wildfires in the western US, Atmos. Chem. Phys., 20, 13319-13341, 10.5194/acp-20-13319-2020, 2020.

Koch, D., Bond, T. C., Streets, D., Unger, N., and van der Werf, G. R.: Global impacts of aerosols from particular source regions and sectors, Journal of Geophysical Research: Atmospheres, 112, 10.1029/2005jd007024, 2007.

Koch, D., Schulz, M., Kinne, S., McNaughton, C., Spackman, J. R., Balkanski, Y., Bauer, S., Berntsen, T., Bond, T. C., Boucher, O., Chin, M., Clarke, A., De Luca, N., Dentener, F., Diehl, T., Dubovik, O., Easter, R., Fahey, D. W., Feichter, J., Fillmore, D., Freitag, S., Ghan, S., Ginoux, P., Gong, S., Horowitz, L., Iversen, T., Kirkev, aring, g, A., Klimont, Z., Kondo, Y., Krol, M., Liu, X., Miller, R., Montanaro, V., Moteki, N., Myhre, G., Penner, J. E., Perlwitz, J., Pitari, G., Reddy, S., Sahu, L., Sakamoto, H., Schuster, G., Schwarz, J. P., Seland, Ø., Stier, P., Takegawa, N., Takemura, T., Textor, C., van Aardenne, J. A., and Zhao, Y.: Evaluation of black carbon estimations in global aerosol models, Atmos. Chem. Phys., 9, 9001-9026, 10.5194/acp-9-9001-2009, 2009.

Kolden, C. A.: We're Not Doing Enough Prescribed Fire in the Western United States to Mitigate Wildfire Risk, Fire, 2, 10.3390/fire2020030, 2019.

Kristiansen, N. I., Stohl, A., Olivié, D. J. L., Croft, B., Søvde, O. A., Klein, H., Christoudias, T., Kunkel, D., Leadbetter, S. J., Lee, Y. H., Zhang, K., Tsigaridis, K., Bergman, T., Evangeliou, N., Wang, H., Ma, P. L., Easter, R. C., Rasch, P. J., Liu, X., Pitari, G., Di Genova, G., Zhao, S. Y., Balkanski, Y., Bauer, S. E., Faluvegi, G. S., Kokkola, H., Martin, R. V., Pierce, J. R., Schulz, M., Shindell, D., Tost, H., and Zhang, H.: Evaluation of observed and modelled aerosol lifetimes using radioactive tracers of opportunity and an ensemble of 19 global models, Atmos. Chem. Phys., 16, 3525-3561, 10.5194/acp-16-3525-2016, 2016.

Kuang, Y., and Shang, J.: Changes in light absorption by brown carbon in soot particles due to heterogeneous ozone aging in a smog chamber, Environmental Pollution, 266, 115273, https://doi.org/10.1016/j.envpol.2020.115273, 2020.

Lack, D. A., Cappa, C. D., Covert, D. S., Baynard, T., Massoli, P., Sierau, B., Bates, T. S., Quinn, P. K., Lovejoy, E. R., and Ravishankara, A. R.: Bias in Filter-Based Aerosol Light Absorption Measurements Due to Organic Aerosol Loading: Evidence from Ambient Measurements, Aerosol Science and Technology, 42, 1033-1041, 10.1080/02786820802389277, 2008.

Lack, D. A., and Cappa, C. D.: Impact of brown and clear carbon on light absorption enhancement, single scatter albedo and absorption wavelength dependence of black carbon, Atmos. Chem. Phys., 10, 4207-4220, 10.5194/acp-10-4207-2010, 2010.

Lack, D. A., Langridge, J. M., Bahreini, R., Cappa, C. D., Middlebrook, A. M., and Schwarz, J. P.: Brown carbon and internal mixing in biomass burning particles, Proceedings of the National Academy of Sciences, 10.1073/pnas.1206575109, 2012a.

Lack, D. A., Richardson, M. S., Law, D., Langridge, J. M., Cappa, C. D., McLaughlin, R. J., and Murphy, D. M.: Aircraft Instrument for Comprehensive Characterization of Aerosol Optical Properties, Part 2: Black and Brown Carbon Absorption and Absorption Enhancement Measured with Photo Acoustic Spectroscopy, Aerosol Science and Technology, 46, 555-568, 10.1080/02786826.2011.645955, 2012b.

Lack, D. A., and Langridge, J. M.: On the attribution of black and brown carbon light absorption using the Ångström exponent, Atmos. Chem. Phys., 13, 10535-10543, 10.5194/acp-13-10535-2013, 2013.

Lan, Z.-J., Huang, X.-F., Yu, K.-Y., Sun, T.-L., Zeng, L.-W., and Hu, M.: Light absorption of black carbon aerosol and its enhancement by mixing state in an urban atmosphere in South China, Atmospheric Environment, 69, 118-123, https://doi.org/10.1016/j.atmosenv.2012.12.009, 2013.

Langridge, J. M., Richardson, M. S., Lack, D., Law, D., and Murphy, D. M.: Aircraft Instrument for Comprehensive Characterization of Aerosol Optical Properties, Part I: Wavelength-Dependent Optical Extinction and Its Relative Humidity Dependence Measured Using Cavity Ringdown Spectroscopy, Aerosol Science and Technology, 45, 1305-1318, 10.1080/02786826.2011.592745, 2011.

Langridge, J. M., Richardson, M. S., Lack, D. A., Brock, C. A., and Murphy, D. M.: Limitations of the Photoacoustic Technique for Aerosol Absorption Measurement at High Relative Humidity, Aerosol Science and Technology, 47, 1163-1173, 10.1080/02786826.2013.827324, 2013.

Laskin, A., Laskin, J., and Nizkorodov, S. A.: Chemistry of Atmospheric Brown Carbon, Chemical Reviews, 115, 4335-4382, 10.1021/cr5006167, 2015.

Laskin, J., Laskin, A., Nizkorodov, S. A., Roach, P., Eckert, P., Gilles, M. K., Wang, B., Lee, H. J., and Hu, Q.: Molecular Selectivity of Brown Carbon Chromophores, Environmental Science & Technology, 48, 12047-12055, 10.1021/es503432r, 2014.

Laumbach, R. J., and Kipen, H. M.: Respiratory health effects of air pollution: Update on biomass smoke and traffic pollution, Journal of Allergy and Clinical Immunology, 129, 3-11, https://doi.org/10.1016/j.jaci.2011.11.021, 2012.

Lee, H. J., Aiona, P. K., Laskin, A., Laskin, J., and Nizkorodov, S. A.: Effect of Solar Radiation on the Optical Properties and Molecular Composition of Laboratory Proxies of Atmospheric Brown Carbon, Environmental Science & Technology, 48, 10217-10226, 10.1021/es502515r, 2014.

Lei, Y., Shen, Z., Zhang, T., Zhang, Q., Wang, Q., Sun, J., Gong, X., Cao, J., Xu, H., Liu, S., and Yang, L.: Optical source profiles of brown carbon in size-resolved particulate matter from typical domestic biofuel burning over Guanzhong Plain, China, Science of The Total Environment, 622-623, 244-251, https://doi.org/10.1016/j.scitotenv.2017.11.353, 2018.

Lewtas, J.: Air pollution combustion emissions: Characterization of causative agents and mechanisms associated with cancer, reproductive, and cardiovascular effects, Mutation Research/Reviews in Mutation Research, 636, 95-133, https://doi.org/10.1016/j.mrrev.2007.08.003, 2007.

Li, C., He, Q., Hettiyadura, A. P. S., Käfer, U., Shmul, G., Meidan, D., Zimmermann, R., Brown, S. S., George, C., Laskin, A., and Rudich, Y.: Formation of Secondary Brown Carbon in Biomass Burning Aerosol Proxies through NO3 Radical Reactions, Environmental Science & Technology, 54, 1395-1405, 10.1021/acs.est.9b05641, 2020.

Li, J., Liu, C., Yin, Y., and Kumar, K. R.: Numerical investigation on the Ångström exponent of black carbon aerosol, Journal of Geophysical Research: Atmospheres, 121, 3506-3518, 10.1002/2015JD024718, 2016.

Limbeck, A., Kulmala, M., and Puxbaum, H.: Secondary organic aerosol formation in the atmosphere via heterogeneous reaction of gaseous isoprene on acidic particles, Geophysical Research Letters, 30, https://doi.org/10.1029/2003GL017738, 2003.

Lin, C.-I., Baker, M., and Charlson, R. J.: Absorption Coefficient of Atmospheric Aerosol: a Method for Measurement, Appl. Opt., 12, 1356-1363, 10.1364/AO.12.001356, 1973.

Lin, G., Penner, J. E., Flanner, M. G., Sillman, S., Xu, L., and Zhou, C.: Radiative forcing of organic aerosol in the atmosphere and on snow: Effects of SOA and brown carbon, Journal of Geophysical Research: Atmospheres, 119, 7453-7476, 10.1002/2013JD021186, 2014.

Lin, P., Laskin, J., Nizkorodov, S. A., and Laskin, A.: Revealing Brown Carbon Chromophores Produced in Reactions of Methylglyoxal with Ammonium Sulfate, Environmental Science & Technology, 49, 14257-14266, 10.1021/acs.est.5b03608, 2015a.

Lin, P., Liu, J., Shilling, J. E., Kathmann, S. M., Laskin, J., and Laskin, A.: Molecular characterization of brown carbon (BrC) chromophores in secondary organic aerosol generated from photo-oxidation of toluene, Physical Chemistry Chemical Physics, 17, 23312-23325, 10.1039/C5CP02563J, 2015b.

Lin, P., Aiona, P. K., Li, Y., Shiraiwa, M., Laskin, J., Nizkorodov, S. A., and Laskin, A.: Molecular Characterization of Brown Carbon in Biomass Burning Aerosol Particles, Environmental Science & Technology, 50, 11815-11824, 10.1021/acs.est.6b03024, 2016.

Lin, P., Bluvshtein, N., Rudich, Y., Nizkorodov, S. A., Laskin, J., and Laskin, A.: Molecular Chemistry of Atmospheric Brown Carbon Inferred from a Nationwide Biomass Burning Event, Environmental Science & Technology, 51, 11561-11570, 10.1021/acs.est.7b02276, 2017.

Liu, D., Whitehead, J., Alfarra, M. R., Reyes-Villegas, E., Spracklen, Dominick V., Reddington, Carly L., Kong, S., Williams, Paul I., Ting, Y.-C., Haslett, S., Taylor, Jonathan W., Flynn, Michael J., Morgan, William T., McFiggans, G., Coe, H., and Allan, James D.: Black-carbon absorption enhancement in the atmosphere

determined by particle mixing state, Nature Geoscience, 10, 184-188, 10.1038/ngeo2901, 2017.

Liu, J., Bergin, M., Guo, H., King, L., Kotra, N., Edgerton, E., and Weber, R. J.: Size-resolved measurements of brown carbon in water and methanol extracts and estimates of their contribution to ambient fine-particle light absorption, Atmos. Chem. Phys., 13, 12389-12404, 10.5194/acp-13-12389-2013, 2013.

Liu, J., Scheuer, E., Dibb, J., Ziemba, L. D., Thornhill, K. L., Anderson, B. E., Wisthaler, A., Mikoviny, T., Devi, J. J., Bergin, M., and Weber, R. J.: Brown carbon in the continental troposphere, Geophysical Research Letters, 41, 2191-2195, 10.1002/2013GL058976, 2014.

Liu, J., Scheuer, E., Dibb, J., Diskin, G. S., Ziemba, L. D., Thornhill, K. L., Anderson, B. E., Wisthaler, A., Mikoviny, T., Devi, J. J., Bergin, M., Perring, A. E., Markovic, M. Z., Schwarz, J. P., Campuzano-Jost, P., Day, D. A., Jimenez, J. L., and Weber, R. J.: Brown carbon aerosol in the North American continental troposphere: sources, abundance, and radiative forcing, Atmos. Chem. Phys., 15, 7841-7858, 10.5194/acp-15-7841-2015, 2015a.

Liu, J., Lin, P., Laskin, A., Laskin, J., Kathmann, S. M., Wise, M., Caylor, R., Imholt, F., Selimovic, V., and Shilling, J. E.: Optical properties and aging of light-absorbing secondary organic aerosol, Atmos. Chem. Phys., 16, 12815-12827, 10.5194/acp-16-12815-2016, 2016.

Liu, P. F., Abdelmalki, N., Hung, H. M., Wang, Y., Brune, W. H., and Martin, S. T.: Ultraviolet and visible complex refractive indices of secondary organic material produced by photooxidation of the aromatic compounds toluene and m-xylene, Atmos. Chem. Phys., 15, 1435-1446, 10.5194/acp-15-1435-2015, 2015b.

Liu, S., Aiken, A. C., Gorkowski, K., Dubey, M. K., Cappa, C. D., Williams, L. R., Herndon, S. C., Massoli, P., Fortner, E. C., Chhabra, P. S., Brooks, W. A., Onasch, T. B., Jayne, J. T., Worsnop, D. R., China, S., Sharma, N., Mazzoleni, C., Xu, L., Ng, N. L., Liu, D., Allan, J. D., Lee, J. D., Fleming, Z. L., Mohr, C., Zotter, P., Szidat, S., and Prévôt, A. S. H.: Enhanced light absorption by mixed source black and brown carbon particles in UK winter, Nature Communications, 6, 8435, 10.1038/ncomms9435, 2015c.

Lopez-Hilfiker, F. D., Pospisilova, V., Huang, W., Kalberer, M., Mohr, C., Stefenelli, G., Thornton, J. A., Baltensperger, U., Prevot, A. S. H., and Slowik, J. G.: An extractive electrospray ionization time-of-flight mass spectrometer (EESI-TOF)

for online measurement of atmospheric aerosol particles, Atmos. Meas. Tech., 12, 4867-4886, 10.5194/amt-12-4867-2019, 2019.

Lund, M. T., Samset, B. H., Skeie, R. B., Watson-Parris, D., Katich, J. M., Schwarz, J. P., and Weinzierl, B.: Short Black Carbon lifetime inferred from a global set of aircraft observations, npj Climate and Atmospheric Science, 1, 31, 10.1038/s41612-018-0040-x, 2018.

Luo, J., Zhang, Y., Wang, F., and Zhang, Q.: Effects of brown coatings on the absorption enhancement of black carbon: a numerical investigation, Atmos. Chem. Phys., 18, 16897-16914, 10.5194/acp-18-16897-2018, 2018.

Marple, V. A., Rubow, K. L., and Behm, S. M.: A Microorifice Uniform Deposit Impactor (MOUDI): Description, Calibration, and Use, Aerosol Science and Technology, 14, 434-446, 10.1080/02786829108959504, 1991.

Mayorga, R. J., Zhao, Z., and Zhang, H.: Formation of secondary organic aerosol from nitrate radical oxidation of phenolic VOCs: Implications for nitration mechanisms and brown carbon formation, Atmospheric Environment, 244, 117910, https://doi.org/10.1016/j.atmosenv.2020.117910, 2021.

McNaughton, C. S., Clarke, A. D., Howell, S. G., Pinkerton, M., Anderson, B., Thornhill, L., Hudgins, C., Winstead, E., Dibb, J. E., Scheuer, E., and Maring, H.: Results from the DC-8 Inlet Characterization Experiment (DICE): Airborne Versus Surface Sampling of Mineral Dust and Sea Salt Aerosols, Aerosol Science and Technology, 41, 136-159, 10.1080/02786820601118406, 2007.

Moharreri, A., Craig, L., Dubey, P., Rogers, D. C., and Dhaniyala, S.: Aircraft testing of the new Blunt-body Aerosol Sampler (BASE), Atmos. Meas. Tech., 7, 3085-3093, 10.5194/amt-7-3085-2014, 2014.

Mohr, C., Lopez-Hilfiker, F. D., Zotter, P., Prévôt, A. S. H., Xu, L., Ng, N. L., Herndon, S. C., Williams, L. R., Franklin, J. P., Zahniser, M. S., Worsnop, D. R., Knighton, W. B., Aiken, A. C., Gorkowski, K. J., Dubey, M. K., Allan, J. D., and Thornton, J. A.: Contribution of Nitrated Phenols to Wood Burning Brown Carbon Light Absorption in Detling, United Kingdom during Winter Time, Environmental Science & Technology, 47, 6316-6324, 10.1021/es400683v, 2013.

Moise, T., Flores, J. M., and Rudich, Y.: Optical Properties of Secondary Organic Aerosols and Their Changes by Chemical Processes, Chemical Reviews, 115, 4400-4439, 10.1021/cr5005259, 2015.

Mok, J., Krotkov, N. A., Arola, A., Torres, O., Jethva, H., Andrade, M., Labow, G., Eck, T. F., Li, Z., Dickerson, R. R., Stenchikov, G. L., Osipov, S., and Ren, X.: Impacts of brown carbon from biomass burning on surface UV and ozone photochemistry in the Amazon Basin, Scientific Reports, 6, 36940, 10.1038/srep36940, 2016.

Moore, R. H., Wiggins, E. B., Ahern, A. T., Zimmerman, S., Montgomery, L., Campuzano Jost, P., Robinson, C. E., Ziemba, L. D., Winstead, E. L., Anderson, B. E., Brock, C. A., Brown, M. D., Chen, G., Crosbie, E. C., Guo, H., Jimenez, J. L., Jordan, C. E., Lyu, M., Nault, B. A., Rothfuss, N. E., Sanchez, K. J., Schueneman, M., Shingler, T. J., Shook, M. A., Thornhill, K. L., Wagner, N. L., and Wang, J.: Sizing response of the Ultra-High Sensitivity Aerosol Spectrometer (UHSAS) and Laser Aerosol Spectrometer (LAS) to changes in submicron aerosol composition and refractive index, Atmos. Meas. Tech., 14, 4517-4542, 10.5194/amt-14-4517-2021, 2021.

Moosmüller, H., Chakrabarty, R. K., Ehlers, K. M., and Arnott, W. P.: Absorption Ångström coefficient, brown carbon, and aerosols: basic concepts, bulk matter, and spherical particles, Atmos. Chem. Phys., 11, 1217-1225, 10.5194/acp-11-1217-2011, 2011.

Myhre, G., Hoyle, C. R., Berglen, T. F., Johnson, B. T., and Haywood, J. M.: Modeling of the solar radiative impact of biomass burning aerosols during the Dust and Biomass-burning Experiment (DABEX), Journal of Geophysical Research: Atmospheres, 113, D00C16, 10.1029/2008jd009857, 2008.

Nguyen, T. B., Laskin, A., Laskin, J., and Nizkorodov, S. A.: Direct aqueous photochemistry of isoprene high-NOx secondary organic aerosol, Physical Chemistry Chemical Physics, 14, 9702-9714, 10.1039/C2CP40944E, 2012.

Nguyen, T. B., Laskin, A., Laskin, J., and Nizkorodov, S. A.: Brown carbon formation from ketoaldehydes of biogenic monoterpenes, Faraday Discussions, 165, 473-494, 10.1039/C3FD00036B, 2013.

O'Dell, K., Bilsback, K., Ford, B., Martenies, S. E., Magzamen, S., Fischer, E. V., and Pierce, J. R.: Estimated Mortality and Morbidity Attributable to Smoke Plumes in the United States: Not Just a Western US Problem, GeoHealth, 5, e2021GH000457, https://doi.org/10.1029/2021GH000457, 2021.

Obregón, M. A., Serrano, A., Costa, M. J., and Silva, A. M.: Validation of libRadtran and SBDART models under different aerosol conditions, IOP Conference Series:

Earth and Environmental Science, 28, 012010, 10.1088/1755-1315/28/1/012010, 2015.

Olson, M. R., Victoria Garcia, M., Robinson, M. A., Van Rooy, P., Dietenberger, M. A., Bergin, M., and Schauer, J. J.: Investigation of black and brown carbon multiple-wavelength-dependent light absorption from biomass and fossil fuel combustion source emissions, Journal of Geophysical Research: Atmospheres, 120, 6682-6697, https://doi.org/10.1002/2014JD022970, 2015.

Orsini, D. A., Ma, Y., Sullivan, A., Sierau, B., Baumann, K., and Weber, R. J.: Refinements to the particle-into-liquid sampler (PILS) for ground and airborne measurements of water soluble aerosol composition, Atmospheric Environment, 37, 1243-1259, https://doi.org/10.1016/S1352-2310(02)01015-4, 2003.

Pagonis, D., Campuzano-Jost, P., Guo, H., Day, D. A., Schueneman, M. K., Brown, W. L., Nault, B. A., Stark, H., Siemens, K., Laskin, A., Piel, F., Tomsche, L., Wisthaler, A., Coggon, M. M., Gkatzelis, G. I., Halliday, H. S., Krechmer, J. E., Moore, R. H., Thomson, D. S., Warneke, C., Wiggins, E. B., and Jimenez, J. L.: Airborne extractive electrospray mass spectrometry measurements of the chemical composition of organic aerosol, Atmos. Meas. Tech., 14, 1545-1559, 10.5194/amt-14-1545-2021, 2021.

Palm, B. B., Peng, Q., Fredrickson, C. D., Lee, B. H., Garofalo, L. A., Pothier, M. A., Kreidenweis, S. M., Farmer, D. K., Pokhrel, R. P., Shen, Y., Murphy, S. M., Permar, W., Hu, L., Campos, T. L., Hall, S. R., Ullmann, K., Zhang, X., Flocke, F., Fischer, E. V., and Thornton, J. A.: Quantification of organic aerosol and brown carbon evolution in fresh wildfire plumes, Proceedings of the National Academy of Sciences, 117, 29469-29477, 10.1073/pnas.2012218117, 2020.

Peltier, R. E., Weber, R. J., and Sullivan, A. P.: Investigating a Liquid-Based Method for Online Organic Carbon Detection in Atmospheric Particles, Aerosol Science and Technology, 41, 1117-1127, 10.1080/02786820701777465, 2007.

Perring, A. E., Schwarz, J. P., Gao, R. S., Heymsfield, A. J., Schmitt, C. G., Schnaiter, M., and Fahey, D. W.: Evaluation of a Perpendicular Inlet for Airborne Sampling of Interstitial Submicron Black-Carbon Aerosol, Aerosol Science and Technology, 47, 1066-1072, 10.1080/02786826.2013.821196, 2013.

Phillips, S. M., Bellcross, A. D., and Smith, G. D.: Light Absorption by Brown Carbon in the Southeastern United States is pH-dependent, Environmental Science & Technology, 51, 6782-6790, 10.1021/acs.est.7b01116, 2017.

Phillips, S. M., and Smith, G. D.: Spectroscopic comparison of water- and methanol-soluble brown carbon particulate matter, Aerosol Science and Technology, 51, 1113-1121, 10.1080/02786826.2017.1334109, 2017.

Pillar-Little, E. A., and Guzman, M. I.: Oxidation of Substituted Catechols at the Air–Water Interface: Production of Carboxylic Acids, Quinones, and Polyphenols, Environmental Science & Technology, 51, 4951-4959, 10.1021/acs.est.7b00232, 2017.

Pio, C. A., Legrand, M., Oliveira, T., Afonso, J., Santos, C., Caseiro, A., Fialho, P., Barata, F., Puxbaum, H., Sanchez-Ochoa, A., Kasper-Giebl, A., Gelencsér, A., Preunkert, S., and Schock, M.: Climatology of aerosol composition (organic versus inorganic) at nonurban sites on a west-east transect across Europe, Journal of Geophysical Research: Atmospheres, 112, 10.1029/2006JD008038, 2007.

Pio, C. A., Legrand, M., Alves, C. A., Oliveira, T., Afonso, J., Caseiro, A., Puxbaum, H., Sanchez-Ochoa, A., and Gelencsér, A.: Chemical composition of atmospheric aerosols during the 2003 summer intense forest fire period, Atmospheric Environment, 42, 7530-7543, https://doi.org/10.1016/j.atmosenv.2008.05.032, 2008.

Pöschl, U., Rudich, Y., and Ammann, M.: Kinetic model framework for aerosol and cloud surface chemistry and gas-particle interactions – Part 1: General equations, parameters, and terminology, Atmos. Chem. Phys., 7, 5989-6023, 10.5194/acp-7-5989-2007, 2007.

Pósfai, M., Gelencsér, A., Simonics, R., Arató, K., Li, J., Hobbs, P. V., and Buseck, P. R.: Atmospheric tar balls: Particles from biomass and biofuel burning, Journal of Geophysical Research: Atmospheres, 109, D06213, 10.1029/2003jd004169, 2004.

Powelson, M. H., Espelien, B. M., Hawkins, L. N., Galloway, M. M., and De Haan, D. O.: Brown Carbon Formation by Aqueous-Phase Carbonyl Compound Reactions with Amines and Ammonium Sulfate, Environmental Science & Technology, 48, 985-993, 10.1021/es4038325, 2014.

Prather, M. J., Zhu, X., Flynn, C. M., Strode, S. A., Rodriguez, J. M., Steenrod, S. D., Liu, J., Lamarque, J. F., Fiore, A. M., Horowitz, L. W., Mao, J., Murray, L. T., Shindell, D. T., and Wofsy, S. C.: Global atmospheric chemistry – which air matters, Atmos. Chem. Phys., 17, 9081-9102, 10.5194/acp-17-9081-2017, 2017.

Rastogi, N., Oakes, M. M., Schauer, J. J., Shafer, M. M., Majestic, B. J., and Weber, R. J.: New Technique for Online Measurement of Water-Soluble Fe(II) in Atmospheric Aerosols, Environmental Science & Technology, 43, 2425-2430, 10.1021/es8031902, 2009.

Regalado, J., Pérez-Padilla, R., Sansores, R., Ramirez, J. I. P., Brauer, M., Paré, P., and Vedal, S.: The Effect of Biomass Burning on Respiratory Symptoms and Lung Function in Rural Mexican Women, American Journal of Respiratory and Critical Care Medicine, 174, 901-905, 10.1164/rccm.200503-479OC, 2006.

Ricchiazzi, P., Yang, S., Gautier, C., and Sowle, D.: SBDART: A Research and Teaching Software Tool for Plane-Parallel Radiative Transfer in the Earth's Atmosphere, Bulletin of the American Meteorological Society, 79, 2101-2114, 10.1175/1520-0477(1998)079<2101:Sarats>2.0.Co;2, 1998.

Rolph, G., Stein, A., and Stunder, B.: Real-time Environmental Applications and Display sYstem: READY, Environmental Modelling & Software, 95, 210-228, https://doi.org/10.1016/j.envsoft.2017.06.025, 2017.

Roman, C., Arsene, C., Bejan, I. G., and Olariu, R. I.: Investigations on the gas-phase photolysis and OH radical kinetics of nitrocatechols: Implications of intramolecular interactions on their atmospheric behavior, Atmos. Chem. Phys. Discuss., 2021, 1-28, 10.5194/acp-2021-553, 2021.

Saleh, R., Robinson, E. S., Tkacik, D. S., Ahern, A. T., Liu, S., Aiken, A. C., Sullivan, R. C., Presto, A. A., Dubey, M. K., Yokelson, R. J., Donahue, N. M., and Robinson, A. L.: Brownness of organics in aerosols from biomass burning linked to their black carbon content, Nature Geoscience, 7, 647, 10.1038/ngeo2220 https://www.nature.com/articles/ngeo2220#supplementary-information, 2014.

Saleh, R., Marks, M., Heo, J., Adams, P. J., Donahue, N. M., and Robinson, A. L.: Contribution of brown carbon and lensing to the direct radiative effect of carbonaceous aerosols from biomass and biofuel burning emissions, Journal of Geophysical Research: Atmospheres, 120, 10,285-210,296, 10.1002/2015JD023697, 2015.

Saleh, R., Cheng, Z., and Atwi, K.: The Brown–Black Continuum of Light-Absorbing Combustion Aerosols, Environmental Science & Technology Letters, 5, 508-513, 10.1021/acs.estlett.8b00305, 2018.

Saleh, R.: From Measurements to Models: Toward Accurate Representation of Brown Carbon in Climate Calculations, Current Pollution Reports, 6, 90-104, 10.1007/s40726-020-00139-3, 2020.

Sareen, N., Moussa, S. G., and McNeill, V. F.: Photochemical Aging of Light-Absorbing Secondary Organic Aerosol Material, The Journal of Physical Chemistry A, 117, 2987-2996, 10.1021/jp309413j, 2013.

Satish, R., and Rastogi, N.: On the Use of Brown Carbon Spectra as a Tool to Understand Their Broader Composition and Characteristics: A Case Study from Crop-residue Burning Samples, ACS Omega, 4, 1847-1853, 10.1021/acsomega.8b02637, 2019.

Schauer, J. J.: Evaluation of elemental carbon as a marker for diesel particulate matter, Journal of Exposure Science & Environmental Epidemiology, 13, 443-453, 10.1038/sj.jea.7500298, 2003.

Scheuer, E., Talbot, R. W., Dibb, J. E., Seid, G. K., DeBell, L., and Lefer, B.: Seasonal distributions of fine aerosol sulfate in the North American Arctic basin during TOPSE, Journal of Geophysical Research: Atmospheres, 108, 8370, 10.1029/2001JD001364, 2003.

Schill, G. P., Froyd, K. D., Bian, H., Kupc, A., Williamson, C., Brock, C. A., Ray, E., Hornbrook, R. S., Hills, A. J., Apel, E. C., Chin, M., Colarco, P. R., and Murphy, D. M.: Widespread biomass burning smoke throughout the remote troposphere, Nature Geoscience, 10.1038/s41561-020-0586-1, 2020.

Schnaiter, M., Linke, C., Möhler, O., Naumann, K.-H., Saathoff, H., Wagner, R., Schurath, U., and Wehner, B.: Absorption amplification of black carbon internally mixed with secondary organic aerosol, Journal of Geophysical Research: Atmospheres, 110, 204, https://doi.org/10.1029/2005JD006046, 2005.

Schnitzler, E. G., Liu, T., Hems, R. F., and Abbatt, J. P. D.: Emerging investigator series: heterogeneous OH oxidation of primary brown carbon aerosol: effects of relative humidity and volatility, Environmental Science: Processes & Impacts, 22, 2162-2171, 10.1039/D0EM00311E, 2020.

Schroeder, W., Prins, E., Giglio, L., Csiszar, I., Schmidt, C., Morisette, J., and Morton, D.: Validation of GOES and MODIS active fire detection products using ASTER and ETM+ data, Remote Sensing of Environment, 112, 2711-2726, https://doi.org/10.1016/j.rse.2008.01.005, 2008.

Schuster, G. L., Dubovik, O., Arola, A., Eck, T. F., and Holben, B. N.: Remote sensing of soot carbon – Part 2: Understanding the absorption Ångström exponent, Atmos. Chem. Phys., 16, 1587-1602, 10.5194/acp-16-1587-2016, 2016.

Schwarz, J. P., Gao, R. S., Fahey, D. W., Thomson, D. S., Watts, L. A., Wilson, J. C., Reeves, J. M., Darbeheshti, M., Baumgardner, D. G., Kok, G. L., Chung, S. H., Schulz, M., Hendricks, J., Lauer, A., Kärcher, B., Slowik, J. G., Rosenlof, K. H., Thompson, T. L., Langford, A. O., Loewenstein, M., and Aikin, K. C.: Single-particle measurements of midlatitude black carbon and light-scattering aerosols from the boundary layer to the lower stratosphere, Journal of Geophysical Research: Atmospheres, 111, 207, https://doi.org/10.1029/2006JD007076, 2006.

Schwarz, J. P., Spackman, J. R., Fahey, D. W., Gao, R. S., Lohmann, U., Stier, P., Watts, L. A., Thomson, D. S., Lack, D. A., Pfister, L., Mahoney, M. J., Baumgardner, D., Wilson, J. C., and Reeves, J. M.: Coatings and their enhancement of black carbon light absorption in the tropical atmosphere, Journal of Geophysical Research: Atmospheres, 113, 03, 10.1029/2007JD009042, 2008.

Sedlacek III, A. J., Lewis, E. R., Kleinman, L., Xu, J., and Zhang, Q.: Determination of and evidence for non-core-shell structure of particles containing black carbon using the Single-Particle Soot Photometer (SP2), Geophysical Research Letters, 39, 802, 10.1029/2012GL050905, 2012.

Selimovic, V., Yokelson, R. J., McMeeking, G. R., and Coefield, S.: Aerosol Mass and Optical Properties, Smoke Influence on O3, and High NO3 Production Rates in a Western U.S. City Impacted by Wildfires, Journal of Geophysical Research: Atmospheres, 125, e2020JD032791, https://doi.org/10.1029/2020JD032791, 2020.

Shen, H., Tao, S., Liu, J., Huang, Y., Chen, H., Li, W., Zhang, Y., Chen, Y., Su, S., Lin, N., Xu, Y., Li, B., Wang, X., and Liu, W.: Global lung cancer risk from PAH exposure highly depends on emission sources and individual susceptibility, Scientific Reports, 4, 6561, 10.1038/srep06561, 2014.

Shetty, N. J., Pandey, A., Baker, S., Hao, W. M., and Chakrabarty, R. K.: Measuring light absorption by freshly emitted organic aerosols: optical artifacts in traditional solvent-extraction-based methods, Atmos. Chem. Phys., 19, 8817-8830, 10.5194/acp-19-8817-2019, 2019.

Shrivastava, M., Lou, S., Zelenyuk, A., Easter, R. C., Corley, R. A., Thrall, B. D., Rasch, P. J., Fast, J. D., Massey Simonich, S. L., Shen, H., and Tao, S.: Global long-

range transport and lung cancer risk from polycyclic aromatic hydrocarbons shielded by coatings of organic aerosol, Proceedings of the National Academy of Sciences, 114, 1246-1251, 10.1073/pnas.1618475114, 2017.

Sokolik, I. N., and Toon, O. B.: Incorporation of mineralogical composition into models of the radiative properties of mineral aerosol from UV to IR wavelengths, Journal of Geophysical Research: Atmospheres, 104, 9423-9444, 10.1029/1998JD200048, 1999.

Spaulding, R. S., Talbot, R. W., and Charles, M. J.: Optimization of a Mist Chamber (Cofer Scrubber) for Sampling Water-Soluble Organics in Air, Environmental Science & Technology, 36, 1798-1808, 10.1021/es011189x, 2002.

Stein, A. F., Draxler, R. R., Rolph, G. D., Stunder, B. J. B., Cohen, M. D., and Ngan, F.: NOAA's HYSPLIT Atmospheric Transport and Dispersion Modeling System, Bulletin of the American Meteorological Society, 96, 2059-2077, 10.1175/BAMS-D-14-00110.1, 2015.

Stephens, M., Turner, N., and Sandberg, J.: Particle identification by laser-induced incandescence in a solid-state laser cavity, Appl. Opt., 42, 3726-3736, 10.1364/AO.42.003726, 2003.

Stith, J. L., Ramanathan, V., Cooper, W. A., Roberts, G. C., DeMott, P. J., Carmichael, G., Hatch, C. D., Adhikary, B., Twohy, C. H., Rogers, D. C., Baumgardner, D., Prenni, A. J., Campos, T., Gao, R., Anderson, J., and Feng, Y.: An overview of aircraft observations from the Pacific Dust Experiment campaign, Journal of Geophysical Research: Atmospheres, 114, https://doi.org/10.1029/2008JD010924, 2009.

Subramanian, R., Roden, C. A., Boparai, P., and Bond, T. C.: Yellow Beads and Missing Particles: Trouble Ahead for Filter-Based Absorption Measurements, Aerosol Science and Technology, 41, 630-637, 10.1080/02786820701344589, 2007.

Sullivan, A. P., Peltier, R. E., Brock, C. A., de Gouw, J. A., Holloway, J. S., Warneke, C., Wollny, A. G., and Weber, R. J.: Airborne measurements of carbonaceous aerosol soluble in water over northeastern United States: Method development and an investigation into water-soluble organic carbon sources, Journal of Geophysical Research: Atmospheres, 111, S46, https://doi.org/10.1029/2006JD007072, 2006.

Sullivan, A. P., May, A. A., Lee, T., McMeeking, G. R., Kreidenweis, S. M., Akagi, S. K., Yokelson, R. J., Urbanski, S. P., and Collett Jr, J. L.: Airborne

characterization of smoke marker ratios from prescribed burning, Atmos. Chem. Phys., 14, 10535-10545, 10.5194/acp-14-10535-2014, 2014.

Sullivan, A. P., Guo, H., Schroder, J. C., Campuzano-Jost, P., Jimenez, J. L., Campos, T., Shah, V., Jaeglé, L., Lee, B. H., Lopez-Hilfiker, F. D., Thornton, J. A., Brown, S. S., and Weber, R. J.: Biomass Burning Markers and Residential Burning in the WINTER Aircraft Campaign, Journal of Geophysical Research: Atmospheres, 124, 1846-1861, 10.1029/2017JD028153, 2019.

Sun, J., Wei, B., Mei, Q., An, Z., Wang, X., and He, M.: Ozonation of 3-methylcatechol and 4-methylcatechol in the atmosphere and aqueous particles: Mechanism, kinetics and ecotoxicity assessment, Chemical Engineering Journal, 358, 456-466, https://doi.org/10.1016/j.cej.2018.10.074, 2019.

Talbot, R. W., Dibb, J. E., Scheuer, E. M., Kondo, Y., Koike, M., Singh, H. B., Salas, L. B., Fukui, Y., Ballenthin, J. O., Meads, R. F., Miller, T. M., Hunton, D. E., Viggiano, A. A., Blake, D. R., Blake, N. J., Atlas, E., Flocke, F., Jacob, D. J., and Jaegle, L.: Reactive nitrogen budget during the NASA SONEX Mission, Geophysical Research Letters, 26, 3057-3060, https://doi.org/10.1029/1999GL900589, 1999.

Teich, M., van Pinxteren, D., Wang, M., Kecorius, S., Wang, Z., Müller, T., Močnik, G., and Herrmann, H.: Contributions of nitrated aromatic compounds to the light absorption of water-soluble and particulate brown carbon in different atmospheric environments in Germany and China, Atmos. Chem. Phys., 17, 1653-1672, 10.5194/acp-17-1653-2017, 2017.

Thompson, M. P., Calkin, D. E., Finney, M. A., Ager, A. A., and Gilbertson-Day, J. W.: Integrated national-scale assessment of wildfire risk to human and ecological values, Stochastic Environmental Research and Risk Assessment, 25, 761-780, 10.1007/s00477-011-0461-0, 2011.

Tian, Z., Zhao, H., Peter, K. T., Gonzalez, M., Wetzel, J., Wu, C., Hu, X., Prat, J., Mudrock, E., Hettinger, R., Cortina, A. E., Biswas, R. G., Kock, F. V. C., Soong, R., Jenne, A., Du, B., Hou, F., He, H., Lundeen, R., Gilbreath, A., Sutton, R., Scholz, N. L., Davis, J. W., Dodd, M. C., Simpson, A., McIntyre, J. K., and Kolodziej, E. P.: A ubiquitous tire rubber–derived chemical induces acute mortality in coho salmon, Science, 371, 185-189, 10.1126/science.abd6951, 2020.

Verma, V., Wang, Y., El-Afifi, R., Fang, T., Rowland, J., Russell, A. G., and Weber, R. J.: Fractionating ambient humic-like substances (HULIS) for their reactive

oxygen species activity – Assessing the importance of quinones and atmospheric aging, Atmospheric Environment, 120, 351-359, https://doi.org/10.1016/j.atmosenv.2015.09.010, 2015.

Vidović, K., Kroflič, A., Šala, M., and Grgić, I.: Aqueous-Phase Brown Carbon Formation from Aromatic Precursors under Sunlight Conditions, Atmosphere, 11, 131, 2020.

Virkkula, A.: Correction of the Calibration of the 3-wavelength Particle Soot Absorption Photometer (3λ PSAP), Aerosol Science and Technology, 44, 706-712, 10.1080/02786826.2010.482110, 2010.

Wang, S., Coggon, M. M., Gkatzelis, G. I., Warneke, C., Bourgeois, I., Ryerson, T., Peischl, J., Veres, P. R., Neuman, J. A., Hair, J., Shingler, T., Fenn, M., Diskin, G., Huey, L. G., Lee, Y. R., Apel, E. C., Hornbrook, R. S., Hills, A. J., Hall, S. R., Ullmann, K., Bela, M. M., Trainer, M. K., Kumar, R., Orlando, J. J., Flocke, F. M., and Emmons, L. K.: Chemical Tomography in a Fresh Wildland Fire Plume: A Large Eddy Simulation (LES) Study, Journal of Geophysical Research: Atmospheres, 126, e2021JD035203, https://doi.org/10.1029/2021JD035203, 2021.

Wang, X., Heald, C. L., Sedlacek, A. J., de Sá, S. S., Martin, S. T., Alexander, M. L., Watson, T. B., Aiken, A. C., Springston, S. R., and Artaxo, P.: Deriving brown carbon from multiwavelength absorption measurements: method and application to AERONET and Aethalometer observations, Atmos. Chem. Phys., 16, 12733-12752, 10.5194/acp-16-12733-2016, 2016.

Wang, X., Heald, C. L., Liu, J., Weber, R. J., Campuzano-Jost, P., Jimenez, J. L., Schwarz, J. P., and Perring, A. E.: Exploring the observational constraints on the simulation of brown carbon, Atmos. Chem. Phys., 18, 635-653, 10.5194/acp-18-635-2018, 2018.

Warner, J. X., Wei, Z., Strow, L. L., Barnet, C. D., Sparling, L. C., Diskin, G., and Sachse, G.: Improved agreement of AIRS tropospheric carbon monoxide products with other EOS sensors using optimal estimation retrievals, Atmos. Chem. Phys., 10, 9521-9533, 10.5194/acp-10-9521-2010, 2010.

Washenfelder, R. A., Attwood, A. R., Brock, C. A., Guo, H., Xu, L., Weber, R. J., Ng, N. L., Allen, H. M., Ayres, B. R., Baumann, K., Cohen, R. C., Draper, D. C., Duffey, K. C., Edgerton, E., Fry, J. L., Hu, W. W., Jimenez, J. L., Palm, B. B., Romer, P., Stone, E. A., Wooldridge, P. J., and Brown, S. S.: Biomass burning dominates

brown carbon absorption in the rural southeastern United States, Geophysical Research Letters, 42, 653-664, 10.1002/2014GL062444, 2015.

Weber, R. J., Orsini, D., Daun, Y., Lee, Y. N., Klotz, P. J., and Brechtel, F.: A Particle-into-Liquid Collector for Rapid Measurement of Aerosol Bulk Chemical Composition, Aerosol Science and Technology, 35, 718-727, 10.1080/02786820152546761, 2001.

Weingartner, E., Saathoff, H., Schnaiter, M., Streit, N., Bitnar, B., and Baltensperger, U.: Absorption of light by soot particles: determination of the absorption coefficient by means of aethalometers, Journal of Aerosol Science, 34, 1445-1463, https://doi.org/10.1016/S0021-8502(03)00359-8, 2003.

Werle, P., Mücke, R., and Slemr, F.: The limits of signal averaging in atmospheric trace-gas monitoring by tunable diode-laser absorption spectroscopy (TDLAS), Applied Physics B, 57, 131-139, 10.1007/BF00425997, 1993.

Williams, J., de Reus, M., Krejci, R., Fischer, H., and Ström, J.: Application of the variability-size relationship to atmospheric aerosol studies: estimating aerosol lifetimes and ages, Atmos. Chem. Phys., 2, 133-145, 10.5194/acp-2-133-2002, 2002.

Wonaschütz, A., Hitzenberger, R., Bauer, H., Pouresmaeil, P., Klatzer, B., Caseiro, A., and Puxbaum, H.: Application of the Integrating Sphere Method to Separate the Contributions of Brown and Black Carbon in Atmospheric Aerosols, Environmental Science & Technology, 43, 1141-1146, 10.1021/es8008503, 2009.

Wong, J. P. S., Nenes, A., and Weber, R. J.: Changes in Light Absorptivity of Molecular Weight Separated Brown Carbon Due to Photolytic Aging, Environmental Science & Technology, 51, 8414-8421, 10.1021/acs.est.7b01739, 2017.

Wong, J. P. S., Tsagkaraki, M., Tsiodra, I., Mihalopoulos, N., Violaki, K., Kanakidou, M., Sciare, J., Nenes, A., and Weber, R. J.: Effects of Atmospheric Processing on the Oxidative Potential of Biomass Burning Organic Aerosols, Environmental Science & Technology, 53, 6747-6756, 10.1021/acs.est.9b01034, 2019a.

Wong, J. P. S., Tsagkaraki, M., Tsiodra, I., Mihalopoulos, N., Violaki, K., Kanakidou, M., Sciare, J., Nenes, A., and Weber, R. J.: Atmospheric evolution of molecular-weight-separated brown carbon from biomass burning, Atmos. Chem. Phys., 19, 7319-7334, 10.5194/acp-19-7319-2019, 2019b.

Wooster, M. J., Roberts, G., Perry, G. L. W., and Kaufman, Y. J.: Retrieval of biomass combustion rates and totals from fire radiative power observations: FRP derivation and calibration relationships between biomass consumption and fire radiative energy release, Journal of Geophysical Research: Atmospheres, 110, 10.1029/2005JD006318, 2005.

Wu, H., Taylor, J. W., Langridge, J. M., Yu, C., Allan, J. D., Szpek, K., Cotterell, M. I., Williams, P. I., Flynn, M., Barker, P., Fox, C., Allen, G., Lee, J., and Coe, H.: Rapid transformation of ambient absorbing aerosols from West African biomass burning, Atmos. Chem. Phys., 21, 9417-9440, 10.5194/acp-21-9417-2021, 2021.

Wu, Y., Cheng, T., Liu, D., Allan, J. D., Zheng, L., and Chen, H.: Light Absorption Enhancement of Black Carbon Aerosol Constrained by Particle Morphology, Environmental Science & Technology, 52, 6912-6919, 10.1021/acs.est.8b00636, 2018.

Yan, J., Wang, X., Gong, P., Wang, C., and Cong, Z.: Review of brown carbon aerosols: Recent progress and perspectives, Science of The Total Environment, 634, 1475-1485, https://doi.org/10.1016/j.scitotenv.2018.04.083, 2018.

Zeng, L., Zhang, A., Wang, Y., Wagner, N. L., Katich, J. M., Schwarz, J. P., Schill, G. P., Brock, C., Froyd, K. D., Murphy, D. M., Williamson, C. J., Kupc, A., Scheuer, E., Dibb, J., and Weber, R. J.: Global Measurements of Brown Carbon and Estimated Direct Radiative Effects, Geophysical Research Letters, 47, e2020GL088747, 10.1029/2020gl088747, 2020.

Zeng, L., Sullivan, A. P., Washenfelder, R. A., Dibb, J., Scheuer, E., Campos, T. L., Katich, J. M., Levin, E., Robinson, M. A., and Weber, R. J.: Assessment of online water-soluble brown carbon measuring systems for aircraft sampling, Atmos. Meas. Tech., 14, 6357-6378, 10.5194/amt-14-6357-2021, 2021.

Zhang, A., Wang, Y., Zhang, Y., Weber, R. J., Song, Y., Ke, Z., and Zou, Y.: Modeling the global radiative effect of brown carbon: a potentially larger heating source in the tropical free troposphere than black carbon, Atmos. Chem. Phys., 20, 1901-1920, 10.5194/acp-20-1901-2020, 2020a.

Zhang, X., Hecobian, A., Zheng, M., Frank, N. H., and Weber, R. J.: Biomass burning impact on PM_{2.5} over the southeastern US during 2007: integrating chemically speciated FRM filter measurements, MODIS fire counts and PMF analysis, Atmos. Chem. Phys., 10, 6839-6853, 10.5194/acp-10-6839-2010, 2010.

Zhang, X., Lin, Y.-H., Surratt, J. D., and Weber, R. J.: Sources, Composition and Absorption Ångström Exponent of Light-absorbing Organic Components in Aerosol Extracts from the Los Angeles Basin, Environmental Science & Technology, 47, 3685-3693, 10.1021/es305047b, 2013.

Zhang, X., Mao, M., Yin, Y., and Tang, S.: The absorption Ångstrom exponent of black carbon with brown coatings: effects of aerosol microphysics and parameterization, Atmos. Chem. Phys., 20, 9701-9711, 10.5194/acp-20-9701-2020, 2020b.

Zhang, Y., Forrister, H., Liu, J., Dibb, J., Anderson, B., Schwarz, J. P., Perring, A. E., Jimenez, J. L., Campuzano-Jost, P., Wang, Y., Nenes, A., and Weber, R. J.: Top-of-atmosphere radiative forcing affected by brown carbon in the upper troposphere, Nature Geoscience, 10, 486, 10.1038/ngeo2960 https://www.nature.com/articles/ngeo2960#supplementary-information, 2017.

Zhang, Y., Favez, O., Canonaco, F., Liu, D., Močnik, G., Amodeo, T., Sciare, J., Prévôt, A. S. H., Gros, V., and Albinet, A.: Evidence of major secondary organic aerosol contribution to lensing effect black carbon absorption enhancement, npj Climate and Atmospheric Science, 1, 47, 10.1038/s41612-018-0056-2, 2018.

Zhao, R., Lee, A. K. Y., Huang, L., Li, X., Yang, F., and Abbatt, J. P. D.: Photochemical processing of aqueous atmospheric brown carbon, Atmos. Chem. Phys., 15, 6087-6100, 10.5194/acp-15-6087-2015, 2015.

Zhong, M., and Jang, M.: Dynamic light absorption of biomass-burning organic carbon photochemically aged under natural sunlight, Atmos. Chem. Phys., 14, 1517-1525, 10.5194/acp-14-1517-2014, 2014.

Zhou, X., Josey, K., Kamareddine, L., Caine, M. C., Liu, T., Mickley, L. J., Cooper, M., and Dominici, F.: Excess of COVID-19 cases and deaths due to fine particulate matter exposure during the 2020 wildfires in the United States, Science Advances, 7, eabi8789, 10.1126/sciadv.abi8789, 2021.